Integrated Multi-Sensor System for Parallel In-Situ Monitoring of Biotechnological Processes

Von der Fakultät für Ingenieurwissenschaften,
Abteilung Elektrotechnik und Informationstechnik
der Universität Duisburg-Essen

zur Erlangung des akademischen Grades

Doktor der Ingenieurwissenschaften

genehmigte Dissertation

von

Stefan Mross, M.Sc.

aus

Düsseldorf

1. Gutachter: Prof. Dr.-Ing. Holger Vogt
2. Gutachter: Prof. Michael Kraft, PhD

Tag der mündlichen Prüfung: 18.08.2016

Danksagung

Die vorliegende Arbeit entstand während meiner Tätigkeit als wissenschaftlicher Mitarbeiter in der Abteilung Mikro- und Nanosysteme am Fraunhofer-Institut für Mikroelektronische Schaltungen und Systeme (IMS) in Duisburg. Zu ihrem Gelingen haben viele Personen beigetragen, denen ich hier danken möchte.

Herrn Professor Holger Vogt und Herrn Professor Michael Kraft danke ich für die freundliche Übernahme und Betreuung der Arbeit, zahlreiche fachliche Hinweise und Anregungen sowie Unterstützung beim Schreiben und Veröffentlichen wissenschaftlicher Arbeiten. Herrn Professor Michael Kraft danke ich weiterhin für die freundliche Übernahme des Zweitgutachtens.

Herrn Dr.-Ing. Tom Zimmermann möchte ich für die vielfältigen, hilfreichen wissenschaftlichen Anregungen, die beständige Motivation und die wertvollen Ratschläge zu allen Facetten des wissenschaftlichen Lebens und Arbeitens, von der Suche nach Masterstudenten über das Schreiben durchdachter Veröffentlichungen bis hin zur Vorbereitung überzeugender Vorträge, besonders danken.

Weiterhin danke ich meinen Kollegen in der Gruppe Biohybride Systeme, Frau Dr.-Ing. Sarah Kißler und Herrn Dr. Sebastien Pierrat, für wertvolle Anregungen, hilfreiche Diskussionen und die sehr angenehme Arbeitsatmosphäre in der Gruppe, dank der ich mich vom ersten Tag an sehr wohl am Institut gefühlt habe.

Danken möchte ich auch den Kollegen der Abteilung TFE, die mich zu Fragen der Prozesstechnik im MST-Labor beraten und mir an den Anlagen geholfen haben.

Dank gebührt ebenfalls Herrn Sebastian Zenzes und Frau Vanessa Hapke, die im Rahmen ihrer Masterarbeit bzw. ihres Praktikums viele Messungen durchgeführt und wertvolle Messergebnisse erzielt haben.

Mein Dank gilt auch Herrn Professor Wilfried Mokwa und Frau Dipl.-Ing. Nadine Winkin für mehrere Aufdampfvorgänge mit Gold und Platin, ohne die

der in dieser Arbeit entwickelte Chip nicht hätte gefertigt werden können.

Abschließend gilt mein Dank meiner Familie und meinen Freunden, die mich während der Zeit der Dissertation immer unterstützt und damit entscheidend zum Gelingen der Arbeit beigetragen haben.

Zusammenfassung

Die wachsende Komplexität heutiger biotechnologischer Prozesse, z.B. in der Herstellung von Antikörpern und Impfstoffen, und immer höhere Anforderungen an die Effizienz der Prozesse und Sicherheit der Produkte erfordern eine präzise Überwachung und Steuerung. In dieser Arbeit wird ein miniaturisiertes Multi-Sensor-System zur parallelen Überwachung vier wichtiger Prozessgrößen entwickelt: Glukose und Laktat in weiten Konzentrationsbereichen, pH und Zelldichte.

Das auf einem Silizium-Chip integrierte System wird in einem CMOS-basierten, für die Massenproduktion geeigneten Fertigungsverfahren hergestellt und hat eine Größe von nur 7,16 mm × 7,16 mm, wodurch es auch in kleinen Bioreaktoren wie Zellkulturflaschen eingesetzt werden kann. Hierdurch und durch die kontinuierliche, parallele Messung direkt im Bioreaktor ist das System gegenüber dem bisher üblichen Messaufbau, der einen separaten Sensor für jeden Parameter und Probennahme und externe Messungen für Glukose und Laktat vorsieht, deutlich im Vorteil. Es ist kleiner, kostengünstiger, einfacher zu handhaben und leichter zu sterilisieren. Weiterhin ermöglicht die räumliche Nähe der Sensoren die gegenseitige Korrektur der Messwerte und das Erkennen von Drifts und anderen Abweichungen.

Das Hauptaugenmerk der Arbeit liegt auf der Entwicklung von amperometrischen Enzymsensoren für Glukose und Laktat, die an die in Bioprozessen üblichen weiten Konzentrationsbereiche von wenigen Millimol pro Liter (mM) bis über 1000 mM angepasst sind. Um in solch weiten Bereichen messen zu können, werden diffusionsbegrenzende Membranen verwendet, die den Stoffstrom zur Enzymschicht auf dem Sensor verringern. Es werden zwei Membranmaterialien, Poly(dimethylsiloxan) (PDMS) und Polyurethan (PU), auf ihre Eignung für diese Anwendung hin untersucht, wobei Untersuchungen zu Oberflächenbeschaffenheit, Durchlässigkeit und Langzeitstabilität der Membranen durchgeführt werden. Mit

Hilfe der PDMS-Membranen können Glukosekonzentrationen bis 200 mM gemessen werden, mit den PU-Membranen Konzentrationen bis 600 mM Glukose und 900 mM Laktat. Diese Messbereiche decken einen Großteil der in Bioprozessen vorkommenden Konzentrationen ab. Die Glukosesensoren werden in Langzeitversuchen eingesetzt und zeigen eine Einsatzdauer von 13 Tagen bei der kontinuierlichen Glukosemessung in einer Hefekultur und 30 Tagen bei wöchentlichen Kalibriermessungen.

Der Zelldichtesensor ist in Form von Fingerelektroden aus Platin ausgeführt und bestimmt die Zelldichte über die Messung der Leitfähigkeit einer Zelllösung. Es werden Messungen bis 20 g/l Trockenzellmasse in Hefekulturen gezeigt, was einen weiten Bereich der in Bioprozessen vorkommenden Zelldichten abdeckt.

Der pH-Wert wird in C-U-Messungen am Chip über die Veränderung der Schwellenspannung bestimmt. Als pH-empfindliches Material wird Ta_2O_5 verwendet, das mittels Atomlagenabscheidung (ALD) auf dem Multi-Sensor-Chip abgeschieden wird. Es wird ein Messbereich von pH 3 bis pH 12 erreicht, der das gesamte pH-Spektrum der in Bioprozessen genutzten Kulturlösungen umfasst. Beide Sensoren werden in der kontinuierlichen Überwachung von Hefekulturen eingesetzt und liefern Messwerte in guter Übereinstimmung mit Referenzmessungen.

Durch die parallele Überwachung von Glukosekonzentration und Zelldichte in einer Hefekultur werden der gleichzeitige Betrieb mehrerer Sensoren auf einem Chip demonstriert und die Vorteile des Multi-Sensor-Systems gegenüber dem Einsatz einzelner Sensoren gezeigt.

Abstract

Due to increasing complexity of bioprocesses in production and research, e.g. in the fabrication of antibodies and vaccines, and high efficiency and product safety requirements, precise monitoring and control in biotechnology becomes increasingly important. In this work a multi-sensor system for the parallel in-situ monitoring of the four important process parameters glucose, lactate, cell density and pH in bioprocesses is developed.

The fabrication process of the sensor chip, based on a CMOS process flow, is suitable for integration into standard processes and mass production of the system. Thanks to the continuous, parallel measurement directly inside the bioreactor the system is considerably simpler, smaller, more cost-effective and easier to sterilize than the state-of-the-art measurement approach, which involves a separate sensor for every parameter and sampling and external measurement for glucose and lactate.

The focus of this thesis is on the development of amperometric enzyme sensors for glucose and lactate that cover the wide concentration ranges found in bioprocesses. These range from a few millimoles per liter (mM) to concentrations above 1000 mM. To achieve such wide measurement ranges diffusion-limiting membranes are employed. Two membrane materials, poly(dimethylsiloxane) (PDMS) and polyurethane (PU), are assessed for this purpose, examining the surface morphology, permeability and long-term performance of fabricated membranes. Using PDMS membranes glucose is measured up to 200 mM, and with sensors covered with PU membranes concentrations up to 600 mM glucose and 900 mM lactate are measured. These ranges include a significant part of the concentrations found in bioprocesses. The glucose sensors are employed in long-term measurements and show good performance in the continuous monitoring of a yeast culture over 13 days and weekly calibration measurements over 30 days.

The cell density sensor is realized as interdigitated platinum electrodes, and cell density is determined via conductivity changes of a cell suspension. Measurements are performed up to 20 g/l dry cell weight, covering a significant part of the cell densities found in bioprocesses.

The pH is determined in C-V measurements via threshold voltage shifts at an electrolyte-insulator-semiconductor structure. Ta_2O_5 is employed as a pH-sensitive material, deposited on the chip surface by an atomic layer deposition (ALD) process. The sensor is able to measure pH in a range from pH 3 to pH 12, being suitable for any medium used in cell cultures. Both sensors show good performance and tight correlation with reference measurements when used in the monitoring of yeast culture.

The glucose and cell density sensor in parallel are successfully employed in the monitoring of a yeast culture, showing good correlation with reference measurements. The feasibility of the parallel operation of multiple sensors on one chip is proven, and the advantage of the multi-sensor system in comparison to single sensors is demonstrated.

Contents

Chapter 1

Introduction - State of the Art and Purpose of This Work

Today, biotechnology comprises a wide variety of processes and products, ranging from yeast cultures for alcoholic fermentation to complex mammalian cultures for tissues, vaccines, monoclonal antibodies and therapeutic proteins [1, 2]. Due to continuous progress in medicine and trends such as personalized medicine especially the demand for sophisticated and customized products with high expression rates, including antibodies and vaccines, is rapidly growing. At the same time high efficiency and product quality are key requirements for various processes, be they new or well-established [3].

In order to meet the increasing requirements and enable cutting-edge processes precise process control is crucial. This, in turn, involves the knowledge of a multitude of parameters that influence the process. A selection of these parameters, as listed in Fig. 1.1, includes concentration of nutrients (e.g., glucose) and metabolites (e.g., lactate), reactor parameters such as pH, pressure, temperature, oxygen and carbon dioxide tension, and product parameters like cell density or concentration of enzymes, antibodies, vaccines etc. [3]. For many of these parameters a continuous measurement that provides real-time data is preferable because this allows detecting small changes quickly, adjusting relevant parameters timely and controlling the process at its optimum. For complex products such as antibodies already small differences in process parameters, acting on small timescales, can significantly affect product attributes such as glycosylation patterns [4] and compromise product quality.

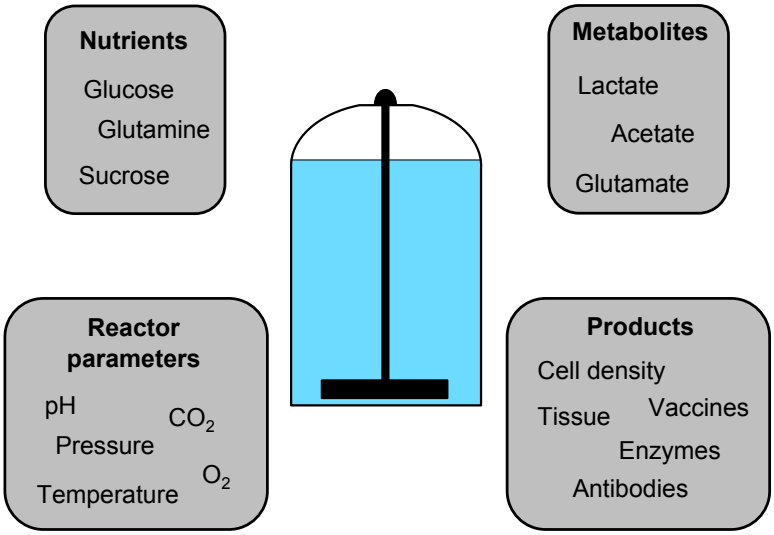

Figure 1.1: Parameters in biotechnological processes, grouped into four main categories; in complex bioprocesses; multiple parameters have to be monitored to achieve high product quality and yield

The benefits gained from the monitoring of multiple parameters are manifold. In Fig. 1.2 the parallel monitoring of cell density, nutrients, metabolites and pH in a batch process is schematically shown. Thanks to the obtained cell density data, scientists and process engineers can derive the growth phase of the cells, detect phase transitions, maintain an optimal cell density and identify contaminations of mammalian cultures by fast growing fungi or bacteria. The parallel monitoring of the nutrient and metabolite concentrations allows verifying the cell density data, maintaining narrow process windows for optimal growth and avoiding inhibition effects, such as the Crabtree effect [5]. Finally, the monitoring of reactor parameters, such as pH, provides data necessary to ensure optimal growth conditions and allows immediate intervention in case of deviations.

Monitoring is required in each of the three stages biotechnological processes typically pass through during their development [3]. In the development stage the characteristics of a new process, which are derived from the measured parameters, have to be understood and optimized. In the process characterization and validation phase control limits, critical process parameters and set points have to be determined since these affect process performance and product quality. In the production phase the process has to be tightly controlled at the set points determined earlier. Each of these tasks relies on the precise knowledge of multiple

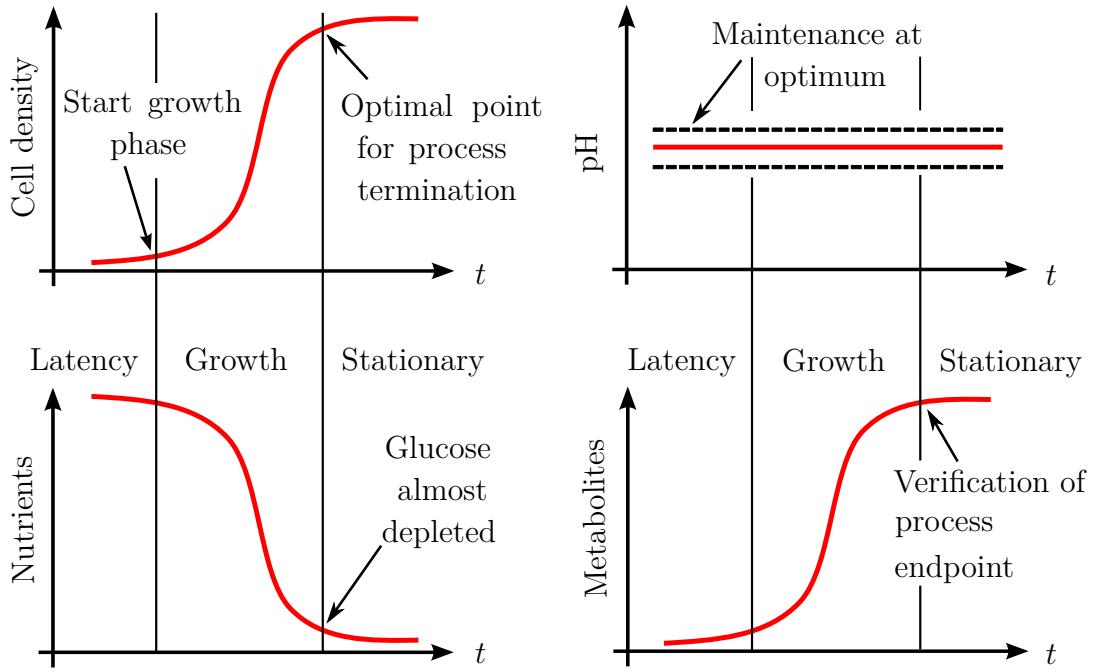

Figure 1.2: Parallel monitoring data of cell density, nutrients, metabolites and pH in a batch process; schematic representation; from the parallel monitoring plenty of process information is gained

parameters.

The high significance of process monitoring and control in biotechnology is reflected in the process analytical technology (PAT) framework, announced by the American Food and Drug Administration (FDA) in 2004. PAT is defined as "a system for designing, analyzing, and controlling manufacturing through timely measurements (i.e., during processing) of critical quality and performance attributes of raw and in-process materials and processes with the goal of ensuring final product quality" [6]. Since its introduction the PAT guidelines have become the standard in biotechnological production, and much work has been done in the field of analytical technologies to meet the requirements of the framework [7]. Sensor systems play a key role in PAT and hence are of high relevance to the biotechnological industry. By implementing the PAT guidelines and increasing the antibody titer in a bioprocess from 0.1 g/l to 1 g/l an average production facility with an annual output of 250 kg of antibodies can save around $300 million per year [8].

Commercial sensors for many parameters in bioprocesses exist, however, they

Figure 1.3: Industrial fermentor with multiple single sensors, © Lambda Instruments [9]; the setup is complicated, requires much space, bears the risk of contamination and increases costs

are typically designed to measure only a single parameter each. The monitoring of multiple parameters therefore requires multiple sensors to be introduced into the bioprocess, leading to a setup as depicted in Fig. 1.3 [9]. Such a setup has considerable drawbacks. Each sensor is provided in its own housing (typically PG 13.5) with a considerable installation space, meaning that the introduction of multiple sensors into a bioreactor can occupy a large portion of the vessel, leaving less space for cultivation. Because of this, for small bioreactors, such as cell culture flasks, sensors in large housings may not be applicable at all. Moreover, the introduction of multiple single sensors complicates the setup, bears the risk of contamination and increases costs. The last aspect is particularly prohibitive for single-use bioreactors, which are increasingly being used and which would profit from cost-effective, single-use sensors [10, 11].

Furthermore, analytes such as glucose, lactate, glutamine and glutamate in bio-

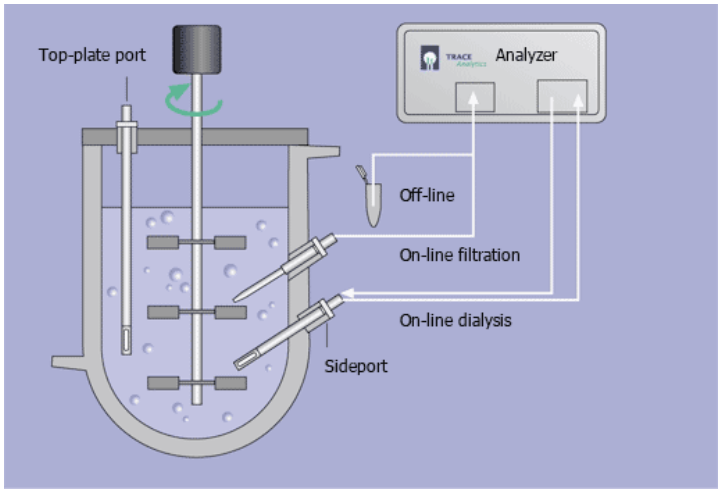

Figure 1.4: Setup for sampling and offline measurement of nutrients and metabolites in bioprocesses, © Trace Analytics GmbH [12]; the setup is complicated and real-time measurements are not possible

processes are mainly measured off-line today using setups as depicted in Fig. 1.4 [12]. This measurement mode involves sample taking through additional ports and fluidic setups and introduces a delay, meaning that no-real time data for these analytes is available. An in-situ sensor for these parameters would simplify the bioreactor setup and provide real-time results. The sensor would, however, also have to meet the requirements of bioprocesses. Among these are high analyte concentrations up to several hundreds of millimoles per liter (mM) and permanent contact with the cell culture medium over days or even weeks. A few in-situ sensors for bioreactors have been reported, however, their measurement range did not exceed 50 mM [13–15].

In this thesis an approach is taken to overcome the drawbacks of the state of the art in bioprocess monitoring by integrating multiple sensors on a single chip. This integration leads to a multi-sensor system for the parallel in-situ monitoring of glucose, lactate, cell density and pH in biotechnological processes. These parameters are chosen because of their high relevance for a broad range of bioprocesses. Glucose is the main nutrient for many cell types. Its control allows keeping cells at the optimal point in their metabolic activity, ensuring high product quality and preventing stuck fermentations [16]. Lactate is one of the key metabolites secreted by mammalian cells and gives information about the health of the cells and their metabolic activity [17]. The cell density is of interest

both in processes where cells are the final product and where metabolites are harvested. Low cell densities reduce the yield of the process, whereas too high densities can lead to metabolic changes affecting the metabolites produced by the cells [3]. Finally, pH is a crucial reactor parameter with significant influence on process performance and product quality [7, 18]. Especially in mammalian cell cultures the pH has to be maintained in tight boundaries to ensure proper cell metabolism and high quality of the metabolic products.

The integration of sensor elements for the four mentioned parameters on a single chip, which for in-situ application in bioreactors is demonstrated for the first time to the author's best knowledge, has some distinct advantages. It miniaturizes the measurement setup, reducing the occupied space and making applications in small bioreactors, such as cell culture flasks, possible. The cost of such a device and the effort of sterilization are considerably lower than with single sensors, qualifying the approach for single-use applications [10,11]. The integrated glucose and lactate sensors allow for in-situ monitoring of these analytes, eliminating the need for sample taking and external measurement equipment.

Thanks to the close proximity of the integrated sensors all parameters are measured virtually at the same spot, and possible concentration differences within the bioreactor, originating from inadequate mixing, become irrelevant. This allows making the signals of the individual sensors more robust and reliable by considering the data of the other sensors. As an example, temperature and pH are two parameters that significantly influence the activity of enzymes and thereby the signal of enzyme sensors. By measuring these parameters in close proximity to the enzyme sensors, the measurement signals can be corrected and more precise data obtained. Furthermore, integrating multiple sensors for the same parameter on one chip provides comparative data and enables detecting drifts and sensor degradation. Finally, the same process parameter can be derived from the data of several sensors, e.g. cell density from a dedicated cell density sensor and glucose and lactate levels [19], to confirm sensor data and observed process behavior.

While multi-sensor platforms have been demonstrated for bioreactors [20–22], sensors for wide concentration ranges of glucose and lactate have not yet been integrated to the author's best knowledge.

The focus of this work will be on the development of enzyme sensors for wide concentration ranges of glucose and lactate. To achieve these ranges diffusion-

limiting membranes will be employed and two membrane materials evaluated. Together with the enzyme sensors an impedance sensor for the determination of cell density and a semiconductor-based pH sensor will be developed. First, the performance of the enzyme sensors and the additional sensor elements will be evaluated individually in calibration measurements and in the monitoring of yeast cultures. Then, the feasibility of sensor integration and parallel application on a single chip will be assessed and applications in yeast cultures demonstrated.

Chapter 2

Theory and Sensor Design

The discussion of the sensor elements in this chapter is based on and extends the author's review on enzyme sensors [23], his publications on glucose sensors with PDMS membranes [16,24], enzyme sensors for the monitoring of biotechnological processes [25] and a multi-sensor system for the monitoring of biotechnological processes [26,27].

2.1 Amperometric Enzyme Sensors

Today, the field of electrochemical biosensors spans a very wide range, including bioreceptors such as nucleic acids, antibodies, aptamers, cells and enzymes [28,29]. In this extensive research field enzyme sensors are among the most popular and most studied devices. This can be explained with the advantages of using enzymes for transduction: they offer high specificity towards their target molecules [30], can remain active for several weeks when kept in an appropriate environment, can be immobilized in various ways and are commercially available for a wide variety of substrates [31,32].

Enzymes are proteins that catalyze a reaction with high specificity for their target molecule [33], making reactions occur faster and with lower activation energy. The catalysis of the chemical reaction takes place at the active site of the enzyme, a three-dimensional structure located at a specific point in the protein structure of the biomolecule. The conformation of the active site is accountable for the high specificity of the enzyme since for most enzymes it exactly matches shape and structure of the substrate molecule. Enzymes can be categorized by

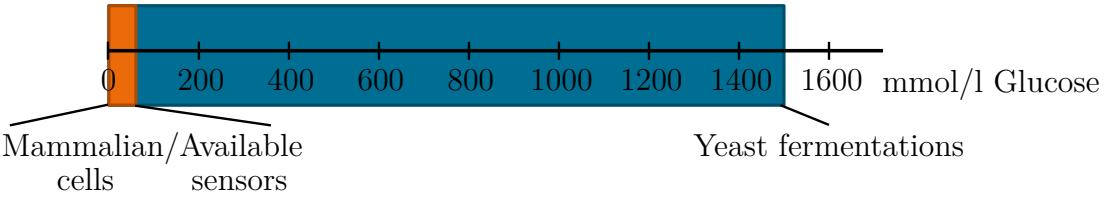

Figure 2.1: Glucose concentrations found in bioprocesses, going from 50 mM in mammalian cultures up to 1500 mM in yeast fermentations [39]; commercially available sensors are limited to the orange range

the chemical reaction they catalyze. The enzymes used in this work belong to the class of oxidoreductases, particularly to the subclass of oxidases, meaning that they catalyze oxidation reactions.

In the context of bioprocess monitoring several key analytes can be measured using enzyme sensors. These include glucose as the main nutrient for a wide variety of cells and lactate as an important metabolite. The precise control of glucose allows increasing antibody yield [34], reducing applied nutrients [35], ensuring reproducible glycosylation [4] and preventing stuck fermentations [36–38] and substrate inhibition, i.e. the Crabtree effect [5]. Similarly, lactate is one of the main metabolites in mammalian cell cultures and gives information about the health of the cells and their metabolic activity [17]. Today, glucose and lactate in bioreactors are typically measured after sampling in external electrochemical analyzers [3]. However, sampling requires additional ports, bears the risk of contamination and delays the measurement results. In contrast to that, continuous in-situ glucose and lactate measurements would provide real-time data and be of great benefit for many applications.

When designing in-situ sensors for glucose and lactate the wide concentration ranges of these analytes in bioprocesses have to be considered. Concentrations go up to around 50 mM for mammalian cell cultures but can reach values up to 1500 mM glucose in alcoholic fermentation [39] or around 1000 mM lactate in the production of biodegradable polymers [40, 41]. The wide range of glucose concentrations found in bioprocesses is depicted in Fig. 2.1. Sensors for such wide concentration ranges have rarely been reported since most of the research in glucose and lactate sensing is directed towards applications in health care, where concentrations stay below 50 mM [42–44]. There are only few reports of sensors for wide concentration ranges [45–47], and demonstrated sensors for

in-situ measurements in bioreactors are limited to concentrations up to 50 mM [13–15]. In this work glucose and lactate sensors for wide concentration ranges for application in bioreactors are developed.

Before dealing with the application of enzymes and diffusion-limiting membranes in biosensing, the mechanism and kinetics of enzymatic reactions will be discussed.

2.1.1 Michaelis-Menten Kinetics

The kinetics of enzymatic reactions can be described by the Michaelis-Menten model. In this model the general form of an enzymatic reaction is written as [33]

$$\mathrm{E} + \mathrm{S} \underset{k_{-1}}{\overset{k_1}{\rightleftharpoons}} \mathrm{ES} \xrightarrow{k_2} \mathrm{E} + \mathrm{P}, \tag{2.1}$$

where E denotes the enzyme, S its substrate, P the product of the enzymatic reaction and k_1, k_{-1} and k_2 are the rate constants for the individual steps of the reaction. The reaction can be described as follows: enzyme E and substrate S bind to form the enzyme-substrate complex ES. The double arrow indicates the fact that this step is potentially reversible, meaning that E and S can separate without a reaction taking place. When the complex ES has formed the enzymatic reaction takes place, leading to the formation of product P and free enzyme E.

The unit of the rate constants is of the form

$$[k] = \left(\frac{\mathrm{l}}{\mathrm{mol}}\right)^{n-1} \cdot \frac{1}{\mathrm{s}}, \tag{2.2}$$

where n is the order of the chemical reaction. The binding of enzyme E and substrate S is a reaction of second order, whereas dissociation of the enzyme-substrate complex ES into educts or products is of first order.

As a measure for the enzyme kinetics the rate at which the product is formed can be derived from the individual reaction rates. A helpful quantity in this regard is the Michaelis constant K_M, which is calculated as the ratio of the reaction rates [33]:

$$K_\mathrm{M} = \frac{k_2 + k_{-1}}{k_1}. \tag{2.3}$$

Under the assumption that the product formation is much faster than dissociation of the enzyme-substrate complex, i.e. $k_2 \ll k_{-1}$, K_M simplifies to

$$K_\mathrm{M} \approx \frac{k_{-1}}{k_1}. \tag{2.4}$$

Since k_1 and k_{-1} denote the binding and dissociation of enzyme and substrate K_M can be seen as a measure for the affinity of the enzyme for its substrate. The lower K_M, the higher the affinity. Considering the facts that k_1 describes a second-order chemical reaction and k_{-1} a first-order reaction, the unit of K_M is

$$[K_\mathrm{M}] = \frac{(\mathrm{l/mol})^{1-1} \cdot 1/\mathrm{s}}{(\mathrm{l/mol})^{2-1} \cdot 1/\mathrm{s}} \tag{2.5}$$

$$= \frac{\mathrm{mol}}{\mathrm{l}}. \tag{2.6}$$

After introducing K_M, the Michaelis-Menten model provides an equation to relate the initial rate of product formation v to the initial substrate concentration s:

$$v = \frac{v_\mathrm{max} s}{K_\mathrm{M} + s}, \tag{2.7}$$

$$\text{with } v_\mathrm{max} = k_2 e_\mathrm{t}, \tag{2.8}$$

where e_t is the enzyme concentration, i.e. the amount of enzyme per volume. When plotting the above relationship a hyperbolic behavior can be identified, as shown in Fig. 2.2. Up to K_M and half of the maximum product formation rate v_max the relationship between v and s can be considered linear [48], and the enzyme kinetics can be described by a first-order equation:

$$v = \frac{k_2 e_\mathrm{t}}{K_\mathrm{M}} s. \tag{2.9}$$

Above K_M the product formation rate asymptotically approaches v_max, meaning that the measurement signal derived from the enzymatic reaction is not a linear measure for the substrate concentration anymore. A convenient quantity that summarizes the rate constants and the Michaelis constant is the enzyme activity. It is defined as the amount of enzyme that converts 1 µmol of substrate in 1 min at 25 °C at the enzyme's optimum pH [33]. The enzyme activity is expressed in units U. The specific enzyme activity states the amount of active enzyme in relation to the total protein mass in a product and is given as units per mg (U/mg). For enzymatic glucose and lactate sensors reported limits of the linear range without diffusion-limiting membranes are typically below 10 mM [42, 43, 49–52].

In this work enzyme sensors for glucose and lactate are developed using the enzymes glucose oxidase (GOx) and lactate oxidase (LOx). The reaction equation for the enzymatic conversion of glucose by glucose oxidase is as follows [29]:

$$\beta\text{-D-glucose} + \mathrm{GOx} + \mathrm{O_2} \rightarrow \delta\text{-D-gluconolactone} + \mathrm{H_2O_2}. \tag{2.10}$$

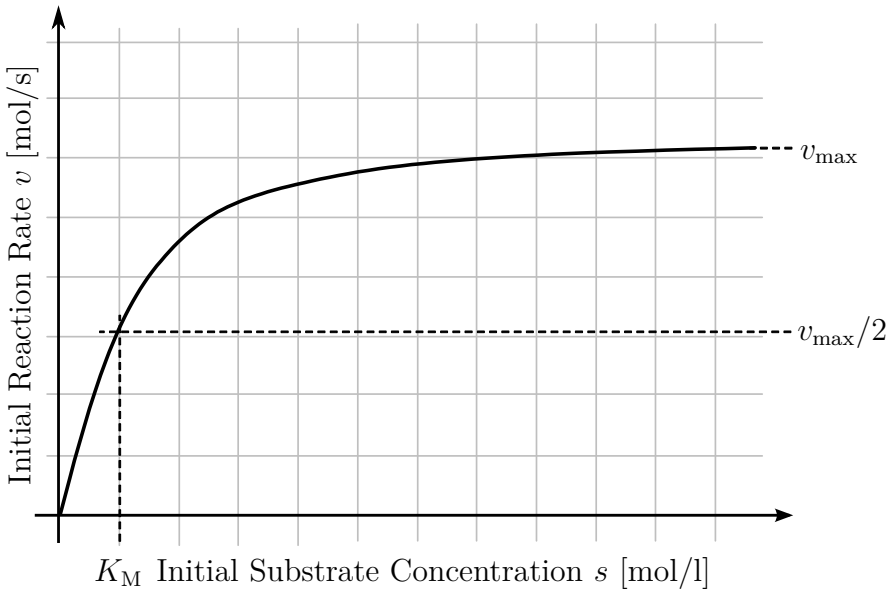

Figure 2.2: Michaelis-Menten kinetics: relationship between substrate concentration s and product formation rate v; up to K_{M} the relationship can be considered linear

Similarly, for lactate oxidase the reaction can be written as [53]

$$\text{L-lactate} + \text{LOx} + \text{O}_2 \rightarrow \text{pyruvate} + \text{H}_2\text{O}_2. \tag{2.11}$$

2.1.2 Influencing Factors

The introduced factors of the enzyme kinetics are influenced by several parameters, such as temperature, pH, immobilization technique and diffusion-limiting membranes [30]. Consequently, they have to be determined for the specific application. Especially temperature and pH are two parameters that either have to be kept constant during the measurement or their influence taken into account for reliable measurements using enzyme sensors. As an example the temperature and pH dependence of the activity of glucose oxidase are depicted in Fig. 2.3, where 100 % is the activity at optimum pH and temperature, respectively [54].

Another important aspect of oxidase enzymes is their dependence on an oxidizing agent or "redox mediator", which accepts electrons from the enzyme molecule after the reaction with its substrate [48]. The redox mediator converts the enzyme back into its native form, making it ready for conversion of the next substrate molecule. Typically, oxygen is used as the redox mediator. If there is a lack of

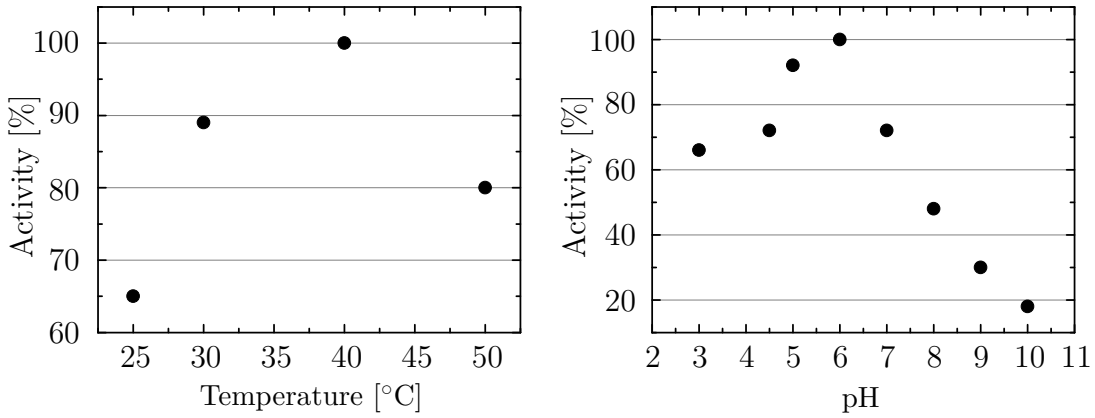

Figure 2.3: Temperature and pH dependence of glucose oxidase [54]

oxygen in the sample solution, the enzyme is not immediately converted back to its initial form and thus is not directly ready for digestion of the next substrate molecule. The reaction rate then becomes limited by the oxygen supply, and the linear range is lower than in solutions saturated with oxygen [42].

Since cell culture media can get depleted of oxygen measures have to be taken to ensure reliable sensor performance in such an environment. One possible solution is the usage of diffusion-limiting membranes with good oxygen permeability. This approach will be discussed in subsection 2.1.4.

2.1.3 Amperometry

In order to translate the enzymatic reaction into an electrical signal a suitable transduction method is required. Here, amperometry is the predominant technique because of its straightforward detection scheme and the widespread availability of dedicated and affordable laboratory instruments [16]. It requires a three-electrode setup in which the working electrode (WE), which is functionalized with an enzyme, is held at a defined potential relative to a reference electrode (RE), which typically is an Ag/AgCl electrode [29]. Stability of the Ag/AgCl electrode can be a critical issue and is subject to ongoing research [55]. The potential is controlled by a potentiostat, a laboratory instrument, resulting in a circuit as shown in Fig. 2.4. The control amplifier of the potentiostat maintains the potential between WE and RE as closely as possible to the desired potential $U_{\mathrm{WE/RE}}$ by providing or draining current through a third counter electrode (CE). The product of the enzymatic reaction (e.g. H_2O_2) is oxidized or reduced at the WE, and

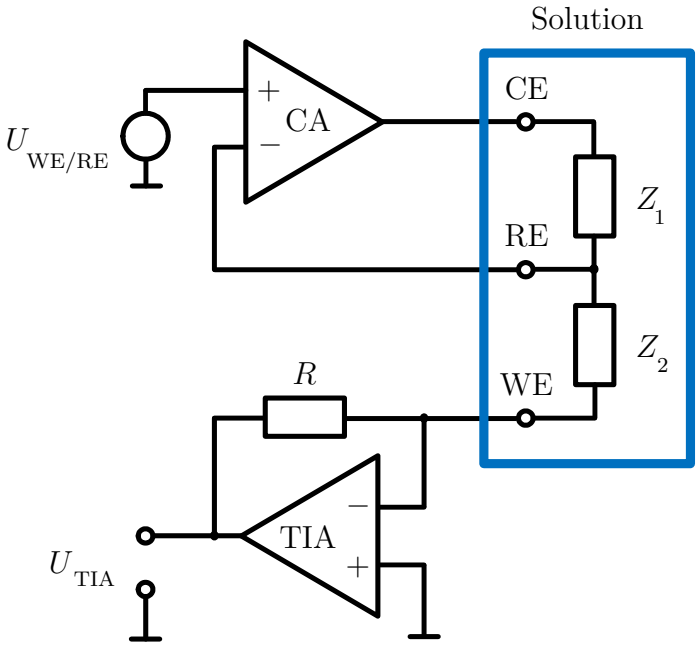

Figure 2.4: Schematic of a potentiostat circuit with control amplifier (CA) and transimpedance amplifier (TIA), working electrode (WE), reference electrode (RE) and counter electrode (CE); Z_1 and Z_2 are solution impedances

the electrons taken from the oxidized molecule or passed to the reduced molecule generate a current through WE. The resulting current I between CE and WE flows through the solution impedances Z_1 and Z_2, representing the solution resistance between the electrodes and the impedances arising from the charge transfer between electrodes and solution. The current is converted by a transimpedance amplifier into a proportional voltage $U_{\mathrm{TIA}} = -R \cdot I$.

WE and CE are typically produced from the highly conductive, inert and biocompatible materials gold or platinum. RE should be positioned in close proximity to WE since the potential drop stemming from the current flowing through the solution resistance between these two electrodes is not compensated by the control amplifier.

Assuming H_2O_2 as the redox species the reaction taking place at the WE can be written as

$$H_2O_2 \rightarrow 2e^- + O_2 + 2H^+. \tag{2.12}$$

The current detected in an amperometric measurement depends both on the rate of the redox reaction at the electrode surface and on the rate of mass transfer of the redox species from the bulk solution to the electrode. If a sufficient potential

is applied between WE and RE, the redox reaction rate reaches a maximum value, and the current is then determined only by mass transfer of the redox species to the electrode. This condition is described by the Cottrell equation [56]:

$$I = nFAc\sqrt{\frac{D}{\pi t}}. \tag{2.13}$$

In Eq. 2.13 n is the number of electrons drained from the oxidized molecule or passed to the reduced molecule, F is the Faraday constant, A is the surface area of the electrode, c and D are the concentration of the redox species and its diffusion coefficient in the solution, and t is time.

The Cottrell equation provides a general description of the current in amperometry, assuming a decreasing flux of redox species to the electrode and a decreasing current over time. This is because a solution volume depleted of redox species spreads around the electrode with time, leading to longer diffusion distances. For the case of an electrode with a membrane on top and a large volume of solution outside the membrane, however, a constant flux to the electrode can be assumed since the depleted layer cannot spread further than the distance to the inner membrane surface, and there is a sufficient amount of redox species outside the membrane. Supposing a membrane with thickness l, a stable concentration c of redox species on the outer side of the membrane and a concentration $c_\mathrm{i} = 0$ on the inner side (i.e. the space between electrode and inner membrane surface is depleted of redox species) the application of Fick's first law of diffusion leads to the following expression for the current I in relation to c [57]:

$$I = nFA\frac{D}{l}c. \tag{2.14}$$

Using this equation the current of a membrane covered electrode can be calculated as a function of the membrane properties D and l, and the area of the electrode.

2.1.4 Diffusion-Limiting Membranes

The Michaelis constants for glucose oxidase and lactate oxidase are around 33 mM and 0.7 mM [58], meaning that a plane enzyme sensor by far does not cover the relevant concentration ranges found in bioprocesses. In fact, the concentration of these substances in bioreactors spans a wide range from a few millimoles per liter to around 1500 mM, e.g. initial nutrient concentrations in ethanol fermentation

using yeast cultures [39] or lactate production with high yield up to 1000 mM for biodegradable polymers [40, 41]. At the same time the response time of the sensor has to fit the characteristics of the monitored bioprocess. Here, the doubling time of the cells in the bioreactor is a useful indicator since it reflects their metabolic activity and thus the speed at which glucose is consumed [3]. Animal cells have a doubling time of 1/day, while bacterial cells, e.g. E. coli, double in 20-30 min [3]. Hence, useful enzyme sensors for biotechnological processes should have a response time below 20 min in order to monitor and control analyte levels fast enough.

Another characteristic of applications in bioreactors is that the sensor is in permanent contact with the culture medium over a period of several days or weeks. A stable signal is necessary over the whole duration of the culture in order to accurately control and adjust the nutrient concentration. Hence, the enzyme layer has to be protected from physical damage and must not be dissolved by the culture medium.

A third aspect associated with electrochemical enzyme sensors is susceptibility of the measurement to interfering substances [44]. Typical ingredients of cell culture media, such as L-cysteine, L-glutathione and ascorbic acid have been shown to interfere with electrochemical glucose measurements, giving too high glucose readings [44, 47]. For applications in bioreactors a sensor must not be affected by such substances in order to provide reliable measurements.

One way to achieve wide linear ranges for enzyme sensors, protect the enzyme against adverse environmental influences and eliminate interfering substances is the application of membranes on top of the enzyme layer [13, 14, 42–44, 59–61]. The extension of the linear measurement range using membranes is based on reducing the flux of analyte molecules to the enzyme, thereby assuring an analyte concentration $c \ll K_{\mathrm{M}}$ at the enzyme layer. The extension of the linear range of a glucose sensor by using a diffusion-limiting membrane is schematically depicted in Fig. 2.5. In the following subsections diffusion processes in membranes will be described from a physical viewpoint. After that, a mathematical description of the transport phenomena in enzyme sensors with diffusion-limiting membranes will be derived.

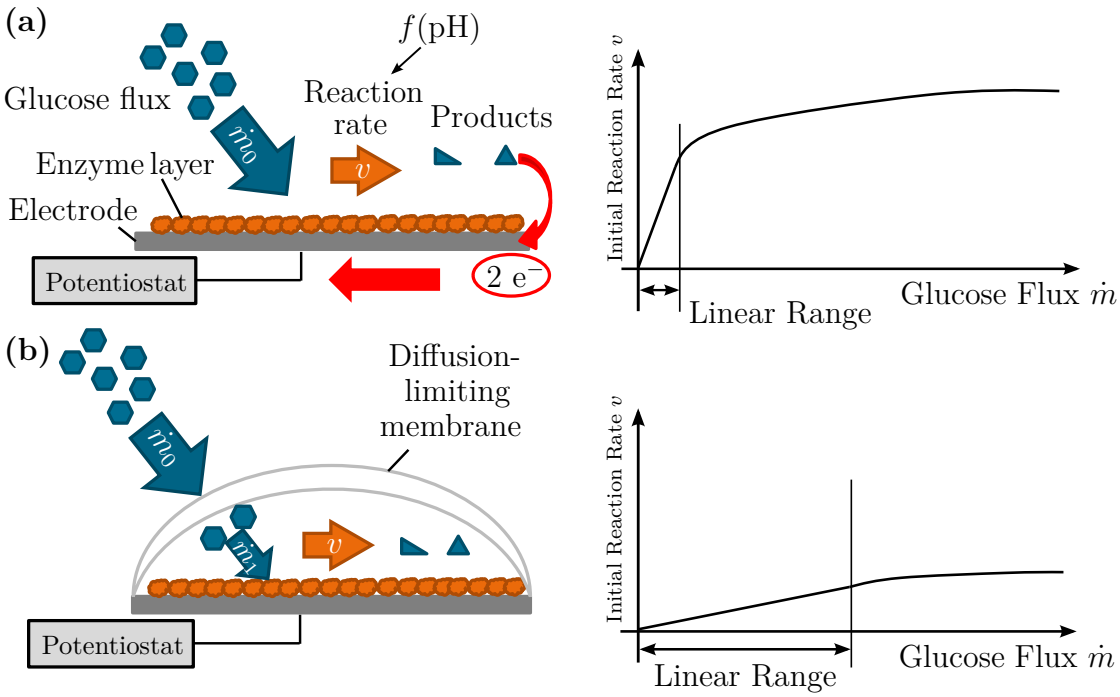

Figure 2.5: Extension of the linear measurement range of a glucose sensor: (a) unhindered flux of glucose molecules to the enzyme layer results in fast saturation of the reaction rate; (b) diffusion-limiting membrane reduces arriving glucose molecules per time and extends linear range

2.1.4.1 Diffusion Processes in Membranes

Membranes are thin material layers that limit or prohibit the transport of mass [62]. Membranes can be divided into two classes: porous and non-porous or dense membranes. In accordance with this classification two general models for mass transport through membranes exist: the pore-flow model and the solution-diffusion model.

Porous membranes contain randomly distributed pores, which can either be interconnected or isolated. The diameter of the pores determines the selectivity of the membrane due to a sieving effect. Molecules with a size greater than the pore diameter are retained, while smaller molecules can pass through. For most membranes pore diameters vary in a certain range and hence an average pore diameter is given. The ratio of the pore volume to the total volume of a membrane is the porosity p [63]. Since pores can be closed at one or both ends an effective porosity p_{eff} is defined that represents the volume fraction of

the membrane through which molecules can effectively cross the membrane. If a material possesses mainly closed pores, it is regarded as a foam rather than a porous membrane. Since pores not necessarily follow a straight path from one side of the membrane to the other the tortuosity factor τ accounts for the route the pores take [64]. The more twisted the pores are, the longer it takes for molecules to pass through the membrane. The tortuosity ranges from $\tau = 1$ for straight pores to $\tau \sim 2.5$ for a membrane with many interconnected, wound pores through which molecules have to find their way. Taking the aforementioned parameters into account an effective diffusion coefficient D_e for a molecule in the membrane can be calculated, which refers to the diffusion coefficient in water D:

$$D_\mathrm{e} = \frac{D p_\mathrm{eff}}{\tau}. \tag{2.15}$$

In non-porous or dense membranes transport of molecules occurs through the membrane material itself. The solution-diffusion model describing the transport assumes that molecules dissolve in the membrane material and permeate from one micro cavity to the next one through temporary, open volume segments in the membrane material [63]. The main parameters characterizing this transport are the sorption coefficient K of the molecule and its diffusion coefficient D in the membrane. The sorption coefficient relates the concentration of a molecule in the membrane to the concentration in the surrounding medium under equilibrium conditions. It is hence an indicator of the solubility of a molecule in the membrane and also accounts for the selectivity of the membrane. The diffusion coefficient describes the mobility of a molecule in the membrane material. It can be derived from the fractional free volume of a polymer, however, these calculations include empirically gained parameters and are specific to certain materials. The two described parameters can be combined into a single parameter, the permeability P [65]:

$$P = KD. \tag{2.16}$$

Mathematically, transport through membranes can be described using one of two general models [62]. One is based on Fick's laws of diffusion and describes the concentration of a substance as a function of place and time. Fick's first law describes the diffusive flux of molecules J as a consequence of a constant concentration difference between to adjacent regions, related by the diffusion

coefficient D. For the one-dimensional case, J is written as

$$J = -D\frac{\partial c}{\partial x}. \tag{2.17}$$

While Fick's first law assumes a constant concentration difference between the two regions and hence a constant flux, the second law describes the case of a changing flux in response to a temporal change in the concentration gradient. Considering the conservation of mass between the regions the infinitesimal concentration difference is

$$\frac{\partial c}{\partial t} = -\frac{\partial J}{\partial x}, \tag{2.18}$$

and combined with Fick's first law:

$$\frac{\partial c}{\partial t} = D\frac{\partial^2 c}{\partial x^2}. \tag{2.19}$$

The other model for membrane transport is based on so-called mass transfer coefficients. In comparison to Fick's laws it is a lumped-parameter model that allows to calculate fluxes across membranes and the resulting concentrations on both sides more easily but does not give information on the time dependence of the transport. For many practical applications, however, equilibrium conditions with steady fluxes can be assumed, which justify the application of membrane transfer coefficients. For a membrane with thickness l, the mass transfer coefficient k for a substance with diffusion coefficient D in the membrane is

$$k = \frac{D}{l}. \tag{2.20}$$

2.1.4.2 Mathematical Description of Enzyme Sensors with Diffusion-Limiting Membranes

A mathematical description of an enzyme sensor with a diffusion-limiting membrane must take into account the transport and reaction processes occurring in the membrane and the enzyme layer. The general structure of the discussed sensor, as adapted from [66] and [67], is shown in Fig. 2.6. The schematic shows the concentration of a substrate, e.g. glucose, in the different layers. For the following discussion the sorption coefficients at all interfaces are assumed as unity, meaning that a constant concentration is maintained at the boundaries between the layers. Also, all fluxes and the enzymatic reaction are assumed to be in steady state. In the solution surrounding the sensor a constant concentration

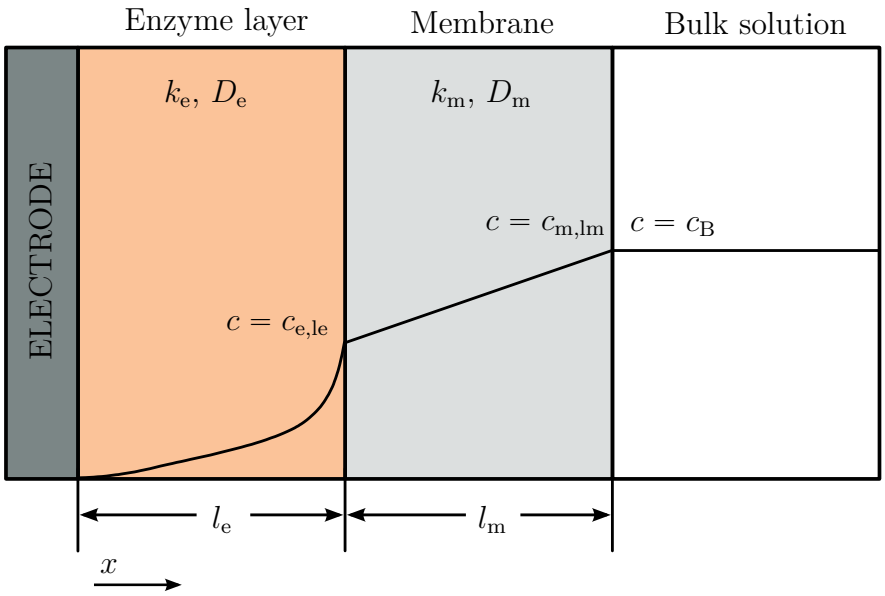

Figure 2.6: Structure of enzyme sensor with diffusion-limiting membrane, with substrate concentration c, mass-transfer coefficients and diffusion coefficients

c_B is assumed, which can be assured by a sufficiently large volume and constant transport of the substrate to the sensor through convection and diffusion. In the membrane with thickness l_m, mass transfer coefficient k_m and diffusion coefficient for the substrate D_m, there is a constant decline of the substrate concentration. The concentration profile $c(x)$ and flux of the substrate J in the membrane can be described by [62, 66]

$$c(x) = c_{e,0} + \frac{c_B - c_{e,le}}{l_m} x \tag{2.21}$$

$$J = \frac{D_m}{l_m}(c_{e,le} - c_B) = k(c_{e,le} - c_B). \tag{2.22}$$

In the enzyme layer the arriving substrate molecules are converted into product molecules by the enzyme. This process starts at the boundary between membrane and enzyme layer, however, not all substrate molecules are directly converted at this point. Instead, substrate molecules that are not converted diffuse further into the enzyme layer where they eventually come into contact with a free enzyme molecule and the enzymatic reaction takes place. Hence, a coupled transport and reaction model has to be derived for this layer. For this, Fick's second law will be applied, augmented by the reaction term derived from the Michaelis-Menten

model, giving [66]:

$$\frac{\partial c}{\partial t} = D_{\mathrm{e}}\frac{\partial^2 c}{\partial x^2} - \frac{v_{\max} c}{K_{\mathrm{M}} + c}. \tag{2.23}$$

Since equilibrium conditions are assumed there is no variation of substrate concentration with time:

$$0 = D_{\mathrm{e}}\frac{\partial^2 c}{\partial x^2} - \frac{v_{\max} c}{K_{\mathrm{M}} + c} \tag{2.24}$$

$$\Leftrightarrow D_{\mathrm{e}}\frac{\partial^2 c}{\partial x^2} = \frac{v_{\max} c}{K_{\mathrm{M}} + c}. \tag{2.25}$$

Equation 2.25 cannot be solved analytically since it is a non-linear differential equation of second order. In order to derive an analytical solution a substrate concentration in the sensor $c \ll K_{\mathrm{M}}$ will be assumed, which is feasible since the sensor is meant to be operated in the concentration range with linear enzyme kinetics. Under this assumption Eq. 2.25 reduces to [66]

$$D_{\mathrm{e}}\frac{\partial^2 c}{\partial x^2} = \frac{k_2 e_{\mathrm{t}}}{K_{\mathrm{M}}} c. \tag{2.26}$$

The solution for this linear second-order differential equation is of the general form [66]

$$c = A_2 \sinh(\frac{x}{X_{\mathrm{k}}}) + B_2 \cosh(\frac{x}{X_{\mathrm{k}}}). \tag{2.27}$$

In this equation A_2 and B_2 are integration constants, and X_{k} is defined as

$$X_{\mathrm{k}} = \sqrt{\frac{K_{\mathrm{M}} D}{v_{\max}}}. \tag{2.28}$$

In order to apply the general solution two boundary conditions are assumed: (1) at the electrode surface there is no change of substrate concentration, hence at $x = 0$, $ds/dx = 0$; (2) at the boundary of enzyme layer and membrane the concentrations are equal, i.e. $c_{\mathrm{m,le}} = c_{\mathrm{e,le}}$. Under these assumptions the following equation for the substrate concentration profile in the enzyme layer can be derived [66]:

$$c(x) = c_{\mathrm{B}} \frac{\cosh(x/X_{\mathrm{k}})}{\cosh(l_{\mathrm{e}}/X_{\mathrm{k}})}. \tag{2.29}$$

The term $l_{\mathrm{e}}/X_{\mathrm{k}}$ is the Thiele modulus [48] and relates the parameters describing transport through the enzyme layer to the parameters characterizing the enzymatic reaction. A large Thiele modulus indicates a slow mass transfer in relation to a fast enzymatic reaction, meaning that substrate transport limits the reaction

rate. In contrast, a small Thiele modulus points to a slow reaction in comparison to fast mass transfer, hence the enzymatic reaction with its velocity v is the rate determining step.

The reaction and transport processes in the enzyme layer can be linked to the transport process in the membrane by means of the Biot number β, relating the mass transfer coefficients of membrane and enzyme layer [48]:

$$\beta = \frac{k_\mathrm{m}}{k_\mathrm{e}}. \tag{2.30}$$

The Biot number allows to estimate which transport process is the slower one, and therefore determines the overall transport rate of the sensor. For small Biot numbers diffusion through the membrane is determining, while for large Biot numbers the diffusion in the enzyme layer dominates. In order to obtain an enzyme sensor for bulk substrate concentrations $c_\mathrm{B} \gg K_\mathrm{M}$ a small Biot number $\beta \ll 1$ and a large Thiele modulus $l_\mathrm{e}/X_\mathrm{k} \gg 1$ have to be achieved so that the substrate concentration reaching the enzyme layer is maintained in the linear regime of the enzymatic reaction. In this case the upper limit Λ of the linear range can be estimated as [48]

$$\Lambda = \frac{K_\mathrm{M} k_2 e_\mathrm{t} l_\mathrm{e} l_\mathrm{m}}{2 D_\mathrm{m}} + 1. \tag{2.31}$$

Hence, there are different ways to adjust the linear range of the enzyme sensor. The thickness l_m of the membrane can be altered, changing the path length the glucose molecules have to diffuse before reaching the enzyme layer. The diffusion coefficient of the substrate in the membrane D_m can be modified, leading to different "resistances" the glucose molecules encounter when passing the membrane. Finally, the properties of the enzyme layer can be varied. However, in this thesis the focus will be on membrane development, i.e. the tuning of D_m and l_m.

2.1.4.3 Materials for Diffusion-Limiting Membranes

Materials for diffusion-limiting membranes in biosensor applications must fulfill a number of requirements. Besides being biocompatible they have to be permeable to the desired analyte molecule and insoluble in the solution in which the sensor is meant to be operated, typically aqueous fluids. Another important feature for enzyme sensors using oxidases is good oxygen permeability if oxygen is used as the redox mediator. The membrane should in fact be more permeable to oxygen

than to the analyte molecule in order to avoid shortage of the redox mediator and a decreased linear measurement range.

A variety of materials has been used for diffusion-limiting membranes, among them cellulose acetate [44], polyurethane [43, 68, 69], polycarbonate [45] and Nafion® [42,70]. While all of these materials have been shown to fulfill the requirements mentioned above, wide linear measurement ranges beyond 50 mM for the important analytes glucose and lactate have rarely been reported. In this work two materials were assessed for their suitability for wide range measurements of glucose and lactate concentrations in biotechnological processes.

Out of the common materials polyurethane was used. Due to its biocompatibility and permeability for oxygen, glucose and lactate, it is well suited for enzyme sensors and has widely been employed for diffusion-limiting membranes [43, 68, 71, 72]. The material consists of polyol and isocyanate components linked together by the characteristic urethane group -NH-CO-O- [73]. A wide range of polyurethanes exists for various applications, such as foam and fibrous materials, coatings and adhesives [72]. In this work Selectophore® polyurethane from Sigma Aldrich, USA, was used, which is a medical-grade aliphatic poly(ether-urethane) [74].

In order to apply the PU on the enzyme layer the material had to be in the form of a solution. PU is easily dissolved in mixtures of the solvents tetrahydrofuran (THF) and dimethylformamide (DMF) [43, 68]. Using a mixture of THF and DMF in varying ratios introduces the possibility to tune the properties of the PU membrane. This can be attributed to the different vapor pressures of the solvents and the time required for their evaporation. The vapor pressures of THF and DMF at 20 °C are 173 hPa and 3.77 hPa [75], respectively, meaning that THF evaporates faster than DMF. By varying the amount of the solvents in the mixture PU solutions with different evaporation rates could be obtained and the influence of this parameter on the morphology and permeability of the membranes studied. As a second parameter the concentration of the PU in the solution was varied since this is one of the key parameters in membrane fabrication [63].

As a second and less characterized material for diffusion-limiting membranes in the context of enzyme sensors poly(dimethylsiloxane) (PDMS) was employed. PDMS belongs to the class of siloxanes and is a polymer built from multiple monomer units with the formula $SiO(CH_3)_2$ [76]. Owing to its biocompatible

and non-toxic nature and its good oxygen permeability it has found applications in many different fields and is used as a material for contact lenses, ingredient in shampoos and other cosmetic products, anti-foaming agent for food and as a lubricant. In this work Sylgard 184 from Dow Corning, USA, was used. Sylgard 184 is a two-part silicone elastomer consisting of a highly viscous base part and a curing agent. The two parts can be mixed in various relations to obtain different grades of crosslinking. The crosslinking occurs over 24 h at room temperature. When applied by spin-coating the membrane thickness can be adjusted by varying the spin speed [77, 78]. This opens up the possibility to produce sensors with different membrane thicknesses and evaluate the influence of the thickness on linear range and response time.

In its natural and fully cross-linked state PDMS is hydrophobic [79] and assumed to be nearly impermeable to glucose and lactate. Because of that the PDMS was chemically modified by bringing it into contact with water during a part of the curing process. Two principles were supposed to change the properties of the material during the partial curing in an aqueous environment. One is the incorporation of water into the membrane. It has been shown that the glucose permeability of a membrane can be adjusted by incorporating different amounts of water into it [80]. For PDMS to the author's best knowledge the diffusion coefficient for glucose has not been adjusted by the addition of water so far. Instead, other hydrophilic compounds have been used. Lin et al. prepared a hydrogel from a PDMS formulation and poly(ethylene glycol) methacrylate (PEGMA) and demonstrated increasing glucose permeability with increasing PEGMA content [81]. However, during fabrication, organic solvents were used, which are known to damage and denature enzymes [82]. In order to preserve the catalytic activity of the enzyme layer water was chosen as the modifying compound in this thesis.

As a second effect the hydrolysis of chemical bonds in the PDMS during the curing in water was assumed, leading to partial chain scission and degradation of the material. These processes have been reported for polymeric sealants in general [83] and partially cured poly(dimethylsiloxane) in contact with water in particular [84] and were assumed here to increase the permeability of the PDMS for glucose and lactate.

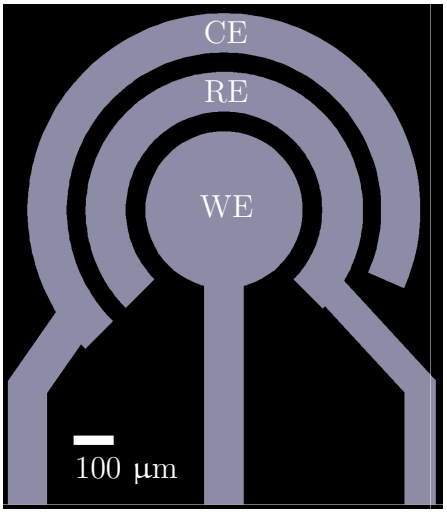

Figure 2.7: Design of three-electrode setup for amperometry; design choices: (1) concentric electrodes ensure even distribution of the electric field lines and independence of the direction of flow; (2) circular shape is similar to shape of fluid drops on surface; (3) minimum diameter for functionalization by hand chosen as 1 mm due to positioning inaccuracy and minimum diameter of droplets on gold surface

2.1.5 Sensor Design

For the design of the amperometric electrodes the three-electrode configuration with working, counter and reference electrode was chosen. The three-electrodes were arranged as concentric circles, which ensured an even distribution of the electric field lines between the electrodes and made the arrangement independent of the direction of flow in stirred solutions in comparison to finger shaped electrodes. The circular shape was also well suited for functionalization by dispensing an enzyme solution by hand since fluids form circular droplets on surfaces.

The working electrode was placed in the middle, surrounded by the reference and counter electrode as depicted in Fig. 2.7. Thus, the reference electrode was in close proximity to the working electrode, while the counter electrode had the biggest area, thereby ensuring the least possible potential drop when providing or draining current.

The size of the electrodes was chosen considering the functionalization procedure. The smallest amount of enzyme solution that could be dispensed using common microliter pipettes was 0.1 µL. This volume was found to form a droplet

with a diameter of approximately 500 µm on a gold film. Since the enzyme solution had to be dispensed by hand during the experimental phase a positioning inaccuracy of 500 µm was assumed. These considerations led to a minimum diameter of 1 mm for the electrode setup. Accordingly, the WE was designed to have a diameter of 400 µm, while CE and RE had a width of 100 µm. The spacing between the electrodes was chosen as 50 µm. To investigate the influence of the electrode area on the sensor signal a second variant with twice the area was designed, having a WE diameter of 566 µm, a RE/CE diameter of 141 µm and a spacing of 71 µm.

While higher electrode areas were expected to give higher currents and thus a higher sensitivity, two circular electrodes with diameters above 1.5 mm could not be placed on the available chip sensor area of 3.3 mm × 3.3 mm. This area was chosen considering the design criteria established in section 2.4. Thus, such variants were not considered in the design phase.

Platinum was chosen as the electrode material since it is inert, conductive and biocompatible. The RE was planned to be galvanically silver-plated and chlorided before experiments were performed. However, due to concerns about the stability of plated silver electrodes, an external Ag/AgCl reference electrode was used in the experiments instead. Nevertheless, the on-chip silver-plated RE is an option for further integration of the sensor chip. As an alternative to silver-plating the electrode could also be produced by evaporation of silver, a method suitable for mass fabrication.

For the evaluation of sensors with PDMS membranes separate three-electrode configurations on ceramics were used (BST GmbH, Germany). These consisted of a gold WE, a Ag/AgCl RE and a platinum CE, all produced by screen printing. The electrode setup and its dimensions are depicted in Fig. 2.8. The WE area of the electrodes on ceramics was 1.02 mm^2.

2.1.6 Sensor Functionalization

For functionalization of the electrodes a protocol based on enzyme crosslinking with bovine serum albumin (BSA), a protein obtained from bovine plasma, was used. In comparison to more complex protocols, such as covalent or bioaffinity bonding, this immobilization method is more straightforward and provides a comparable long-term stability up to 10 weeks [52]. Crosslinking is understood here

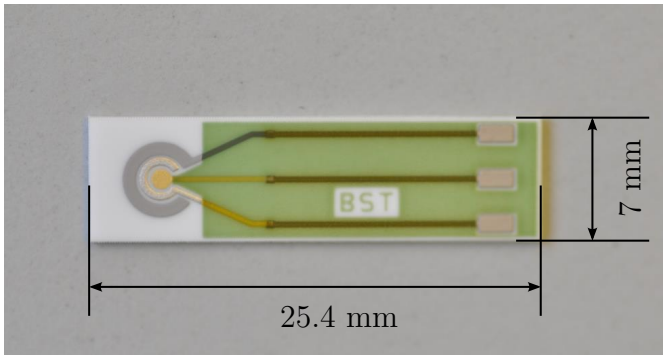

Figure 2.8: Three-electrode setup on ceramics with screen-printed electrodes (WE: gold, CE: platinum, RE:Ag/AgCl) for evaluation of sensors with PDMS membranes

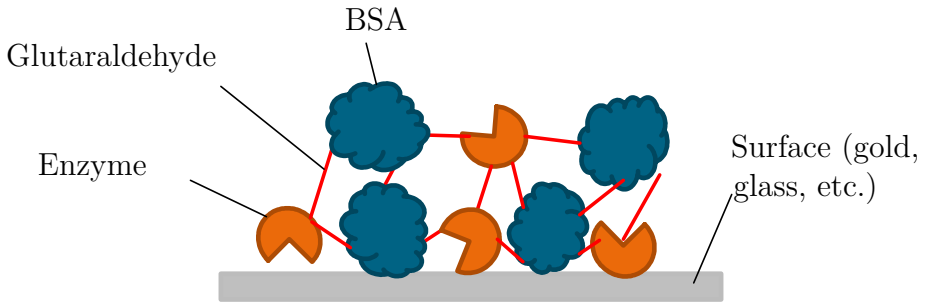

Figure 2.9: Crosslinked film of enzyme, bovine serum albumin (BSA) and glutaraldehyde on a surface; crosslinking is more straightforward than covalent or bioaffinity bonding and provides a similar long-term stability up to 10 weeks [52]

as the process of linking together two biomolecules by means of an intermediate molecule, in this case glutaraldehyde. Glutaraldehyde is a homobifunctional crosslinker, possessing an aldehyde group at both ends, which is able to covalently bind to amino groups present at the surface of biomolecules [31]. By crosslinking the enzyme with BSA a matrix is formed in which the natural conformation of the enzyme is preserved. The crosslinked matrix is schematically depicted in Fig. 2.9.

The enzyme solution was prepared by dissolving 10 mg glucose oxidase (activity 100 - 250 U/mg) or 10 mg lactate oxidase (activity 30 U/mg) and 20 mg bovine serum albumin in 500 µL of 10 mM phosphate buffered saline (all chemicals obtained from Sigma Aldrich, USA). After thorough mixing 25 µL of 8 % glutaraldehyde (v/v) (Polysciences, USA) were added and the solution mixed

again. These quantities had been determined to give the highest sensor signal per applied mass of enzymes and showed reliable sensor behavior when used with diffusion-limiting membranes. Other compositions proved to give a low number of functioning sensors per fabricated batch or had a very limited linear range. An amount of 0.1 µL was then dispensed on the three-electrode setup using a microliter pipette and left to dry in air.

The diffusion-limiting membrane was prepared from either poly(dimethylsiloxane) (PDMS) or polyurethane (PU). PDMS membranes were fabricated by first mixing the base polymer with the curing agent in a ratio of 20:1 (w/w) and degassing the mixture. This ratio had been found to produce permeable membranes when partially cured in water. Lower base ratios gave non-permeable membranes, whereas higher ratios turned out to be too viscous to be reliably processed. The PDMS was then spin-coated onto the enzyme electrodes at spin speeds of 3000 rpm or 6000 rpm for 30 s with an acceleration of 500 rpm/s^2 using a spin-coater (WS650MZ, Laurell, USA). Spin speeds lower than 3000 rpm lead to bad reproducibility of the membrane thickness, whereas speeds higher than 6000 rpm lowered the membrane thickness only slightly further. Higher spin speeds gave thinner membranes.

Two curing schemes were employed in the fabrication. The first one, for simplicity called scheme 1 in the following, included 12 h curing in air followed by 12 h curing in buffer solution. The second scheme, called scheme 2 in the following, involved a longer curing period in air of 16 h followed by 8 h curing in buffer solution.

To measure the thickness and water content of the membranes PDMS was spin-coated onto glass slides and cured with the parameters mentioned above. The thickness of the thick membranes was measured using an optical microscope with a scale and determined to be 35 µm. Thin membranes were measured using an atomic force microscope and determined to have a thickness of 4.5 µm. Water content of the membranes was determined by weighing samples in surface-dried wet state and after dehydration in an oven at 150 °C for 120 min. Water content ranged from 0.2 % to 1.4 %.

Polyurethane membranes were prepared by dissolving PU pellets in a mixture of the solvents tetrahydrofuran (THF) and dimethylformamide (DMF). In order to evaluate the influence of different fabrication parameters on the linear range a

series of membranes was produced. PU solutions in concentrations of 4 %, 6 %, 8 % and 10 % (w/w) were prepared with a mixture of THF and DMF. Higher polymer concentrations were found to be indissoluble in the used solvents. The THF-DMF ratio was adjusted to 9:1, 7:3, 5:5, 3:7 and 1:9, respectively, giving five series of solutions with four concentrations each. PU was found to be indissoluble in the mixture with ratio THF:DMF 1:9 even after several days so this series was not employed in the further experiments. 0.15 µL of the PU solution were applied on the enzyme layer and dried in air.

Surface morphology and thickness of the fabricated membranes were examined using a scanning electron microscope (S-4700, Hitachi, Japan) and an atomic force microscope (MFP-3D, Asylum Research, USA).

The diffusion coefficient for glucose in the membranes was determined using a custom-made diffusion cell. To this end, PU solutions were inserted into silicone tubing to form a plug of defined thickness. The tubing was connected to a stirred reservoir containing a 2.5 M glucose solution and to a second stirred reservoir containing deionized water. Samples were drawn regularly from the reservoirs, the glucose concentrations measured and the diffusion coefficient D determined according to the formula [62]

$$D = \frac{1}{\beta t} \ln \left(\frac{c_{\mathrm{I}}^0 - c_{\mathrm{II}}^0}{c_{\mathrm{I}} - c_{\mathrm{II}}} \right), \tag{2.32}$$

$$\text{with } \beta = \frac{A}{l} \left(\frac{1}{V_{\mathrm{I}}} + \frac{1}{V_{\mathrm{II}}} \right). \tag{2.33}$$

In these formulas c_{I} and c_{II} are the glucose concentrations in the first and second reservoir at time t, c_{I}^0 and c_{II}^0 are the respective glucose concentrations at time $t = 0$, A and l are the total area and thickness of the membrane and V_{I} and V_{II} are the volumes of the two reservoirs.

The thickness of the PU membranes was determined for a THF-DMF ratio of 5:5 by dispensing PU solutions of different concentrations onto an oxidized silicon substrate, breaking the substrate through the middle of the polymer droplet and examining the cross section using an scanning electron microscope. The thickness ranged from 1.5 µm for membranes with 4 % PU to 2.5 µm for membranes with 10 % PU.

Before amperometric measurements electrodes were conditioned in phosphate buffered saline (PBS) for 12 h. Glucose solutions were prepared in PBS. Measure-

ments were performed at room temperature using an Autolab µAUTIII (Metrohm Autolab, The Netherlands) or a MultiEmStat3 potentiostat (PalmSens, The Netherlands). The potential between the working and reference electrode was set to 700 mV, ensuring oxidation of the H_2O_2 generated in the enzymatic reactions.

2.2 Cell Density Sensor

Cell density is one of the key parameters in biotechnological processes. This is both true for processes where the cells are the final product as well as those where metabolites are harvested and the cell mass has to be maintained at an optimum level. A range of methods exist for measuring cell density, among these weighing of dried cells, manual or automated cell counting and several optical techniques, such as turbidity and fluorescence measurements [85, 86]. Besides these direct measurement approaches indirect techniques exist, which correlate parameters such as the oxygen consumption rate or the carbon dioxide production rate to the cell density.

Two important distinctions have to be made between these techniques. One is whether the total number of cells or the number of viable cells is measured, the other if the measurement can be integrated into the process to operate continuously or has to be conducted externally and discontinuously. The number of viable cells is mainly determined by counting cells either manually under a microscope using a hemocytometer or by the help of an automated cell counter. This method allows to distinguish between live and dead cells but is limited to off-line usage. Optical methods on the other hand can be employed for continuous on-line measurements but typically cannot distinguish between live and dead cells because both absorb light. An optimum measurement technique should be able to measure the viable cell density continuously and integrated into the biotechnological process.

A method that fulfills the mentioned requirements is impedance spectroscopy. It is based on the phenomenon that live cells get polarized in an electrical field, whereas dead cells do not respond to the electrical field because they lack an intact cell membrane [87,88]. The polarization occurs up to a certain frequency, which is characteristic for the cell type. When the characteristic frequency f_{char} is exceeded

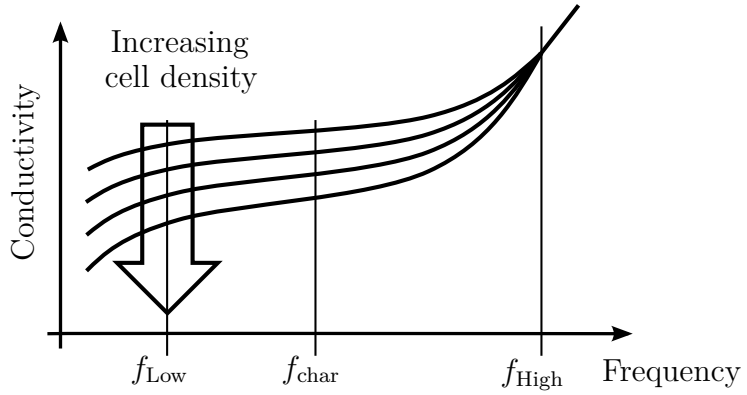

Figure 2.10: Measurement principle of cell density sensor: conductivity at lower measurement frequency f_{Low} is related to conductivity at higher measurement frequency f_{High} and the cell density is derived from this relation; f_{char} is the characteristic frequency of the cells

the charges at the cell membrane cannot follow the electric field, and the cells then do not contribute to the measured impedance anymore. Since the conductivity of the cell suspension below f_{char} is related to the cell density [89] the cell density can be derived from the measured impedance spectrum by calculating the ratio of the conductivity well below and above f_{char}. The measurement principle is schematically shown in Fig. 2.10. In [89] the relationship between the conductivity change $\Delta\sigma$ and the viable cell density N_{c} for spherical cells has been derived as

$$\Delta\sigma \approx 6\pi r^3 N_{\mathrm{c}} \sigma_{\mathrm{a}} \left(\frac{\sigma_{\mathrm{i}}/\sigma_{\mathrm{a}}}{2 + \sigma_{\mathrm{i}}/\sigma_{\mathrm{a}}} \right), \tag{2.34}$$

with r being the cell radius and σ_{i} and σ_{a} the conductivity of the cell cytoplasm and background conductivity of the cell culture medium, respectively. For yeast cells f_{char} is around 5 MHz, for E. coli cells around 14 MHz [90].

2.2.1 Impedance Spectra in Aqueous Solutions

The measurement of impedance spectra in aqueous solutions requires careful electrode design since several factors influence the frequency response, the five main factors being

- the capacitance of the electrical double layer on the electrodes C_{DL}
- the capacitance between the electrodes C_{Elec}
- the solution resistance R_{Sol}

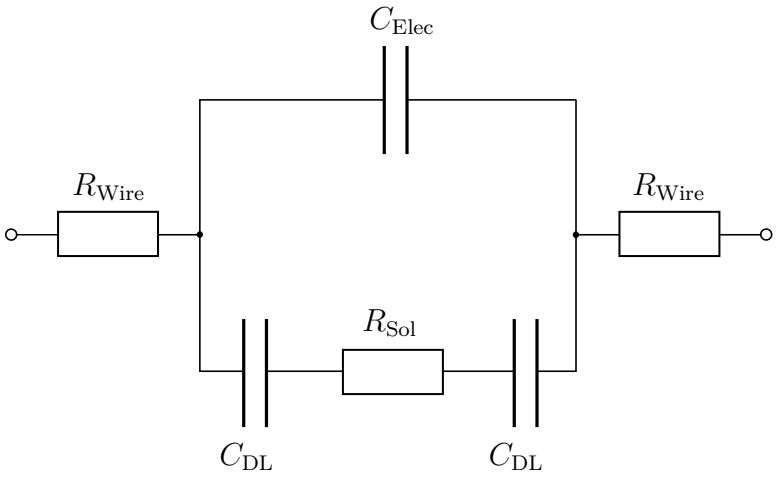

Figure 2.11: Equivalent circuit diagram of electrodes in an aqueous solution; C_{DL}: capacitance of electrical double layer, C_{Elec}: capacitance between electrodes, R_{Sol}: solution resistance, R_{Wire}: wiring resistance

- the wiring resistance R_{Wire}
- the wiring capacitance C_{Wire}.

Considering these five factors an equivalent circuit diagram can be derived with an impedance spectrum exhibiting two cutoff frequencies, as depicted in Fig. 2.11 and Fig. 2.12 [91].

The impedance of the equivalent circuit $\underline{Z}$ can be calculated as

$$\underline{Z} = 2R_{\mathrm{Wire}} + (\underline{Z}_{\mathrm{Elec}} || (\underline{Z}_{\mathrm{DL}} + R_{\mathrm{Sol}})) \tag{2.35}$$

$$= 2R_{\mathrm{Wire}} + \left(\frac{1}{j\omega C_{\mathrm{Elec}}} \parallel \left(\frac{2}{j\omega C_{\mathrm{DL}}} + R_{\mathrm{Sol}} \right) \right) \tag{2.36}$$

$$= 2R_{\mathrm{Wire}} + \frac{(R_{\mathrm{Sol}} + 2/(j\omega C_{\mathrm{DL}})) \cdot 1/(j\omega C_{\mathrm{Elec}})}{R_{\mathrm{Sol}} + 2/(j\omega C_{\mathrm{DL}}) + 1/(j\omega C_{\mathrm{Elec}})} \tag{2.37}$$

$$= 2R_{\mathrm{Wire}} + \frac{R_{\mathrm{Sol}} + 2/(j\omega C_{\mathrm{DL}})}{j\omega C_{\mathrm{Elec}} \cdot (R_{\mathrm{Sol}} + 2/(j\omega C_{\mathrm{DL}})) + 1}. \tag{2.38}$$

The lower frequency part of the spectrum up to the first cutoff frequency f_{Low} is dominated by the capacitance of the electrical double layer C_{DL} formed on each electrode. This layer develops as a reaction to the potential applied between the two electrodes, leading to a potential difference between each electrode and the surrounding solution [56]. This difference attracts ions in the solution that build up a charged layer at the electrode surface. Together with the opposite charges

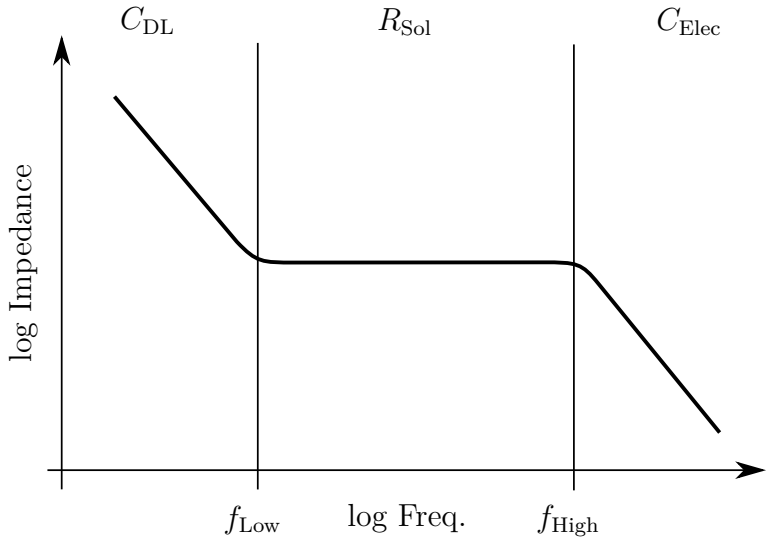

Figure 2.12: Schematic impedance spectrum of electrodes in an aqueous solution with two cutoff frequencies f_{Low} and f_{High} and ohmic plateau in between; spectrum of cell density sensor had to include characteristic frequency of desired cells in ohmic plateau

in the electrode material this setup is called the electrical double layer and can be regarded as the two plates of a capacitor. One plate is formed by the electrode surface, the other one by the plane through the ion layer at the electrode, which is referred to as the outer Helmholtz plane. The distance between the two plates is half the radius of the solvated ions. It depends on the ion sort and the ion concentration. Adjacent to the outer Helmholtz plane a diffuse layer of ions forms that are electrically attracted to the electrode surface while at the same time being drawn away by thermal movement. The two ionic layers are described by the Gouy-Chapman-Stern model. For ionic concentrations above 0.1 mM the diffuse layer can be disregarded and the solution part of the double layer assumed to consist only of the outer Helmholtz plane [56]. In this case the capacitance of the electrical double layer can be estimated as $C_{\mathrm{DL}} \approx C_{\mathrm{o.H.}} \approx 0.2\,\mu\mathrm{F/cm^2}$ [92].

Since each electrode bears a double layer the element C_{DL} is added twice to the equivalent circuit diagram. Furthermore, the solution resistance R_{Sol} is added in series to the capacitances because of the charging current of the double layers flowing through the solution surrounding the electrodes. Under the assumption that the impedance of C_{Elec} can be disregarded in this frequency range the lower

cutoff frequency can be estimated as

$$f_{\mathrm{Low}} \approx \frac{1}{\pi R_{\mathrm{Sol}} C_{\mathrm{DL}}}. \tag{2.39}$$

The middle part of the impedance spectrum is determined by the solution resistance R_{Sol} alone. Here, the impedance of the electrical double layer becomes insignificant, whereas the branch with the capacitance between the electrodes C_{Elec} poses a too big impedance yet and is therefore omitted by the flowing current. An ohmic plateau forms, providing a favorable frequency range for cell density measurements, where capacitive influences are avoided and changes in conductivity can be detected without distortions.

When the measurement frequency exceeds the second cutoff frequency f_{High} the impedance of C_{Elec} falls below the solution resistance R_{Sol}. Current then increasingly flows through the branch with C_{Elec}, which has to be regarded as a capacitor with the solution as its electrolyte. In this region the parasitic wiring capacitance C_{Wire}, stemming from instrument cables and leads on printed circuit boards, has to be considered in parallel to the capacitance between the electrodes. This capacitance is estimated as $C_{\mathrm{Wire}} \approx 100\,\mathrm{pF/m}$ [93]. Disregarding the impedance of C_{DL} the upper cutoff frequency can be estimated as

$$f_{\mathrm{High}} \approx \frac{1}{2\pi R_{\mathrm{Sol}}(C_{\mathrm{Elec}} + C_{\mathrm{Wire}})}. \tag{2.40}$$

2.2.2 Design of Interdigitated Electrodes

In order to determine the cell density by measuring conductivity values below and above the characteristic frequency f_{char} electrodes with an appropriate impedance spectrum had to be designed. The main requirement for the impedance spectrum was that the ohmic plateau included f_{char} and extended several megahertz below and above. This was important because due to variations in cell attributes such as size and shape the characteristic frequency is not limited to a single value but rather extends over a frequency range. Hence, to ensure that at the lower measurement frequency all cells contribute to the conductivity while at the upper frequency there is no cellular influence on the conductivity anymore, the measurement frequencies should be chosen a few megahertz away from f_{char}.

In order to design the electrodes the design parameters had to be related to the factors and cutoff frequencies introduced in section 2.2.1. In this work interdigitated electrodes (IDE) were used, which allow to derive these relationships

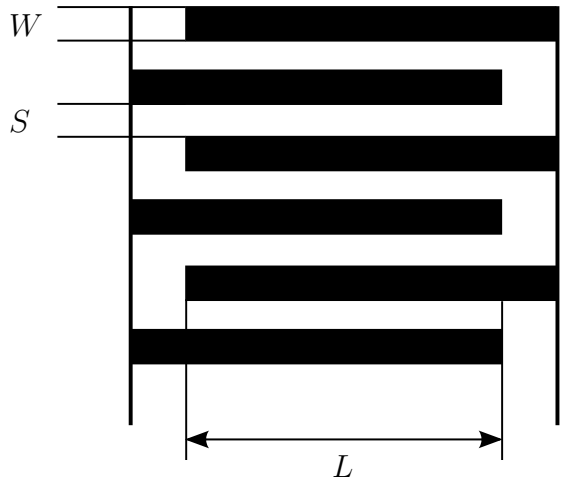

Figure 2.13: Interdigitated electrodes with design parameters finger length L, width W and spacing S; number of fingers N is 6 in this case

using the so-called cell constant K_{Cell} [94]. The cell constant takes into account the number of fingers N, the finger length L, width W and spacing S as depicted in Fig. 2.13. It is calculated using the complete elliptic integral of the first kind $K(k)$:

$$K_{\mathrm{Cell}} = \frac{2}{(N-1)L} \cdot \frac{K(k)}{K(\sqrt{1-k^2})}, \tag{2.41}$$

$$\text{with } K(k) = \int_0^1 \frac{1}{\sqrt{(1-t^2)(1-k^2t^2)}} \mathrm{d}t \tag{2.42}$$

$$\text{and } k = \cos\left(\frac{\pi}{2} \cdot \frac{W}{S+W}\right). \tag{2.43}$$

With K_{Cell} known the resistance R_{Sol} measured with the IDE and the capacitance C_{Elec} could be expressed as [94]

$$R_{\mathrm{Sol}} = \frac{K_{\mathrm{Cell}}}{\sigma_{\mathrm{Sol}}} \tag{2.44}$$

$$C_{\mathrm{Elec}} = \frac{\epsilon_0 \epsilon_{\mathrm{r,Sol}}}{K_{\mathrm{Cell}}}, \tag{2.45}$$

with σ_{Sol} and $\epsilon_{\mathrm{r,Sol}}$ being the solution conductivity and permittivity. Furthermore, the double layer capacitance C_{DL} could be calculated as [91]

$$C_{\mathrm{DL}} = WLNC_{\mathrm{o.H.}}. \tag{2.46}$$

Using these relationships the estimations of the cutoff frequencies given in the last subsection were rewritten as (adapted from [95])

$$f_{\mathrm{Low}} \approx \frac{\sigma_{\mathrm{Sol}}}{\pi W L N C_{\mathrm{o.H.}} K_{\mathrm{Cell}}} \tag{2.47}$$

$$f_{\mathrm{High}} \approx \frac{\sigma_{\mathrm{Sol}}}{2\pi(\epsilon_0 \epsilon_{\mathrm{r,Sol}} + K_{\mathrm{Cell}} C_{\mathrm{Wire}})}. \tag{2.48}$$

The above estimation of f_{Low} was simplified by taking into consideration that the widest ohmic plateau has been found for a ratio $S/W = 0.54$ [96]. Using this ratio the formulas for the cell constant and the lower cutoff frequency simplified to

$$k^* = \cos\left(\frac{\pi}{2} \cdot \frac{1}{1.54}\right) = \cos\left(\frac{\pi}{3.08}\right) = 0.523 \tag{2.49}$$

$$K(k^*) = 1.65,\ K(\sqrt{1 - k^{*2}}) = 2.15 \tag{2.50}$$

$$K_{\mathrm{Cell}}(k^*) = \frac{1.53}{(N-1)L} \tag{2.51}$$

and

$$f_{\mathrm{Low}} \approx \frac{\sigma_{\mathrm{Sol}}}{0.48W} \cdot \frac{N}{N-1}. \tag{2.52}$$

By means of the derived estimations of the cutoff frequencies the design parameters of the IDE could be chosen to match the cell type. In this work the electrodes were designed to measure the density of yeast cells with $f_{\mathrm{char}} \approx 5\,\mathrm{MHz}$ and E. coli cells with $f_{\mathrm{char}} \approx 14\,\mathrm{MHz}$ [90]. For yeast cells, the lower and upper measurement frequencies were chosen as 1 MHz and 10 MHz, for E. coli as 1 MHz and 20 MHz. These values defined the range of the ohmic plateau.

Electrodes were designed in different variants with an ohmic plateau extending to either 10 MHz or 20 MHz. The conductivity of the cell medium was assumed as 1 S/m [97] and an instrument cable length of 2 m was considered, giving a wiring capacitance of $C_{\mathrm{Wire}} = 200\,\mathrm{pF}$. Considering the expression for the upper frequency f_{High} the required cell constants were calculated by rearrangement:

$$f_{\mathrm{High}} \approx \frac{\sigma_{\mathrm{Sol}}}{2\pi(\epsilon_0 \epsilon_{\mathrm{r,Sol}} + K_{\mathrm{Cell}} C_{\mathrm{Wire}})} \tag{2.53}$$

$$\Rightarrow K_{\mathrm{Cell}} = \frac{\sigma_{\mathrm{Sol}}}{2\pi C_{\mathrm{Wire}} f_{\mathrm{High}}} - \frac{\epsilon_0 \epsilon_{\mathrm{r,Sol}}}{C_{\mathrm{Wire}}} \tag{2.54}$$

$$K_{\mathrm{Cell,10MHz}} = 0.76 \frac{1}{\mathrm{cm}} \tag{2.55}$$

$$K_{\mathrm{Cell,20MHz}} = 0.36\frac{1}{\mathrm{cm}}. \tag{2.56}$$

During the design of the IDE several constraints had to be obeyed. First, the size available for the finger electrodes was limited by the sensor area on the chip. This area was chosen as 3.3 mm × 3.3 mm, as explained in section 2.4. Second, the smallest producible distance between structures using a lift-off procedure was assumed to be 10 µm [98], giving a smallest finger width of 18.5 µm. Since the parameters W, L and N were related to each other, W and L were specified at fixed values and N expressed as a function of K_{Cell} and L.

The finger width was chosen as either 18.5 µm, 37 µm, 50 µm or 100 µm. It has been shown that 99 % of the electric field lines between finger electrodes run through a volume element with a height twice the spacing of the electrodes [99]. Since yeast cells have a diameter between 2 µm and 10 µm [89] the smallest finger spacing was expected to detect approximately two yeast cells in z-direction if cells were assumed to be directly adjacent to each other. The maximum spacing on the other hand should detect around 10 cells, which was expected to give a high signal sensitivity, and hence no wider spacings were considered.

The finger length was set to values between 100 µm and 3000 µm with corresponding numbers of fingers. For all combinations of parameters the total width of the IDE G was calculated and variants with $G > 3.3$ mm were discarded. Nine feasible variants with the design parameters differing as much as possible were set up, as shown in Fig. 2.14 and listed in Tab. 2.1.

The impedance spectra of the variants were evaluated in 10 mM phosphate buffered saline (PBS) and the measurement capability in yeast suspensions of increasing concentrations determined. Measurements were performed using a network analyzer with an impedance probe (MS4630B, Anritsu, Japan). The measurement data were transferred to a computer via a GPIB-USB interface and processed by a LabVIEW program. To measure the cell density in yeast suspensions the impedances and phase angles at 1 MHz and 10 MHz were measured, the conductances calculated from these values, converted to the conductivity with the aid of the finger spacing, and the relation $\sigma_{\mathrm{10MHz}}/\sigma_{\mathrm{1MHz}}$ taken as a measure for the cell density.

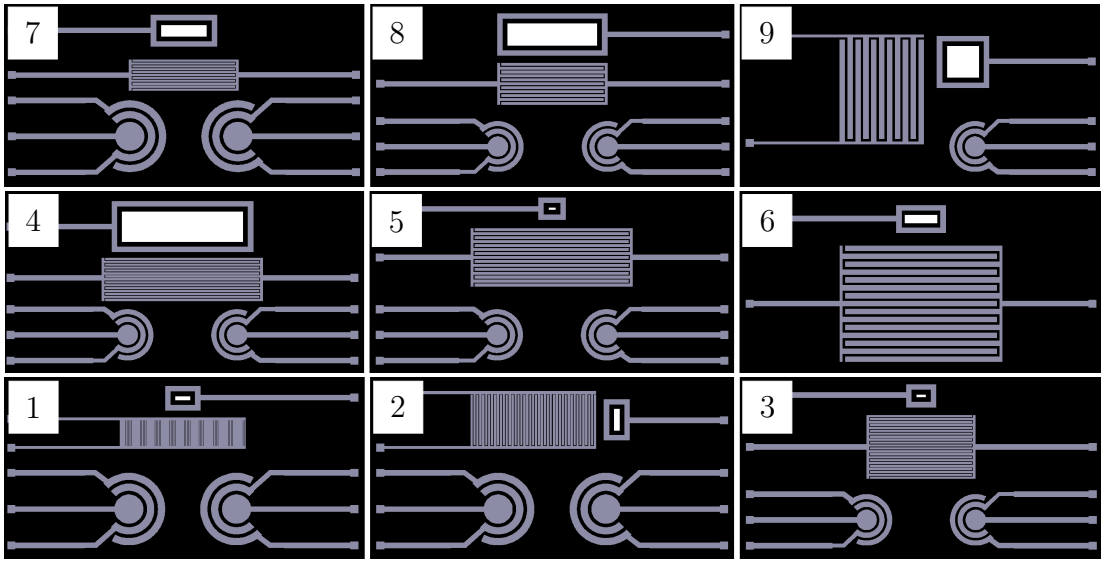

Figure 2.14: Design variants of interdigitated electrodes with enzyme electrodes and pH sensor; platinum layer is shown in gray color, pH sensitive area in white color; figures show detailed views of chip variants

Var	f_{High} [MHz]	f_{Low} [kHz]	R [Ω]	L [µm]	N	W [µm]	G [µm]
1	20	112	36	500	86	18.5	2427
2	20	56.3	36	1000	43	37	2445
3	20	56.3	36	2000	22	37	1241
4	20	56.3	36	3000	15	37	840
5	20	41.6	36	3000	15	50	1135
6	20	20.8	36	3000	15	100	2270
7	10	56.3	76	2000	11	37	611
8	10	41.6	76	2000	11	50	825
9	10	20.8	76	2000	11	100	1650

Table 2.1: Design variants of interdigitated electrodes with cutoff frequencies, resistance and design parameters finger length L, number of fingers N, finger width W and total sensor width G

2.3 pH Sensor

A process parameter of equal importance as the previously discussed ones is pH. It can have significant influence on process performance and product quality and

therefore has to be tightly monitored and controlled [7,18]. The classical pH glass electrode has been used in bioprocesses for decades [3]. However, it is breakable and cannot be integrated in miniaturized setups, such as the one proposed in this work. The ion-sensitive field-effect transistor (ISFET), based on an electrolyte-insulator-semiconductor (EIS) structure, was introduced as an alternative [100]. Its working principle is based on the ability of the insulator - typically an oxide with a high density of hydroxy groups - to attract a surface charge, which varies with the pH of the surrounding solution. When a capacitance-voltage (C-V) measurement is performed over the EIS structure the surface charge on the insulator causes a potential drop, shifting the C-V curve, as depicted in Fig. 2.15. The shift, which is a function of the solution pH, can be taken as a measure for the pH.

2.3.1 Site-Binding Model and Charges at the Insulator Surface

In order to describe the formation of a surface charge on the insulator surface an understanding of the interaction of the surface with the surrounding electrolyte is required. For this, the site-binding theory has been introduced [101]. It assumes the existence of sites, typically OH groups, on the insulator surface, which can bind or release ions, building up a positive or negative charge. Only the hydrogen ions present in the solution are able to bind to these sites or be released from them since all other ions are surrounded by a layer of water molecules, which prevents their interaction with the OH groups [102]. The binding and release mechanism and the working principle of the pH sensor are shown in Fig. 2.15. As the pH of a solution is defined as the negative decadic logarithm of the activity of hydrogen ions [56] the surface charge is dependent on the pH and thus a measure for this parameter.

The equations for the binding and release reactions can be written as [101]

$$\text{A-OH} \rightleftharpoons \text{A-O}^- + \text{H}^+ \tag{2.57}$$

$$\text{A-OH}_2^+ \rightleftharpoons \text{A-OH} + \text{H}^+, \tag{2.58}$$

where A is an atom of the insulator material and H^+ is a hydrogen ion. For these reactions dissociation constants can be derived relating the density of charged

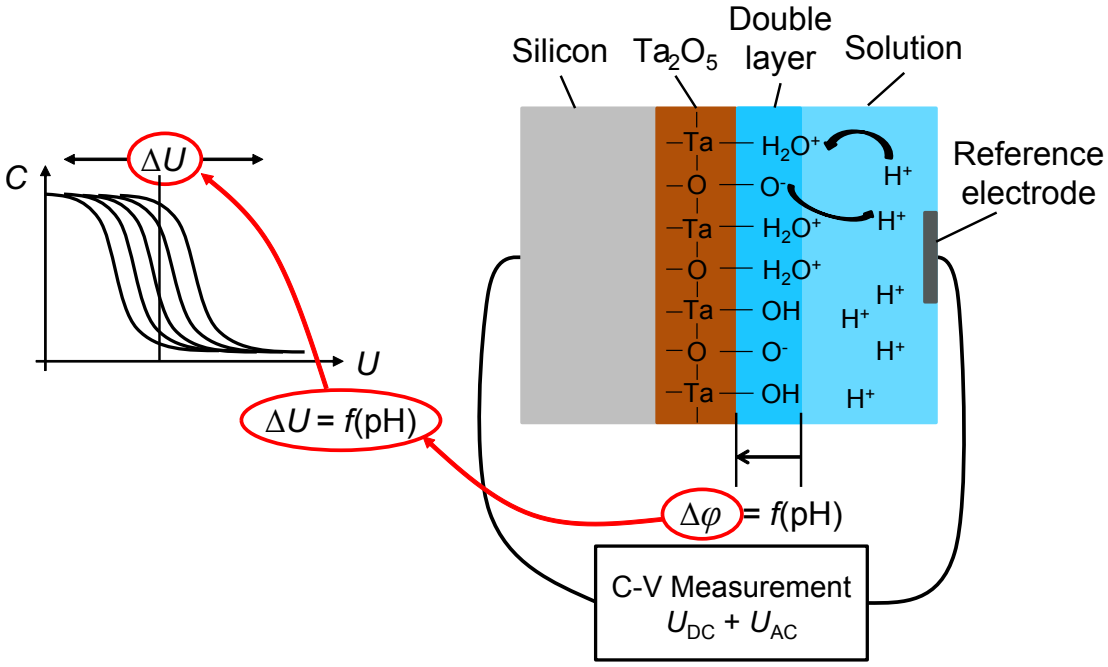

Figure 2.15: pH measurement setup with binding and release of hydrogen ions at Ta_2O_5 surface; potential difference over electrical double layer is related to solution pH and shifts C-V curve; not drawn to scale

groups, i.e. [A-O^-] and [A-OH_2^+], to the density of neutral OH groups [A-OH] and the activity of H^+ ions a_{H^+} [92]:

$$K_a = \frac{[\text{A-O}^-]a_{H^+}}{[\text{A-OH}]} \tag{2.59}$$

$$K_b = \frac{[\text{A-OH}]a_{H^+}}{[\text{A-OH}_2^+]}. \tag{2.60}$$

The above reactions charge the surface either positive or negative, the prevalent reaction depending on the material and the activity of hydrogen ions. The total density of OH groups N_{OH} is a material parameter and depends on the electronegativity of the metal [103]. In this work Ta_2O_5 was used because of its high pH sensitivity and the ability to withstand autoclaving as a common cleaning method for bioreactors [104]. For this material N_{OH} is approximately $1 \times 10^{19}/\text{cm}^2$ [105].

For a certain pH value the number of oppositely charged surface sites balances, so in total there is no surface charge. This pH value, which is specific for every material, is called the pH of zero charge or pH_{pzc}. For Ta_2O_5 $pH_{pzc} = 3$ [105].

The activity of hydrogen ions at the insulator surface is different from the activity in the bulk solution. This is due to the fact that the potential at the

insulator surface is different from the potential in the bulk solution. This potential drop is caused by an electrical double layer forming due to the surface charge on the insulator surface and the voltage applied over the EIS structure during the pH measurement. The activity of the hydrogen ions at the insulator surface $a_{\mathrm{H_s^+}}$ is related to the bulk activity $a_{\mathrm{H^+}}$ through Boltzmann statistics [106]:

$$a_{\mathrm{H_s^+}} = a_{\mathrm{H^+}} e^{-q\phi_0/kT}, \tag{2.61}$$

where q is elementary charge, ϕ_0 is the potential at the insulator surface, k is the Boltzmann constant and T is temperature.

For the further calculations the insulator surface charge per unit area σ_0 has to be derived. This can be done by multiplying the sum of charge carrying surface sites with the elementary charge:

$$\sigma_0 = q([\mathrm{A\text{-}OH_2^+}] - [\mathrm{A\text{-}O^-}]) = q[\mathrm{B}]. \tag{2.62}$$

By expressing the fractions of N_{OH} carrying charge through the dissociation constants established in Eq. 2.60 σ_0 can be written as [92]

$$\sigma_0 = qN_{\mathrm{OH}} \left(\frac{a_{\mathrm{H_s^+}}^2 - K_{\mathrm{a}}K_{\mathrm{b}}}{K_{\mathrm{a}}K_{\mathrm{b}} + K_{\mathrm{b}}a_{\mathrm{H_s^+}} + a_{\mathrm{H_s^+}}^2} \right). \tag{2.63}$$

As a material parameter the so-called intrinsic buffer capacity β_{int} is introduced [92], relating a pH change at the insulator surface to a change in the surface charge density:

$$\frac{\delta\sigma_0}{\delta \mathrm{pH_s}} = q\frac{\delta[\mathrm{B}]}{\delta \mathrm{pH_s}} \tag{2.64}$$

$$= q\beta_{\mathrm{int}}. \tag{2.65}$$

The charge at the insulator surface is balanced by the charge bound in the electrical double layer forming at the surface. As mentioned above this double layer is attracted by the charge on the insulator surface as well as the potential applied between the chip and the reference electrode during the pH measurement. The double layer can be treated with the Gouy-Chapman-Stern model, which has already been introduced in the treatment of the cell density sensor in section 2.2.1. The charge density in the double layer σ_{DL} can be calculated as [92]

$$\sigma_{\mathrm{DL}} = -\sqrt{8kT\epsilon\epsilon_0 c^0}\sinh\left(\frac{zq\phi_{\mathrm{o.H.}}}{2kT}\right) \tag{2.66}$$

$$= -\sigma_0. \tag{2.67}$$

In Eq. 2.65 ϵ and ϵ_0 are the permittivity of the solution and vacuum, $\phi_{\text{o.H.}}$ is the potential at the outer Helmholtz plane and c^0 is the concentration of ions except hydrogen ions. Besides the total charge in the double layer the capacitance change of the double layer as a response to a potential change is of importance. This so-called differential capacitance C_{diff} is defined as [107]

$$C_{\text{diff}} = -\frac{\delta\sigma_{\text{DL}}}{\delta\phi_0} \tag{2.68}$$

$$= \frac{\delta\sigma_0}{\delta\phi_0}. \tag{2.69}$$

Equating the insulator surface charge density in Eq. 2.65 and the charge density in the double layer in Eq. 2.69 gives [92]:

$$\frac{\delta\phi_0}{\delta\text{pH}_\text{s}} = \frac{\delta\phi_0}{\delta\sigma_0}\frac{\delta\sigma_0}{\delta\text{pH}_\text{s}} \tag{2.70}$$

$$= \frac{-q\beta_{\text{int}}}{C_{\text{diff}}}. \tag{2.71}$$

The above formula includes the pH at the insulator surface pH_s. The parameter of interest, however, is the pH in the bulk solution. These are related through Eq. 2.61. Using this relationship Eq. 2.71 can be rewritten as

$$\frac{\delta\phi_0}{\delta\text{pH}} = 2.3\frac{kT}{q}\alpha, \tag{2.72}$$

$$\text{with } \alpha = \frac{1}{(2.3kTC_{\text{diff}}/q^2\beta_{\text{int}}) + 1}. \tag{2.73}$$

The sensitivity parameter α combines the material dependent factors C_{diff} and β_{int} and varies between 0 and 1. For Ta_2O_5, with $C_{\text{diff}} = 0.16\,\text{F/m}^2$ and $\beta_{\text{int}} = 3 \times 10^{18}$ charged groups per m^2 at pH_{pzc} [92], α amounts to 0.981, giving a theoretical pH sensitivity of 58.2 mV/pH at a temperature of 25 °C. This voltage shift can be measured in the C-V curve of the EIS structure.

The theoretical limit of the pH sensitivity given by the Nernst equation is 59.1 mV/pH [56]. The connection between classical pH electrodes and the semiconductor-based EIS structures is the binding and release reactions of hydrogen ions. These can be regarded as oxidation and reduction reactions taking place both at the surface sites of the Ta_2O_5 and at the ion-sensitive glass membrane

of pH electrodes. Considering these redox reactions the theoretical voltage shift ΔU in a galvanic cell can be calculated using the Nernst equation [56]:

$$\Delta U = \frac{RT}{zF} \ln\left(\frac{a_{\mathrm{Ox}}}{a_{\mathrm{Red}}}\right), \tag{2.74}$$

with R being the Avogadro constant, F the Faraday constant, z the number of electrons involved in the redox reaction and a_{Ox} and a_{Red} the activities of the oxidized and reduced species, respectively. Considering the values of R and F the factor for the conversion from the natural logarithm to the decadic logarithm and $z = 1$ for the number of electrons exchanged in every binding or release reaction the voltage shift can be rewritten as

$$\Delta U = 59.1\,\mathrm{mV} \cdot \log\left(\frac{a_{\mathrm{Ox}}}{a_{\mathrm{Red}}}\right). \tag{2.75}$$

Since the pH is defined as the negative decadic logarithm of the activity of hydrogen ions this gives the theoretical limit of the pH sensitivity of 59.1 mV/pH as an absolute value.

2.3.2 Sensor Design

The C-V measurement over the EIS structure was conducted between a reference electrode located in the solution and the backside of the chip, as shown in Fig. 2.15. The shift of the C-V curve had to be measured in the depletion region of the EIS structure since only here a quasi-linear behavior of the capacitance signal was anticipated, allowing to easily distinguish the shifted curves from each other. In this region a fixed capacitance had to be chosen for which the voltage would be determined at the different pH values. A schematic C-V curve with the voltage shift as a function of pH is shown in Fig. 2.16.

Due to the fact that the electrolyte surrounding the chip was highly conductive the capacitance measurement could not be confined to the pH-sensitive area with the capacitance C_{pH}, but the remaining chip area with the capacitance C_{Rem} contributed to the measurement as well. These two parallel capacitances added up to the capacitance detected in the C-V measurement. The capacitance step $C_{\mathrm{pH,Step}}$, stemming from the depletion layer forming in the silicon under the pH-sensitive area, had to be so pronounced that it could be reliably detected in the measurement curve and its shift determined. This requirement lead to the

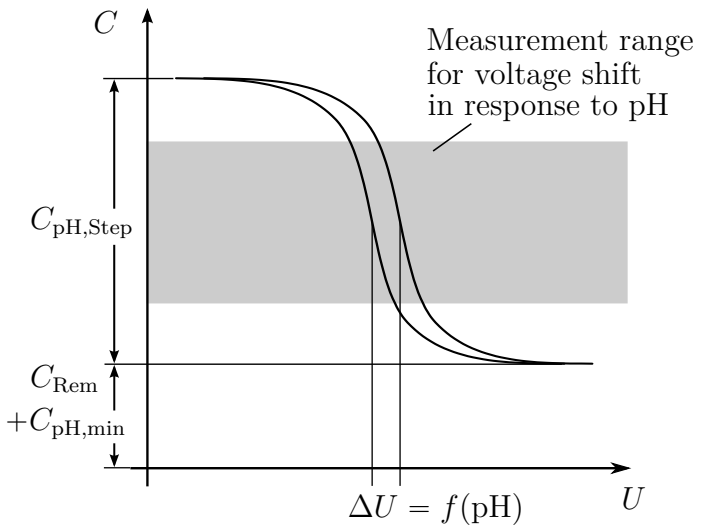

Figure 2.16: Schematic C-V curve of electrolyte-insulator-semiconductor (EIS) structure with voltage shift $\Delta U = f(\mathrm{pH})$; the capacitance step $C_{\mathrm{pH,Step}}$, stemming from the depletion layer forming in the silicon under the pH-sensitive area, had to be distinguished from the remaining capacitances and its shift reliably detected

question how large the pH-sensitive area had to be in relation to the remaining chip area. Hence, the maximum and minimum capacitance of the sensor chip and the ratio of the areas A_{pH} and A_{Rem} were identified as the key parameters to be considered during the design phase. The general design of the sensor chip with the pH-sensitive area is shown in Fig. 2.17.

To make the contribution of C_{pH} in the C-V measurement as high as possible and minimize C_{Rem} the pH-sensitive area was defined in two ways. The thermal oxide below the Ta_2O_5, required to minimize trapped charges at the interface with the pH-sensitive insulator and enhance its adhesion, was kept to about 20 nm in the pH-sensitive area, but grown to a thickness of around 350 nm in the remaining area. These thicknesses were chosen according to the standard process parameters in the CMOS fabrication line of the Fraunhofer IMS. The thick thermal oxide reduced C_{Rem} and lead to a higher potential drop in this area. As a second measure the remaining chip area was implanted with boron ions, leading to a highly positively doped silicon layer, marked with "p^{++}" in Fig. 2.17. This layer prevented the formation of a depletion layer in the remaining chip area during the C-V measurement and hence assured that the measured capacitance change originated from the pH-sensitive area.

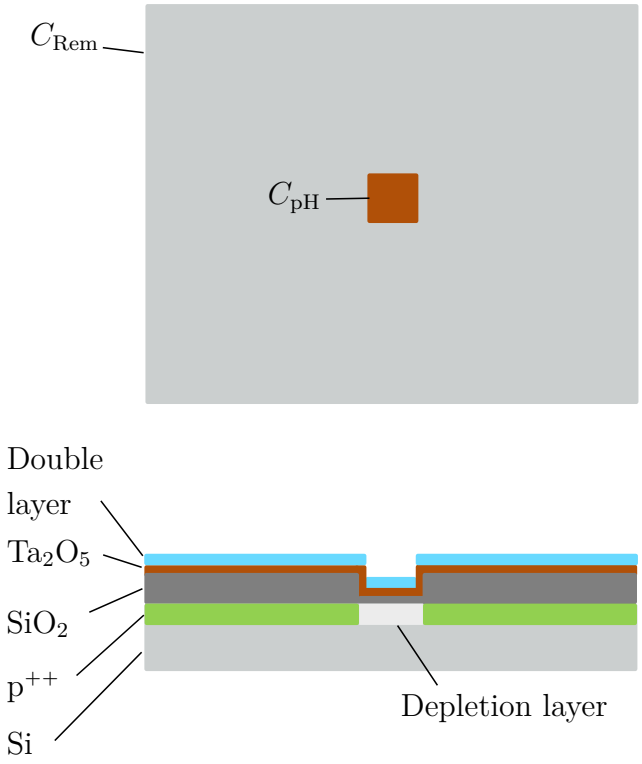

Figure 2.17: Top view and cross section of sensor chip with pH-sensitive area and capacitances C_{pH} and C_{Rem}; ratio of pH-sensitive area and remaining chip area was determined as an important design parameter

In the design of the pH sensor the following capacitances of the EIS stack had to be considered as indicated in Fig. 2.17:

- the capacitance of the electrical double layer C_{DL}
- the capacitance of the Ta_2O_5 layer C_{Ta2O5}
- the capacitance of the SiO_2 layer C_{SiO2}
- the capacitance of the depletion layer C_{Dep}.

The capacitance of the electrical double layer was estimated as $C_{\mathrm{DL}} \approx C_{\mathrm{o.H.}} \approx 0.2\,\mu\mathrm{F/cm^2}$ [92]. This estimation holds for ionic concentrations above 0.1 mM [56], which are common in cell culture media.

The capacitances of the Ta_2O_5 and SiO_2 layer were calculated using the formula

$$C = \epsilon_0 \epsilon_{\mathrm{r}} \frac{A}{d}, \tag{2.76}$$

where the relative permittivities were assumed as $\epsilon_{\mathrm{r,Ta2O5}} = 27$ [108] and $\epsilon_{\mathrm{r,SiO2}} = 3.9$ [109], d was the thickness of the layer and A the areas A_{pH} and A_{Rem}, respectively.

To calculate the capacitance C_{Dep} the width of the depletion layer d_{Dep} was required. This parameter varies between 0 when there is no depletion layer, and the maximum width $d_{\mathrm{Dep,max}}$, depending on the voltage applied to the EIS structure. Since the relevant capacitances for the C-V measurement were the maximum and minimum capacitance of the structure only the capacitances $C_{\mathrm{Dep,min}}$ and $C_{\mathrm{Dep,max}}$ were calculated.

Without a depletion layer there is no capacitance, hence $C_{\mathrm{Dep,min}} = 0$. For the capacitance at the maximum depletion layer width $d_{\mathrm{Dep,max}}$ was calculated according to the formula [110]

$$d_{\mathrm{Dep,max}} = \sqrt{\frac{2\epsilon_0\epsilon_{\mathrm{r,Si}}\phi_{\mathrm{t}}}{qN_{\mathrm{a}}}}, \tag{2.77}$$

with ϕ_{t} and N_{a} being the threshold voltage and doping density of the silicon epitaxial layer, and the relative permittivity of silicon $\epsilon_{\mathrm{r,Si}} = 11.7$ [109]. The used silicon substrate had a slightly positively doped epitaxial silicon layer, where the depletion layer formed, on top of a highly positively doped silicon bulk layer. The highly doped bulk layer enabled good electrical connection from the chip backside to the top layer during the C-V measurements. For the epitaxial layer with a resistivity of 35 Ωcm, a doping density of $N_{\mathrm{a}} = 3.73 \times 10^{14}$ of boron atoms per cm^3 was assumed. The threshold voltage was calculated as (adapted from [110])

$$\phi_{\mathrm{t}} \approx 2\phi_{\mathrm{f}} + \frac{Q_{\mathrm{Dep}}}{C_{\mathrm{Ox}}} \tag{2.78}$$

$$\approx 2\phi_{\mathrm{f}} + \frac{\sqrt{4\epsilon_{\mathrm{r,Si}}qN_{\mathrm{a}}\phi_{\mathrm{f}}}}{C_{\mathrm{Ox}}}, \tag{2.79}$$

where ϕ_{f} is the bulk potential of the silicon, Q_{Dep} is the depletion layer charge and C_{Ox} is the capacitance of the stack of Ta_2O_5 and SiO_2. In this calculation the flatband voltage of the EIS structure was neglected since it could not be determined for a structure with the gate electrode detached from the oxide. Hence, Eq. 2.79 was treated as an estimation of ϕ_{t} rather than an exact calculation. The bulk potential of the silicon ϕ_{f} was calculated as [110]

$$\phi_{\mathrm{f}} = V_{\mathrm{t}} \ln\left(\frac{N_{\mathrm{a}}}{n_{\mathrm{i}}}\right). \tag{2.80}$$

In this formula V_t and n_i are the thermal voltage and the intrinsic carrier concentration of the silicon, which were assumed to be 25.9 mV and $1.45 \times 10^{10}/\mathrm{cm}^3$ [111], respectively, at 300 K.

With the maximum depletion layer width $d_{\mathrm{Dep,max}}$ known the capacitance $C_{\mathrm{Dep,max}}$ at this measurement point could be calculated as

$$C_{\mathrm{Dep,max}} = \epsilon_0 \epsilon_{\mathrm{r,Si}} \frac{A_{\mathrm{pH}}}{d_{\mathrm{Dep,max}}}. \tag{2.81}$$

Having calculated the capacitances of the individual layers of the EIS structure, the maximum and minimum capacitance of the pH-sensitive area could be calculated by adding up the serial capacitances of the individual layers:

$$C_{\mathrm{pH,max}} = \frac{1}{1/C_{\mathrm{DL}} + 1/C_{\mathrm{Ta2O5}} + 1/C_{\mathrm{SiO2}}} \tag{2.82}$$

$$C_{\mathrm{pH,min}} = \frac{1}{1/C_{\mathrm{DL}} + 1/C_{\mathrm{Ta2O5}} + 1/C_{\mathrm{SiO2}} + 1/C_{\mathrm{Dep,max}}}. \tag{2.83}$$

Similarly, the capacitance of the remaining chip area C_{Rem} could be calculated, not considering a depletion layer. The capacitance step in the C-V curve was then calculated as

$$C_{\mathrm{pH,Step}} = C_{\mathrm{pH,max}} - C_{\mathrm{pH,min}}. \tag{2.84}$$

Using Eq. 2.79 and Eq. 2.77 the threshold voltage of the pH-sensitive area was estimated as 559 mV, and the maximum depletion layer width was calculated as 1.32 µm. Considering the calculated pH sensitivity of 58.2 mV/pH and the $\mathrm{pH_{pzc}}$ of 3 for Ta_2O_5 the threshold voltage was anticipated to vary between 501 mV at pH 2 and 1083 mV at pH 12.

As mentioned earlier the ratio of the pH-sensitive area and the remaining chip area was identified as an important design parameter. The question was, how big the pH-sensitive area had to be so that the capacitance step in the C-V curve, originating from the depletion layer in the pH-sensitive area, could be reliably detected in the measurement signal and distinguished from the remaining chip capacitance. As an aid in the design process the ratio Γ of the capacitance step and the total capacitance of the chip was introduced:

$$\Gamma = \frac{C_{\mathrm{pH,Step}} A_{\mathrm{pH}}}{C_{\mathrm{pH,max}} A_{\mathrm{pH}} + C_{\mathrm{Rem}} A_{\mathrm{Rem}}}. \tag{2.85}$$

In this formula the capacitances were normalized to 1 mm^2. With a calculated capacitance step $C_{\mathrm{pH,Step}} = 2.5\,\mathrm{nF/mm}^2$, a maximum capacitance $C_{\mathrm{pH,max}} =$

Var	Γ	A_{pH} [mm^2]	$C_{\mathrm{pH,Step}}$	C_{Total}
1	0.05	0.021	51.5 pF	1.03 nF
2	0.1	0.043	108.4 pF	1.09 nF
3	0.02	0.008	20 pF	1 nF
4	0.8	1.370	3.43 nF	4.28 nF
5	0.01	0.004	9.9 pF	1 nF
6	0.2	0.097	242.6 pF	1.21 nF
7	0.33	0.19	474 pF	1.44 nF
8	0.67	0.741	1.85 nF	2.77 nF
9	0.5	0.378	945.3 pF	1.89 nF

Table 2.2: Design variants of pH sensor with pH-sensitive area A_{pH}, ratio Γ of A_{pH} and remaining chip area, calculated capacitance step $C_{\mathrm{pH,Step}}$ in the C-V measurement and total capacitance of the chip C_{Total}

2.6 nF/mm^2 and a remaining chip area capacitance $C_{\mathrm{Rem}} = 90\,\mathrm{pF/mm^2}$, A_{pH} could be expressed as a function of Γ:

$$A_{\mathrm{pH}} = \frac{A_{\mathrm{Total}}}{27.8(1 - 1.04\Gamma)/\Gamma + 1}. \tag{2.86}$$

The smallest capacitance step that could be reliably measured using the available measurement equipment in form of an LCR meter HP4284 was considered to be 10 pF, leading to a minimum value for Γ of 1 % of the total capacitance. Taking into account the total sensor area of 3.3 mm × 3.3 mm, stemming from the considerations about the sensor integration in section 2.4, the pH-sensitive area for this variant resulted in $A_{\mathrm{pH}} = 0.004\,\mathrm{mm^2}$. Further variants with Γ going up to 80 % were designed to evaluate the influence of increasing area on the sensitivity of the signal. Higher values of A_{pH} were not chosen since an increasing area was expected to increase the number of defects in the oxide layer, which were thought to lead to higher leakage currents and unreliable measurement performance. The resulting nine variants are listed in Tab. 2.2 with C_{Total} being the overall chip capacitance. The design can be seen in Fig. 2.14 in the description of the cell density sensor (section 2.2.2).

C-V measurements were performed with an AC amplitude of 20 mV using an LCR meter (HP4284, Japan). This empirically determined value ensured reliable

measurement results while at the same time keeping the measurement current to around 1 µA. Higher currents had been found to significantly lower the lifetime of the Ag/AgCl reference electrode used in the measurements. The AC frequency was chosen as 1 kHz. This value was low enough to keep the measurement current to around 1 µA and limit the contribution of parasitic capacitances to the measurement signal. Capacitance was measured between the backside of the chip and an Ag/AgCl (SI Analytics, Germany) reference electrode in the electrolyte. All measurements were conducted in a Faraday cage at a constant temperature. The measurement data were transferred to a computer via a GPIB-USB interface and processed by a LabVIEW program.

2.4 Sensor Integration, Fabrication and Measurement Setup

After designing the individual sensor elements, these had to be integrated on a single multi-sensor chip. The chip dimensions and the arrangement of the sensor elements had to satisfy several requirements. First, all sensor elements had to be contacted using only one metal layer since this layer was fabricated as the last step in an external cleanroom. Further processing of wafers with platinum or gold on top, e.g. fabrication of isolation layers necessary for chips with multiple metal layers, was not possible in the cleanroom of the Fraunhofer IMS. At the same time the arrangement had to minimize mutual interferences between the sensor elements in case the sensor would be used with a microfluidic chamber under laminar flow conditions. Since the enzyme sensors produce species such as H_2O_2 and H^+ during operation, which could influence the other sensors, these sensors had to be placed downstream of the other elements.

Second, the chip had to fit the standard PG 13.5 sensor housings used in bioprocesses. These are tubular housings with an inner diameter of approx. 10 mm. The sensor chip is incorporated into the housing in a way that allows the sensing area of the chip to contact the reactor medium while the rest of the chip and the readout electronics are protected from the reactor environment. Hence, the maximum chip size had to be around 7 mm × 7 mm and the design had to include a circumferential edge for bond pads and a sealing gasket.

Third, a maximum design area of 22 mm × 22 mm for the lithographic masks

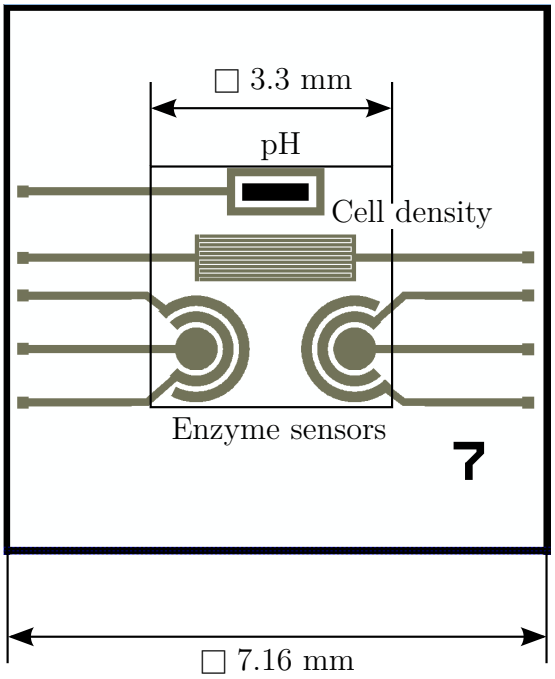

Figure 2.18: Integration of sensor elements on one chip; design choices: (1) all sensor elements contacted using one metal layer; (2) enzyme sensors placed downstream of other sensor elements to minimize chemical interferences; (3) maximum chip size of ca. 7 mm × 7 mm to fit into PG 13.5 sensor housing; (4) circumferential edge for sealing gasket and bond pads

used in the fabrication of the chips had to be considered.

Taking into account the above requirements the sensor elements were arranged as shown in Fig. 2.18. The concentric electrodes of the enzyme sensors were placed at the bottom of the chip so that under laminar flow conditions species produced in the enzyme reactions would be transported away without reaching the other sensor elements.

The placing was chosen in a way that allowed to place the bond pads on the left and right side of the chip so that the inlet and outlet of a microfluidic chamber could be placed at the top and bottom parts of the chip edge. Since electrodes, leads and bond pads were produced from the same material, i.e. platinum, the fabrication of these elements could be carried out in the same process steps.

The reference electrode for the pH sensor was placed around the sensor area, ensuring an even distribution of the electric field lines from the electrode to the sensor. However, due to concerns about the stability of silver-plated platinum

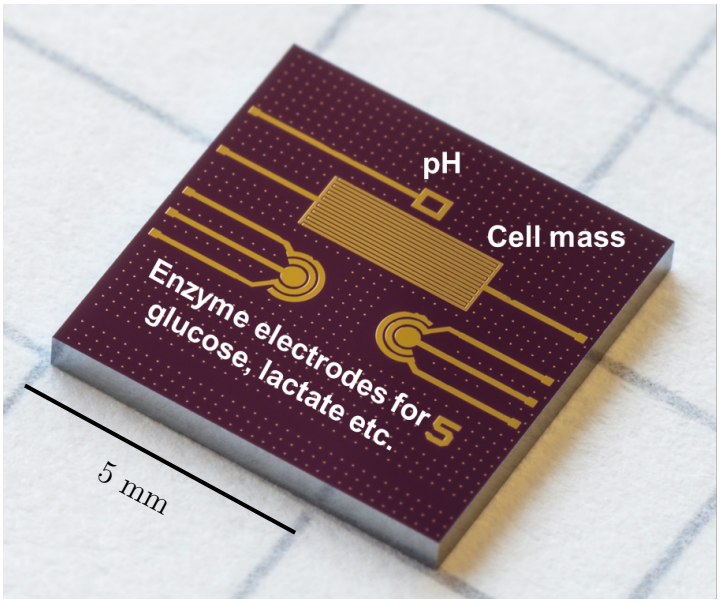

Figure 2.19: Photograph of multi-sensor chip

chip electrodes, an external Ag/AgCl reference electrode was used during the measurements. Nevertheless, the on-chip silver-plated reference electrode remains an option for further integration of the sensor chip.

The width of the leads connecting the sensor elements with the bond pads was chosen to give a low resistance but on the other hand minimize the area for unspecific electrochemical reactions, which could distort the sensor signals. Hence, the width was chosen as 150 µm, which gave a resistance of around 10 Ω. A photograph of a fabricated chip is shown in Fig. 2.19.

The chip size was chosen as 7.16 mm × 7.16 mm with a circumferential edge of 1.93 mm width, leaving a sensor area of 3.3 mm × 3.3 mm, determining the maximum size of the individual sensor elements. The chip dimensions allowed to place nine variants on the lithographic masks and left enough space around the chip sensor area to place a microfluidic chamber or sealing gasket.

Chip Fabrication

The fabrication process is schematically shown in Fig. 2.20. Sensor prototypes were fabricated on highly p-doped silicon wafers ($N_a = 2.7 \times 10^{18}/cm^3$) with a less p-doped epitaxial silicon layer on top ($N_a = 3.73 \times 10^{14}/cm^3$). The highly doped silicon enabled good electrical connection from the chip backside to the top layer

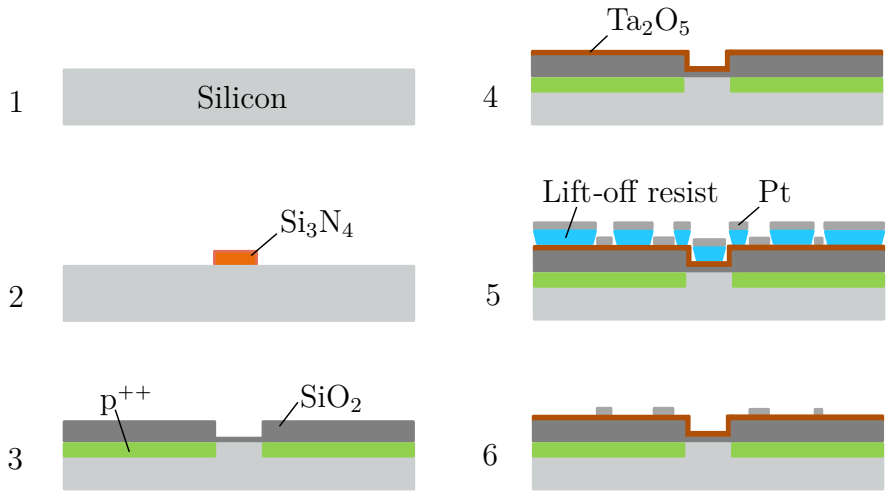

Figure 2.20: Fabrication of multi-sensor chip: 1 start with p-doped silicon; 2 definition of pH sensor area; 3 thermal oxidation and boron implantation; 4 Ta_2O_5 deposition; 5 structuring of lift-off resist and metal evaporation; 6 lift-off

during the C-V measurements. The pH-sensing area was defined by depositing and structuring silicon nitride and thermally oxidizing the wafer. This resulted in a thin thermal oxide of about 20 nm in the pH-sensitive area, whereas the rest of the chip area was covered by a thick thermal oxide of ca. 350 nm to reduce its contribution to the C-V measurement. Additionally, to confine the formation of a depletion layer to the pH-sensing area the remaining chip area was implanted with boron ions. For this the standard process parameters in the CMOS fabrication line of the Fraunhofer IMS were used, i.e. a dose of 3.44×10^{-12} boron ions/cm^2 and an energy of 210 keV. These regions are highlighted green and marked with "p^{++}" in Fig. 2.20.

As a pH-sensitive material Ta_2O_5 was deposited by an atomic layer deposition process with a thickness of 25 nm. For this thickness a reproducible fabrication with predetermined number of process cycles could be ensured.

The electrodes for the enzyme sensors and the cell density sensor were fabricated by a lift-off process. A negative photoresist (AZ nLof 2020, Microchemicals GmbH, Germany) was spin coated with a thickness of 2 µm. The coated substrate was exposed using a stepper (PAS 5500, ASML, The Netherlands) with an energy of 60 mJ and developed. Then, 200 nm platinum on an adhesion layer of 20 nm titanium were evaporated and the lift-off performed using N-Methyl-2-pyrrolidone as a solvent.

After production the wafer backside was grinded to remove any oxides and the wafer diced into single chips.

Measurement Setup

In order to bring the chip in contact with a measurement solution the chip was directly immersed into solution instead of using the initially planned microfluidic setup. The decision in favor of the immersion approach was made since it allowed to effectively conduct in-situ measurements, whereas the microfluidic setup would rather have been an in-line setup. Hence, the chosen setup corresponded closely to the intended application in bioprocesses where the chip is integrated into a PG 13.5 sensor housing and immersed into a bioreactor. Additionally, discarding the microfluidics distinctly simplified the measurement setup.

The chip was mounted on one end of an elongated printed circuit board (PCB) using conductive adhesive (Epotek H20E, USA) to make the backside contact for the C-V measurements. The PCB could be partly immersed in the solution. On the other end electrical connections could be made. Electrical connections to the chip electrodes were made by wire bonding, and the chip edges were protected by a potting compound with little water uptake (Delo Monopox 6095, Germany). The PCB and the measurements were found to be stable even after several days of permanent contact with solutions, resolving initial concerns about the stability of the PCB when immersed into solutions over longer time periods.

The PCB and the measurement setup with a sample immersed in a yeast suspension and held by a laboratory clamp are shown in Fig. 2.21.

Parallel measurements were performed using a setup as shown in Fig. 2.22. The beaker with the measurement solution - either a calibration solution or a yeast culture - was put in a water bath on a combined hot/stirring plate to keep the solution temperature on a constant value. The solution was continuously stirred and air was continuously passed into the solution at a rate of 100 L/min using an air pump connected to an air stone in the beaker. This was necessary to ensure sufficient oxygen supply for the enzyme sensors. The pH was monitored for reference using a commercial pH glass electrode (Sentix 980, WTW GmbH, Germany) and kept constant by adding potassium hydroxide solution as necessary. Laboratory stands were positioned on both sides of the water bath to hold the PCB with the multi-sensor chip, the clips and probes of the measurement

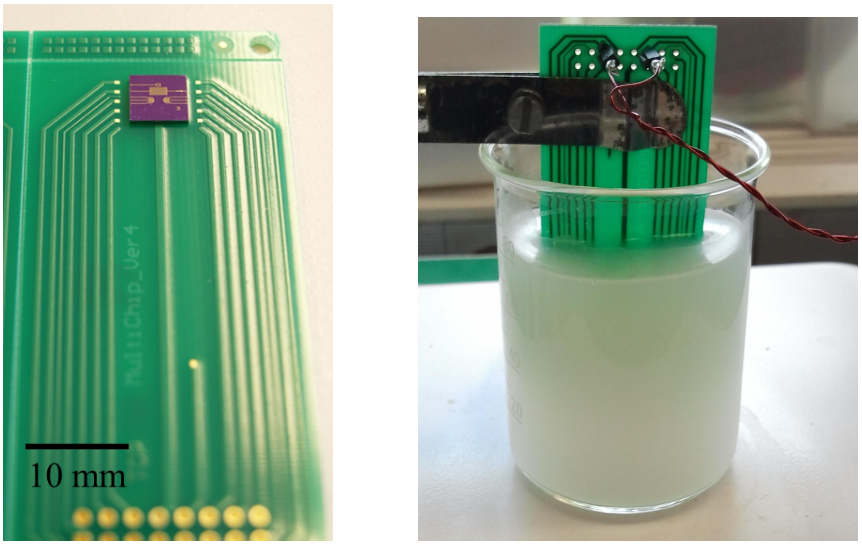

Figure 2.21: Chip mounted on PCB and measurement setup with PCB partly immersed into solution

instruments and the other equipment.

The yeast used in all experiments was instant active dry yeast from Hambleton Bard Ltd., UK. It was suspended in phosphate buffered saline and allowed to rehydrate before measurements were started.

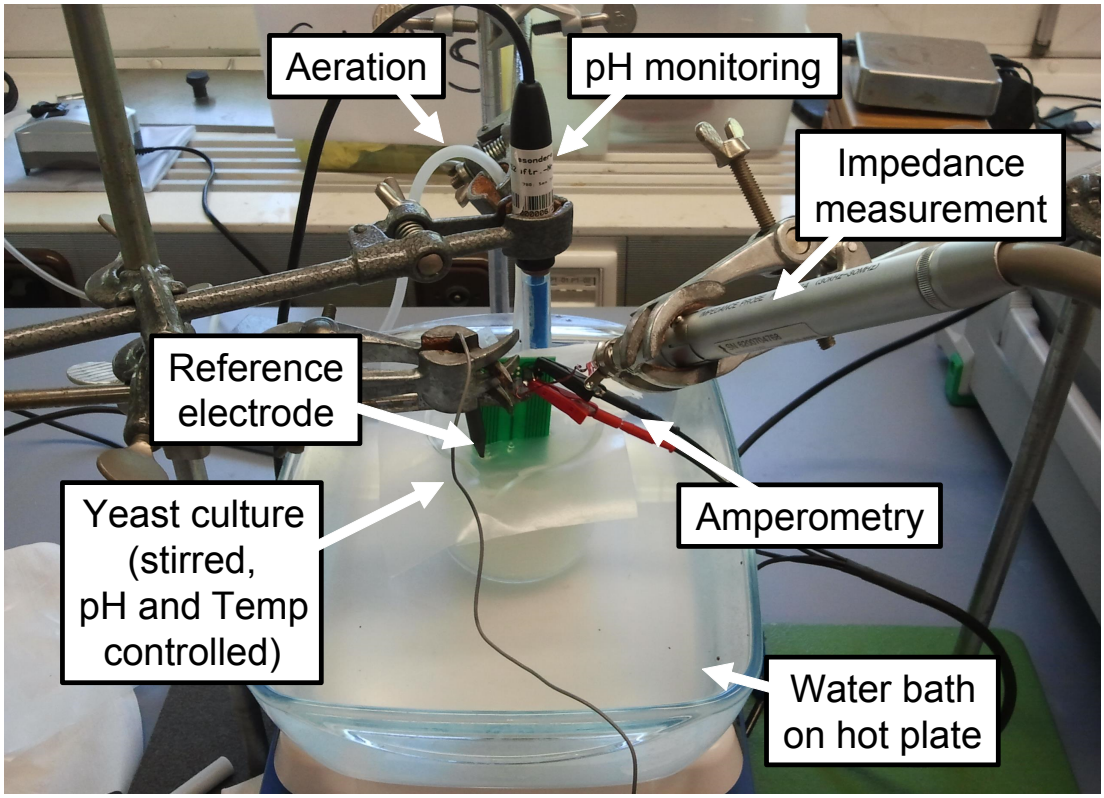

Figure 2.22: Parallel measurement setup in water bath on hot/stirring plate to keep temperature of yeast culture constant

Chapter 3

Results and Discussion

The results and discussion in this chapter are based on and extend the author's publications on glucose sensors with PDMS membranes [16, 24], enzyme sensors for the monitoring of biotechnological processes [25] and a multi-sensor system for the monitoring of biotechnological processes [26, 27].

3.1 Amperometric Enzyme Sensors

3.1.1 Enzyme Sensors with PDMS Membranes

As a first step in the evaluation of the fabricated enzyme sensors measurements were carried out with enzyme electrodes on ceramics without a membrane to determine linear current range and response time. In Fig. 3.1 the response after immersion into 500 µM glucose is shown. The electrodes showed a linear range up to 1 mM with a response time of approximately 200 s and a sensitivity between 60 nA/mM and 65 nA/mM. Response time was measured from the addition of glucose to the point the current reached 95 % of its steady state value. While the sensitivity was comparable to values reported in the literature [46], the response time was higher than typically reported values that range between 20 s and 30 s [43,46]. The longer response time pointed to a reduced permeability of the enzyme layer for glucose and H_2O_2 in comparison to other work. However, since the enzyme layer had been optimized for high sensitivity and long-term stability, and longer response times were regarded as tolerable for in-situ application in bioreactors, the established enzyme layer formulation was used throughout the

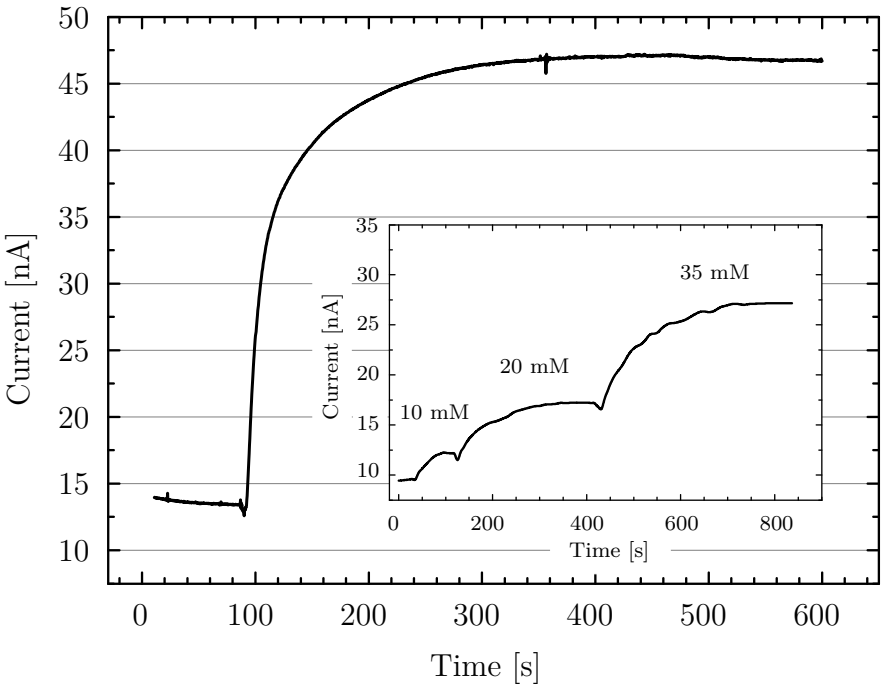

Figure 3.1: Response curve of enzyme electrode on ceramics without membrane after addition of 500 µM glucose; inset shows response of electrode with thick PDMS membrane cured according to scheme 1

experiments with diffusion-limiting membranes.

Influence of Membrane Thickness

To determine the influence of the membrane thickness on the linear measurement range PDMS was spin-coated onto enzyme electrodes with a spin speed of 3000 rpm or 6000 rpm and then cured according to scheme 1. The two used curing schemes are listed in Tab. 3.1 for reference. As can be seen from Fig. 3.2 membranes spun at 6000 rpm increased the linear range to 5 mM. The resolution, measured as the smallest step of glucose that gave a measurable change of the

Scheme	Curing time in air	Curing time in buffer
1	12 h	12 h
2	16 h	8 h

Table 3.1: Curing schemes of PDMS membranes

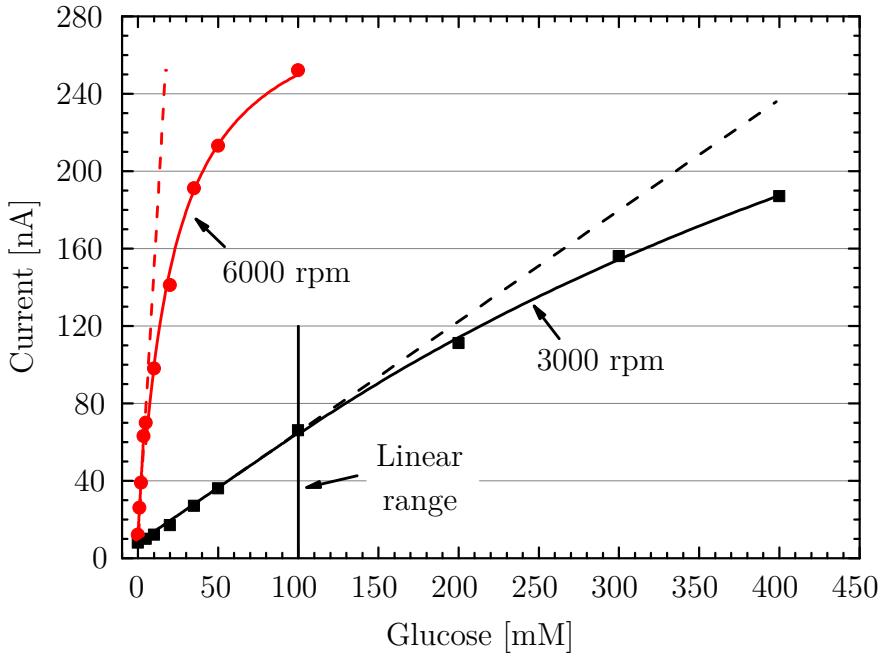

Figure 3.2: Calibration curves of enzyme electrodes with PDMS membrane spun at 3000 rpm and 6000 rpm, curing scheme 1; thick membrane extends linear range to 100 mM, making measurements in mammalian cell cultures possible

output signal, was 1 mM. The sensitivity was calculated to be 9 nA/mM. Membranes spun at 3000 rpm gave a linear range up to 100 mM with a resolution of 5 mM and a sensitivity of 0.6 nA/mM. In the inset of Fig. 3.1 an exemplary current response of an electrode with a thick PDMS membrane is shown. Response times varied with glucose concentrations. Thin membranes had response times between 80 s and 530 s, whereas for thick membranes 90 s to 1150 s was measured.

The relationship between membrane thickness and linear measurement range was not linear as suggested by the estimation introduced in Eq. 2.31 in section 2.1.4.2. The linear range of sensors with thick membranes was 20-fold the range of those with thin membranes. However, the thickness ratio with thicknesses of 35 µm and 4.5 µm, respectively, was only 7:1. From this observation it was concluded that other factors such as differing water uptake of the membranes [80] or different oxygen supply to the enzyme layer [13, 42] played a role in the sensor performance. Comparisons between theoretical sensor behavior and experimental performance have not been published yet to the author's best knowledge. Therefore, the reasons for this deviating sensor behavior have to be

investigated in future research. In the meantime the stated estimation of the linear range should be regarded as a rough guideline for sensor development instead of a definite prediction of sensor performance.

A linear range up to 100 mM qualifies the glucose sensors with thick membranes for applications in mammalian cell cultures, where concentrations go up to 50 mM, as well as fermentations with moderate glucose levels. Response times around 20 min and sensitivities below 1 nA/mM have been described for glucose sensors with wide concentration ranges using polycarbonate or poly(vinyl chloride) diffusion-limiting membranes [45, 47] and thus could be seen as a drawback of such sensors. However, such response times are regarded as acceptable in the context of bioprocess monitoring. Also, the developed sensors are intended for monitoring of wide concentration ranges rather than fine differentiations. Hence, the found sensor performance is considered to be feasible for application in bioreactors.

To evaluate the reproducibility of the measurements electrodes were stored in PBS at room temperature and the measurements repeated after 16 h. Electrodes with thin membranes showed a decrease of the linear range to 3.5 mM and an increase of sensitivity to 13 nA/mM. In contrast to that, sensors with thick membranes exhibited a stable linear range and a decreased sensitivity of 0.4 nA/mM. This behavior was likely to be due to differing water uptake and hydrolysis of the membranes with different thicknesses and also due to variations in the small scale production of the sensors. Long-term behavior of the sensors was investigated in further experiments.

Influence of Curing Scheme

To investigate the influence of the curing scheme of the PDMS membrane on the linear measurement range PDMS membranes spin-coated at 3000 rpm or 6000 rpm were partially cured according to scheme 2. Calibration measurements were then performed and compared to the results obtained for curing scheme 1. Before measurements were performed the electrodes remained in buffer solution for another 12 h for conditioning.

As is shown in Fig. 3.2 and Fig. 3.3 the curing time had significant influence on the linear measurement range. For thin membranes the first curing scheme gave only a slight extension of the linear range to 5 mM, whereas curing scheme 2

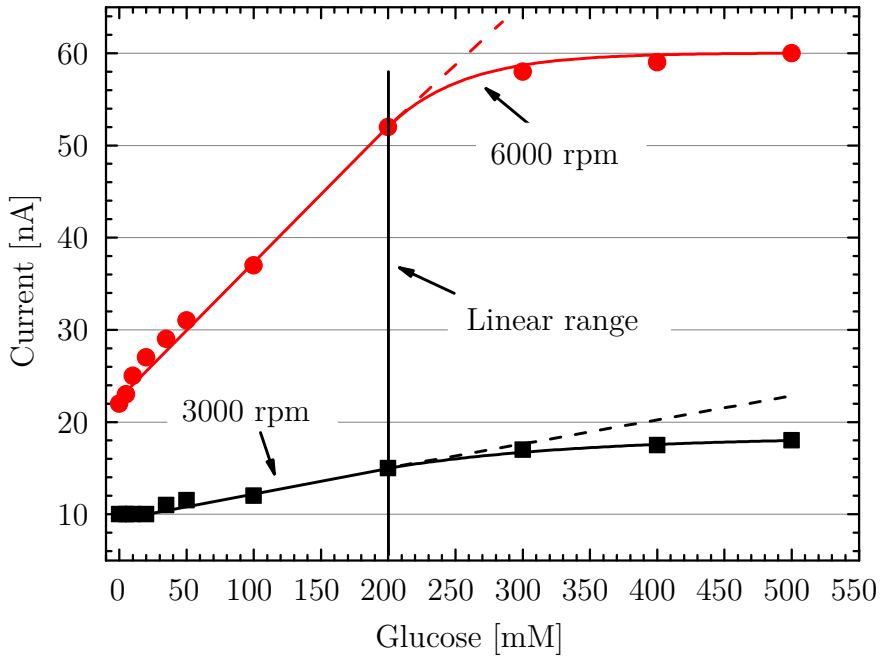

Figure 3.3: Calibration curves of enzyme electrodes with PDMS membrane spun at 3000 rpm and 6000 rpm, curing scheme 2; both sensors showed linear range up to 200 mM, covering concentrations in mammalian cultures as well as many fermentation processes

extended the range significantly to 200 mM. At the same time the sensitivity and resolution of the sensors decreased to 0.13 nA/mM and 10 mM for curing scheme 2, making the sensors more suited for wide-range measurements than determination of small changes in glucose concentrations. The quiescent current of the sensors rose to about 19 nA in comparison to around 11 nA for the shorter curing time in air, the reason of which has to be investigated in further experiments.

The significant difference in performance between the curing schemes of 12 h/12 h and 16 h/8 h could be explained with the different amounts of water incorporated into the membrane [80] and the different grades of hydrolysis of the PDMS chains [83, 84]. Both effects were supposed to change the membrane permeability for glucose. From the found results it could be inferred that the permeability of the PDMS for glucose decreased by approximately a factor of 40 when the curing time in air was changed from 12 h to 16 h. The influence of the curing time on the membrane permeability was far more pronounced than the reported influence of varying water amounts on the permeability of hydrogels [80] or

Membrane	Lin. Range [mM]	Sensitiv. [nA/mM]	Response Time [s]
Scheme 1, thick	100	0.6	90-1150
Scheme 1, thin	5	9	80-530
Scheme 2, thick	200	0.02	120-1470
Scheme 2, thin	200	0.13	90-570

Table 3.2: Linear range, sensitivity and response time of sensors with PDMS membranes cured according to scheme 1 (12 h air/12 h buffer) and scheme 2 (16 h air/8 h buffer)

the influence of hydrophilic PEGMA incorporated in PDMS [81]. Therefore and because the water uptake of the PDMS membranes ranged only between 0.2 % and 1.4 %, the hydrolysis of PDMS chains was assumed to be the determining factor for the membrane permeability.

Electrodes with thick membranes showed an extension of the linear measurement range to 100 mM for curing scheme 1 with a sensitivity of 0.6 nA/mM and a resolution of 5 mM. Curing scheme 2 extended the linear range to 200 mM, which, however, was not better than the linear range of the thin membranes cured using the same scheme. Furthermore, the sensitivity decreased distinctly to 0.02 nA/mM, and the electrodes only showed a response from a glucose concentration of 35 mM upwards. Presumably, the combination of a thick PDMS membrane and a curing scheme with a long curing time in air impeded the oxygen supply to the sensor so much that no higher measurement range in comparison to the thin membrane could be achieved [13, 42]. This fabrication scheme was therefore considered inappropriate for diffusion-limiting membranes for glucose.

For the thin membranes response times for the first curing scheme were between 80 s for small glucose concentrations and 530 s for high glucose concentrations. For membranes cured according to scheme 2 response times varied between 90 s and 570 s.

The relation between linear range, sensitivity and response time of the sensors with membranes cured according to scheme 1 and scheme 2 is listed in Tab. 3.2.

The two applied curing schemes demonstrated a second option to adjust the linear range of the sensors by altering the diffusion coefficient for glucose in the PDMS membrane. In comparison to modification of the membrane thickness

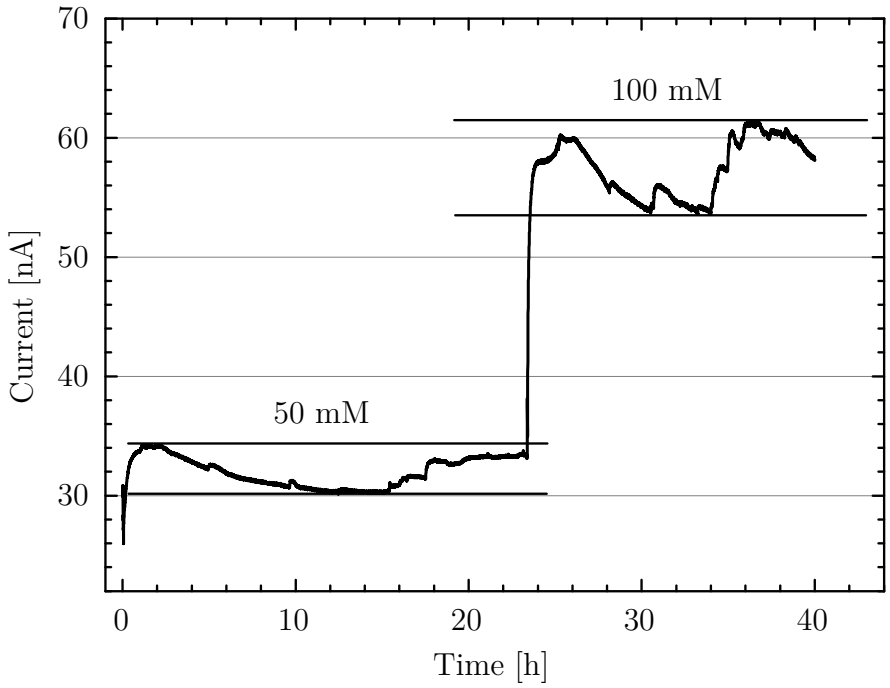

Figure 3.4: Signal over 40 h of enzyme electrode coated with thick PDMS membrane, cured according to scheme 1: glucose 50 mM (0 - 24 h), 100 mM (24 h - 40 h)

using curing scheme 1, changing the membrane permeability to scheme 2 proved to give faster response times and wider measurement ranges and hence was found to be the better way to produce glucose sensors for wide concentration ranges.

Evaluation of Long-Term Performance

For in-situ measurements in bioreactors glucose sensors have to provide a stable signal when in permanent contact with culture medium over several days or weeks. The continuous measurement performance of an electrode with a thick membrane cured according to scheme 1 was tested in a measurement run over 40 h, as shown in Fig. 3.4. The initial glucose concentration was 50 mM. After 24 h glucose was added to give a concentration of 100 mM. During the first 24 h of the experiment the current varied around a mean value of 32 nA with a standard deviation of 1.3 nA. After addition of glucose the mean value was 57.5 nA with a standard deviation of 2.4 nA. The signal showed a kind of cyclic variation. While this behavior could be explained by variations of the membrane permeability, these were rather expected to act on longer time scales, as investigated above.

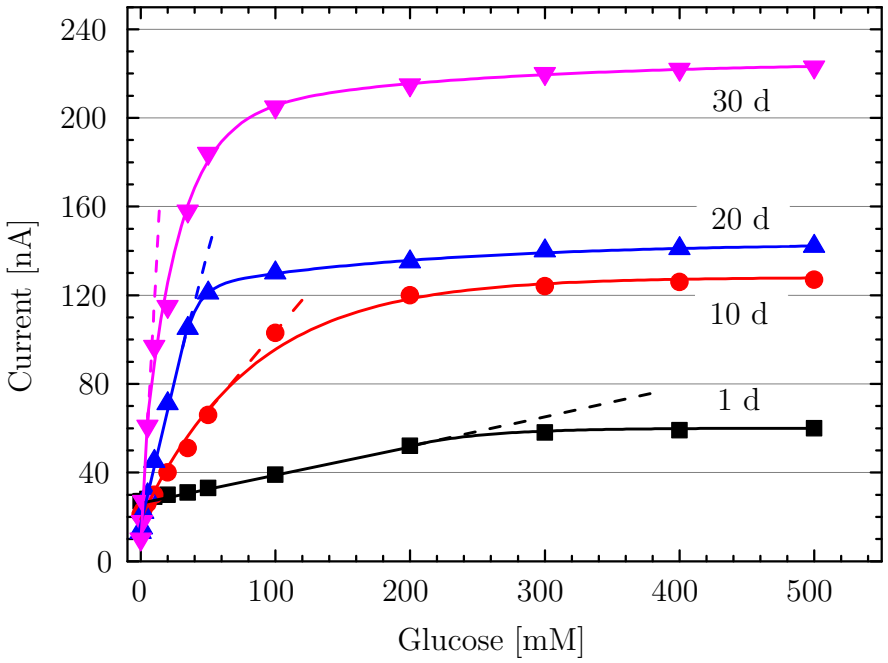

Figure 3.5: Calibration curves of electrodes with membranes spun at 6000 rpm cured according to scheme 2 over 30 days; increase of sensitivity and decrease of linear range suggests that the PDMS membrane permeability increased

It was therefore assumed that the signal variation was caused by instability of temperature or the reference potential.

During the partial curing in buffer solution an uptake of water into the PDMS membrane and partial hydrolysis of the PDMS chains was anticipated. These processes were expected to end when the 24 h curing period of the material had ended. However, further incorporation of water and hydrolysis of PDMS chains might be possible when the sensor is kept in an aqueous solution for a prolonged period, as is the case for continuous measurements in environments such as bioreactors. In order to examine possible effects of prolonged contact with aqueous solutions electrodes with thin membranes cured according to scheme 2 were exemplarily chosen to be kept in PBS over 30 days, and regular calibration measurements were performed. The results in Fig. 3.5 show that signal and sensitivity of the sensors grew over time while the linear range decreased. The sensitivity increased from 0.13 nA/mM on the first day to 37 nA/mM on day 30. At the same time the linear range decreased from 200 mM to 5 mM.

The found results suggest that a constant change of the PDMS properties took place while the material was in contact with solution, altering its transport

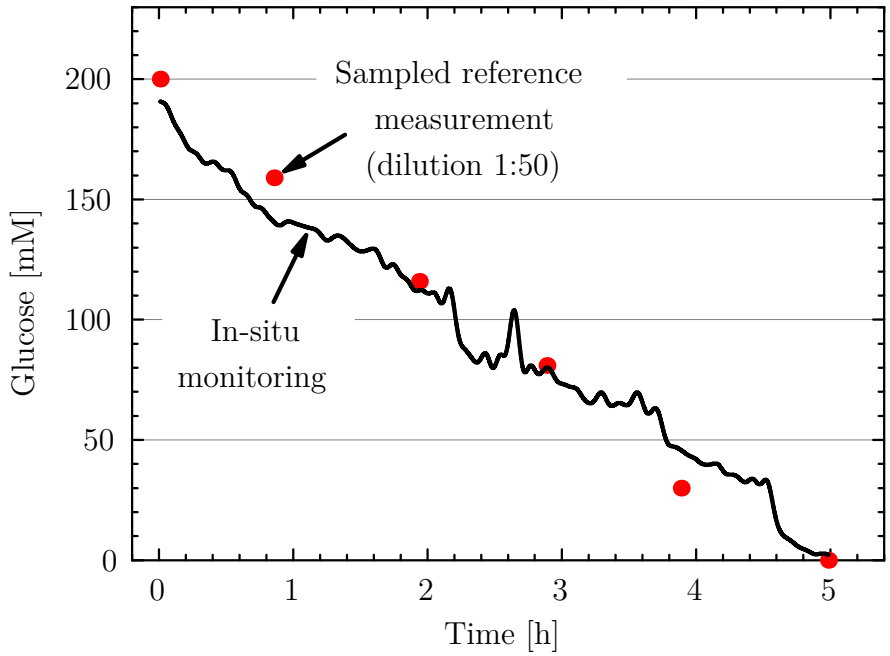

Figure 3.6: Glucose monitoring in yeast culture, initial concentration 200 mM; good agreement with reference measurements, performed using a commercial glucose meter (Accu Check, Roche, USA) with dilution 1:50

characteristics for glucose. As a consequence, for longer measurement runs regular calibrations of the glucose sensors may be necessary. As an alternative the loss of linearity may be corrected by using a model for the decrease. However, this loss is likely to depend on the composition of the surrounding medium, thus further experiments of the behavior of partially cured PDMS in different solutions are necessary. Alternatively, the change of the membrane properties over time could be reduced by curing the PDMS completely in air. In this case the diffusion coefficient would have to be adjusted by mixing the PDMS with hydrophilic compounds as demonstrated in [81].

Glucose Monitoring in Cell Culture

To assess the suitability of the proposed glucose sensors for applications in bioreactors the glucose consumption of a yeast culture was monitored. The culture was prepared in PBS with a cell density of 15 g/l and a high initial glucose concentration of 200 mM. During the culture duration temperature and pH were held constant at 30 °C and pH 4.7, respectively.

The glucose concentration was constantly measured with a glucose electrode with a thin membrane cured according to scheme 2, which had the appropriate linear range up to 200 mM. Samples were taken every hour, filtered and the glucose concentration measured using a commercial glucose meter (Accu Check, Roche, USA) with 50-fold dilution. As depicted in Fig. 3.6 there was good correlation between the continuous measurement signal and the reference measurements over the whole culture duration of five hours, demonstrating the suitability of the developed sensors for application in bioreactors.

After the measurement the sensor electrode was inspected for biofilm growth under an optical microscope. No biofilm could be found on the electrode surface. However, in longer experiments over several days the formation of a biofilm might be possible.

Elimination of Interfering Species

Glucose sensors based on oxidation of hydrogen peroxide are prone to interference by substances contained in the measurement solution that are oxidized at the same potential as H_2O_2 [44]. In cell culture media such as McCoy's 5a medium, L-cysteine, L-glutathione and ascorbic acid are three ingredients that have been shown to interfere with the measurement, giving too high glucose readings [44,47]. For accurate measurements in bioreactors it must be ensured that the sensor is insensitive to those substances. Cellulose acetate (CA) membranes have been shown to retain charged molecules [44], making it an appropriate material for elimination of the interfering substances mentioned.

The suitability of commercially available cellulose acetate membranes for elimination of interferences by L-glutathione, L-cysteine and ascorbic acid was examined. Membranes were cut to size and firmly attached to enzyme electrodes with a PDMS membrane spun at 3000 rpm and cured according to scheme 1, using adhesive tape. The electrodes were then immersed into PBS containing 0.1 mM L-glutathione, 0.2 mM L-cysteine and 0.1 mM ascorbic acid and the measurement compared to electrodes without a membrane. As can be seen from Fig. 3.7 the membrane reduced the current generated by the three substances from 19 nA to 14 nA, i.e. a reduction of 71 % based on the quiescent current was achieved.

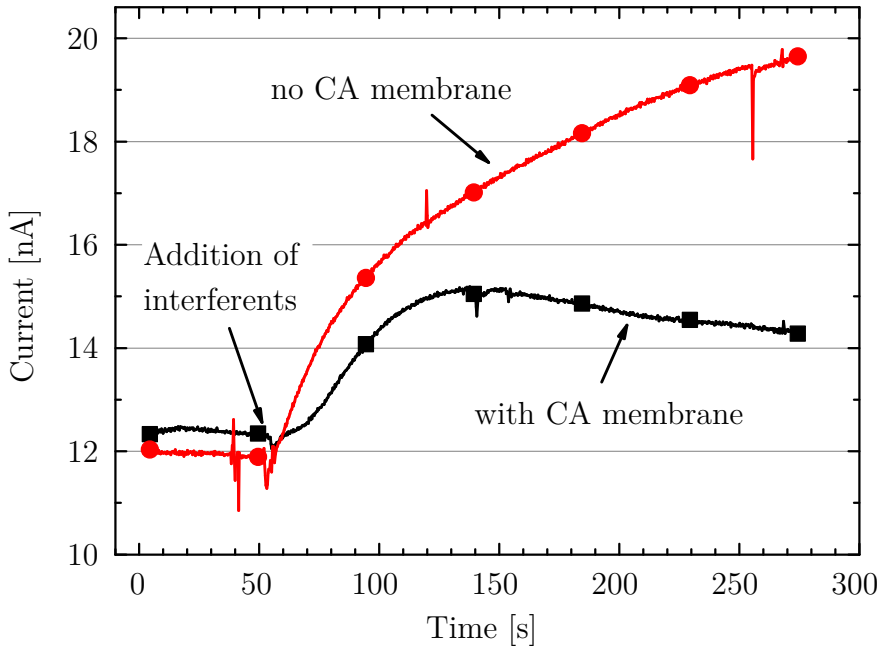

Figure 3.7: Current response of electrodes with and without cellulose acetate (CA) membrane after addition of L-glutathione, L-cysteine and ascorbic acid; CA membrane reduced current generated by interfering substances by 71 %

3.1.2 Enzyme Sensors with PU Membranes

Sensors with PDMS membranes were found to have wide linear measurement ranges and be suitable for the monitoring of cell cultures. However, the fabrication of the membrane, including spin-coating, was found to be ill-suited for the multi-sensor system, where the membrane had to be confined to the enzyme sensors and was not allowed to cover the other sensor elements. Diluting the PDMS with hexane [79] allowed to dispense the polymer solely on the enzyme sensors but distinctly lowered the measurement range. Consequently, for the multi-sensor chip polyurethane was used as membrane material since it could be dispensed specifically on the glucose and lactate sensors without dilution. PU membranes proved to give a wide measurement range, as will be shown in the following subsections.

3.1.2.1 Characterization of Morphology and Permeability

Before fabricating enzyme sensors with polyurethane membranes the influence of varying PU concentrations and solvent compositions on the membrane morphol-

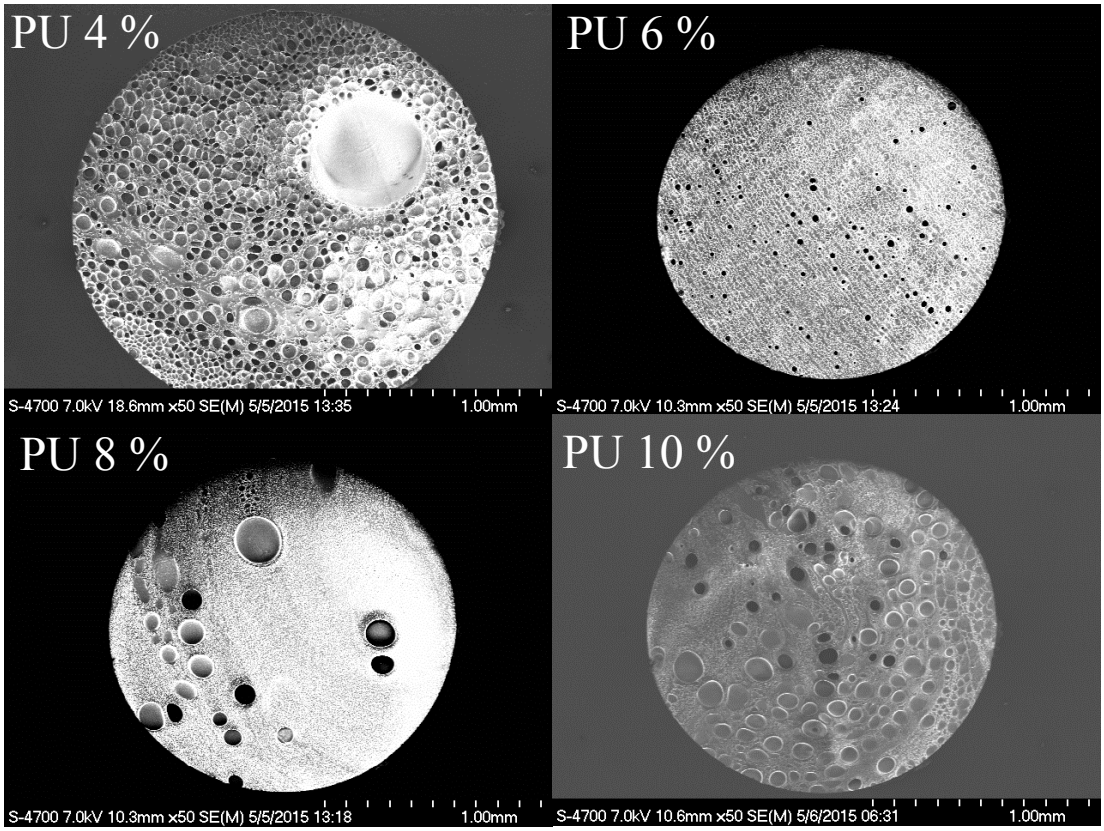

Figure 3.8: SEM images showing surface morphology of polyurethane membranes with PU concentrations of 4 %, 6 %, 8 % and 10 %, prepared with THF:DMF 9:1; morphology became finer with increasing PU concentration

ogy were assessed using a scanning electron microscope (SEM) and an atomic force microscope (AFM).

First, the influence of the PU concentration was evaluated using a fixed solvent composition of THF:DMF 9:1. Solvent compositions with such high THF contents are common in the fabrication of diffusion-limiting PU membranes [43, 68]. As is shown in Fig. 3.8 the surface of a membrane with 4 % PU contained pores with diameters from about 30 µm to 100 µm and some randomly distributed larger pores. Most of the pores did not run through the whole membrane thickness, suggesting that the membrane was predominantly made up of blind pores and hence should be regarded as a foam.

With increasing PU concentration pore diameter and depth of the pores decreased, leading to areas with higher material density. The AFM images shown in the upper row of Fig. 3.9 confirmed that with increasing polymer concentration

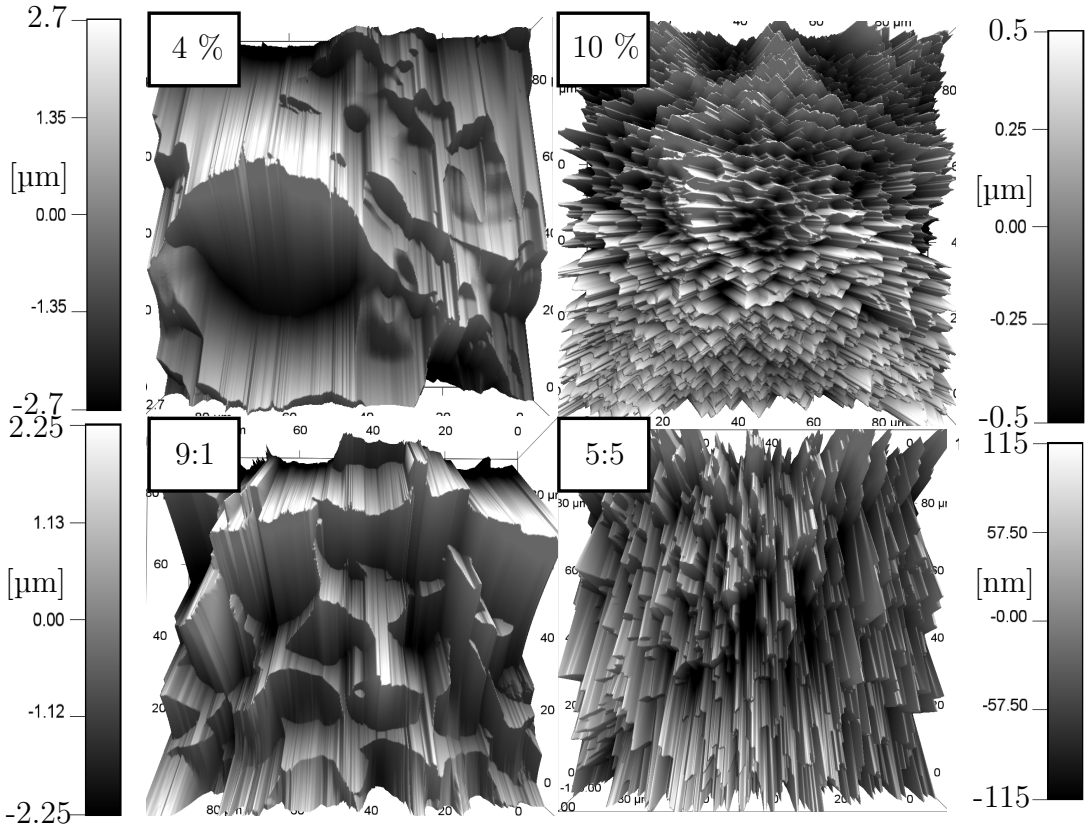

Figure 3.9: AFM images of polyurethane membranes; upper row: PU concentration of 4 % and 10 % with THF:DMF 9:1, lower row: THF-DMF ratio of 9:1 and 5:5 with PU 6 %; image size is 90 µm × 90 µm; morphology became finer with increasing PU concentration and increasing DMF content

a finer surface structure was achieved also on a smaller scale of 90 µm × 90 µm. The differences in morphology can be seen in more detail in the SEM pictures in Fig. 3.10, comparing membranes with PU concentrations of 4 % and 10 %. These detailed pictures confirm the observation that a higher polymer concentration lead to less and shallower pores. The observed increase in membrane density with increasing polymer concentration was in good agreement with well-known relations in membrane fabrication [112] and was expected to distinctly influence the membrane permeability for analytes such as glucose and lactate since a denser material with finer pores was thought to resist diffusion more than a highly porous material.

As a second fabrication parameter the ratio of the solvents tetrahydrofuran and dimethylformamide was varied as THF:DMF 9:1, 7:3, 5:5 and 3:7, using a fixed

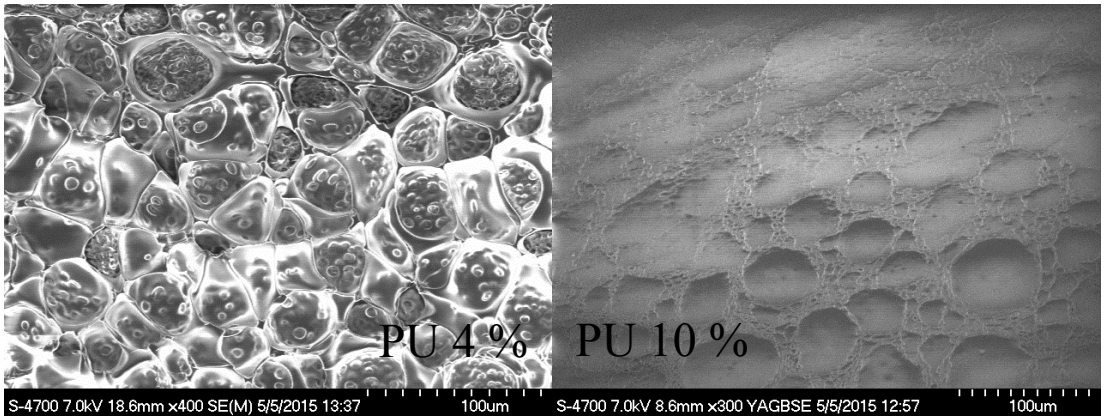

Figure 3.10: SEM images with detailed surface morphology of polyurethane membranes, PU concentrations of 4 % and 10 %, prepared with THF:DMF 9:1; a higher PU concentration gave a finer morphology with less and shallower pores

PU concentration of 6 %. The images in Fig. 3.11 indicate that with the solvent ratio changing from 9:1 to 7:3, the pore density declined and fewer, larger pores formed. A ratio of 5:5 gave a homogeneous membrane with very few, small and shallow pores, which was confirmed by an image taken at a higher magnification, shown in Fig. 3.12. The same trend could be found in the AFM pictures in the lower row of Fig. 3.9, showing a finer morphology for an increasing DMF ratio. The ratio 3:7 lead to a rather dense surface, which, however, contained big voids and defects. These were believed to increase the membrane permeability and therefore lower the measurement range for glucose and lactate. The solvent mixture with 90 % DMF did not dissolve the PU even after several days and was not considered in the following experiments. From this observations it was concluded that the PU material used in this thesis was more soluble in THF than in DMF.

In conclusion, the microscope images showed a clear relationship between increasing polymer concentration and increasing membrane homogeneity, and the THF-DMF ratio of 5:5 was determined to give the most homogeneous membranes.

Characterization of Membrane Permeability

To assess the influence of PU concentration and solvent composition on the permeability of membranes and confirm the observations from the microscope pictures, diffusion coefficients for glucose were measured for PU concentrations from

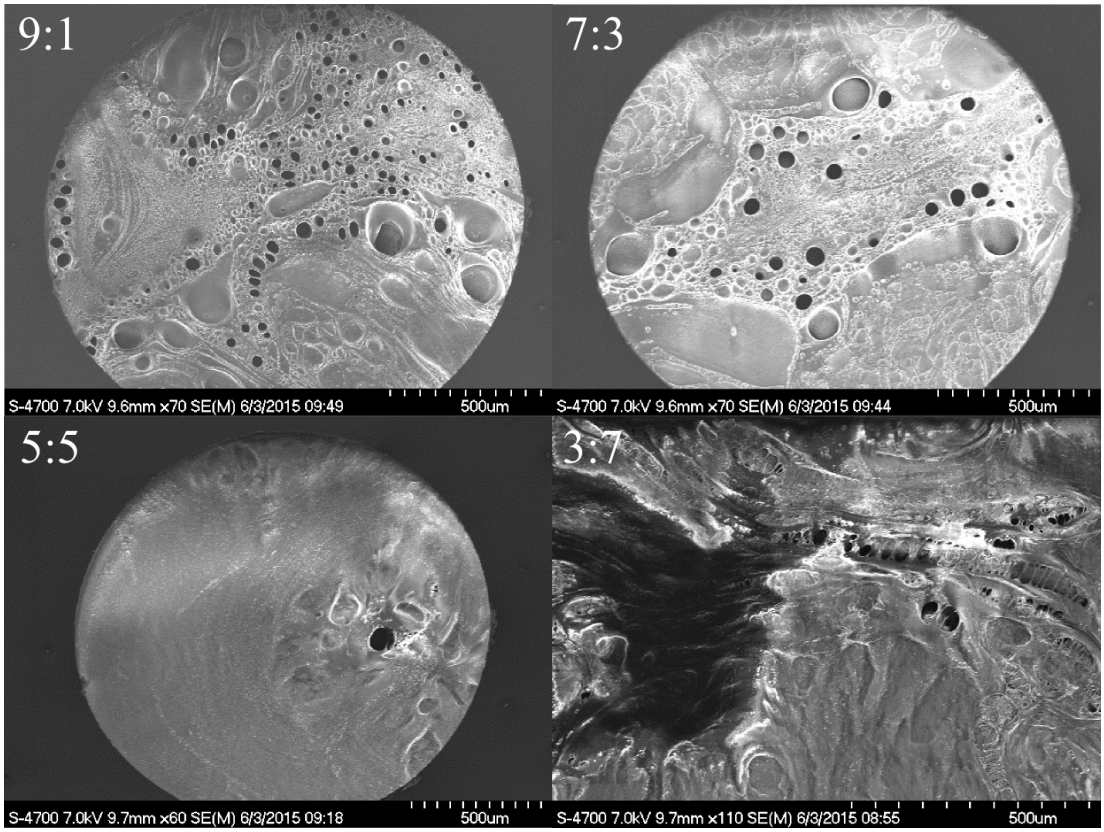

Figure 3.11: SEM images with surface morphology of polyurethane membranes with THF-DMF ratios of 9:1, 7:3, 5:5 and 3:7, PU concentration 6 %; morphology became finer with increasing DMF content up to THF:DMF 5:5

4 % to 10 % and THF-DMF ratios between 9:1 and 3:7. The results depicted in Fig. 3.13 confirm the anticipated influence of the observed surface morphology on membrane permeability. With increasing PU concentration the diffusion coefficient declined from $4.7 \times 10^{-11}\,\mathrm{m^2/s}$ to $9.7 \times 10^{-12}\,\mathrm{m^2/s}$ with a square reciprocal relationship. A similar relationship could be found for THF-DMF ratios between 9:1 and 5:5 with diffusion coefficients ranging from $2.6 \times 10^{-11}\,\mathrm{m^2/s}$ to $1.51 \times 10^{-11}\,\mathrm{m^2/s}$. A further increase of the DMF amount led to an increased diffusion coefficient of $3.21 \times 10^{-11}\,\mathrm{m^2/s}$. These results pointed to the fact that both an increased PU concentration and a higher amount of DMF up to ratio of 5:5 lead to a membrane that was less permeable to glucose and thus was thought to increase the measurement range of enzyme sensors.

The influence of the THF-DMF ratio was likely to be due to the different vapor pressures of the solvent compositions. The more DMF was contained in the sol-

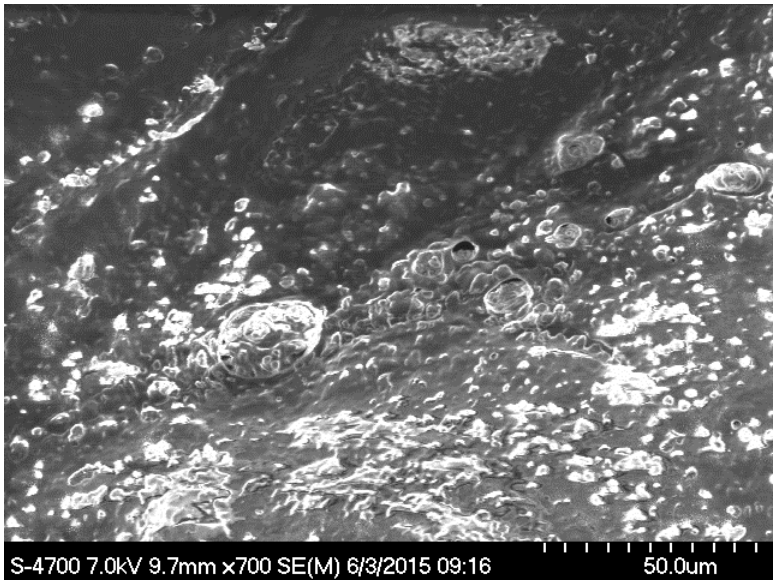

Figure 3.12: Surface morphology of polyurethane membrane with THF-DMF ratio of 5:5, PU concentration 6 %; morphology, obtained with this solvent composition, showed small, shallow pores with diameters mostly around 5 µm

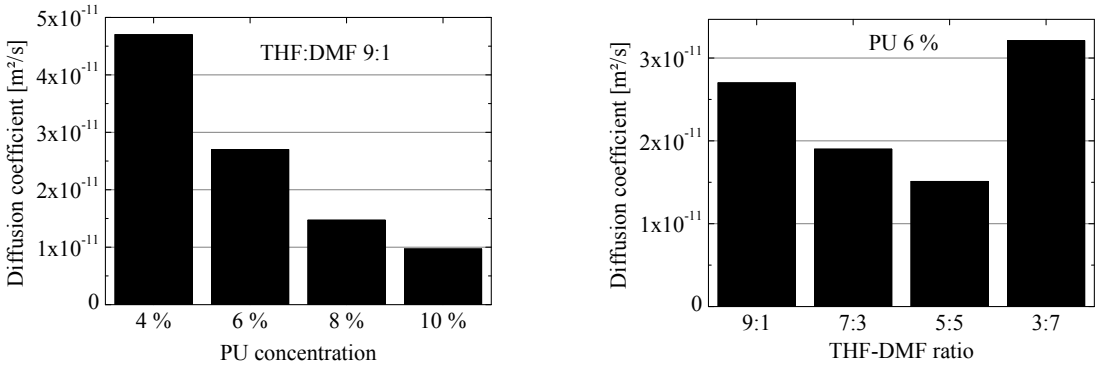

Figure 3.13: Diffusion coefficients of PU membranes for glucose with varying PU concentrations and THF-DMF ratios; an inversely proportional, square relationship was found, confirming the results of the microscope images

vent mixture, the slower the solvent evaporated, leading to a more homogeneous surface with less pores and a lower permeability. The fact that a solvent ratio of THF:DMF 3:7 lead to a surface with large defects and a ratio of 1:9 failed to dissolve the polyurethane might, however, point to a second explanation of the observed membrane morphology and permeability. While the THF evaporated the polyurethane was enriched in the DMF. Assuming the used polyurethane to be less soluble in DMF than in THF conceivably the polymer precipitated in the

DMF, already formed pores collapsed, and a dense membrane formed instead of a porous one [112]. This phenomenon is well-known in phase inversion processes for membrane fabrication [63] and is proposed here as an alternative explanation for the observed relationship between solvent composition and membrane properties.

3.1.2.2 Evaluation of Enzyme Sensors with PU Membranes

After the morphology and permeability of the polyurethane membranes had been evaluated, the linear measurement range of enzyme sensors coated with these membranes was studied. As a preliminary step the amperometric signals of the small and big electrode variant on the multi-sensor chip without enzyme and membrane layers were recorded in 100 µM and 1 mM H_2O_2 solutions to determine the influence of the electrode area on the oxidation current. In 100 µM solution small electrodes gave a current around 30 nA and big electrodes had a current around 60 nA. The twofold current of the big electrode with twice the area of the small variant confirmed the linear relationship between electrode area and oxidation current described by the Cottrell equation (see Eq. 2.13 in section 2.1.3). In 1 mM solution currents of approx. 500 nA and 900 nA were recorded for the small and big variant, respectively. The observed deviation from the linear relationship was ascribed to the high H_2O_2 concentration, leading to small gas bubbles at the electrode surface and complicated determination of the oxidation current.

As a first step in the investigation of the enzyme sensors glucose sensors were fabricated on multi-sensor chips and the signal without a diffusion-limiting membrane evaluated. All studies were first performed with glucose sensors before being extended to lactate sensors. The response of a glucose sensor to 5 mM glucose is shown in Fig. 3.14. The sensor had a linear range of around 2 mM with a sensitivity between 90 nA/mM and 100 nA/mM. Response times varied with glucose concentrations and ranged from 45 s to 120 s.

No clear relationship between electrode area and current in response to glucose could be established. It was concluded that due to variations in the manual electrode functionalization the behavior of the enzyme layer was not consistent enough to determine the influence of the electrode area. Nevertheless, the achieved sensitivity was in good agreement with reported high values for enzyme electrodes [43, 44] with slightly longer response times, which were acceptable for

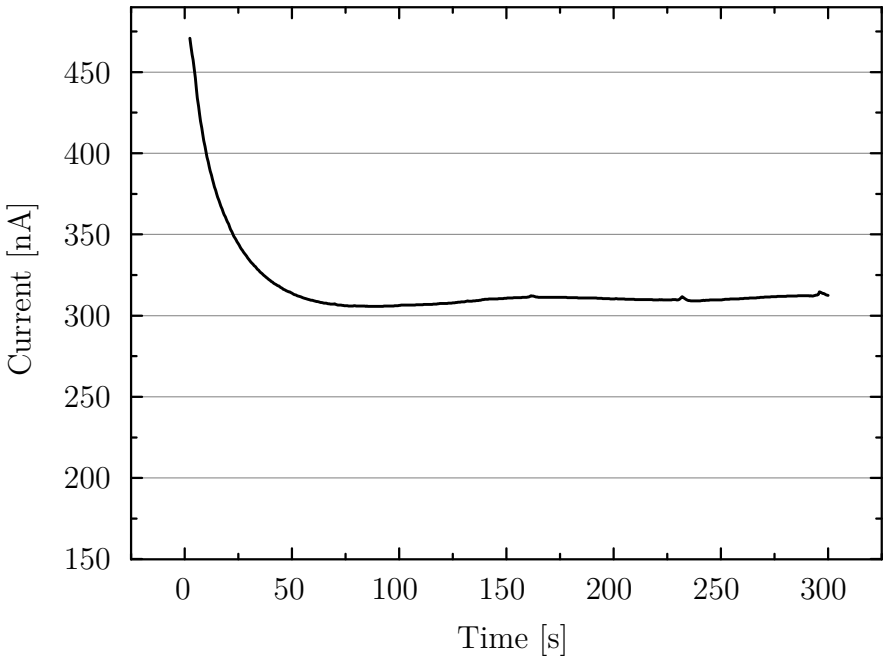

Figure 3.14: Signal of glucose sensor without PU membrane after immersion into 5 mM glucose; response time of around 70 s was in accordance with enzyme sensors demonstrated by others

bioprocess monitoring. Hence, the found performance was expected to enable good performance of membrane-covered electrodes.

The differences in response time of the on-chip glucose electrodes in comparison to the ceramic electrodes were attributed to the smaller amount of enzyme solution dispensed onto the chip, leading to a thinner enzyme layer. It has been shown that the thickness of the enzyme layer is inversely related to the sensor response time [57]. The higher sensitivity of the on-chip electrodes could not be ascribed to a single factor; however, deviations in enzyme activity or differences in the surface morphology between screen-printed and evaporated metal electrodes could have played a role.

Influence of PU concentration

Fig. 3.15 shows the linear measurement range of glucose sensors with PU membranes fabricated with polymer concentrations of 4 % to 10 % with a THF-DMF ratio of 9:1. In general, the relation between PU concentration, linear range and sensitivity corresponded with the relation found for the morphology and diffusion

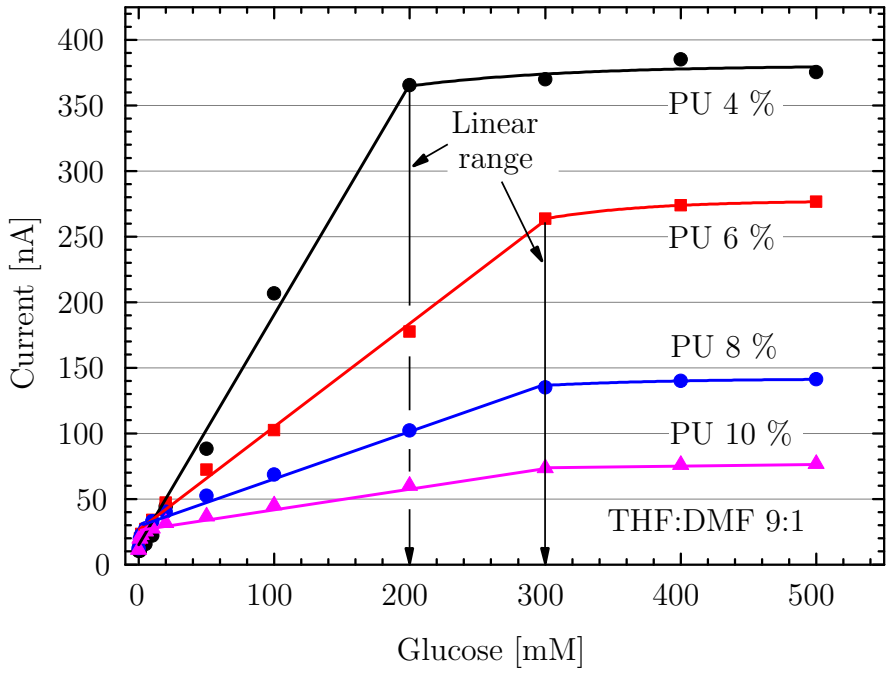

Figure 3.15: Calibration curve of glucose sensor with PU membranes, PU concentration 4 % to 10 %, ratio THF:DMF 9:1; linear range up to 300 mM

coefficients of the membranes. A PU concentration of 4 % extended the linear range to 200 mM, while higher concentrations gave an extension to 300 mM. With increasing concentration the sensitivity of the sensors decreased, ranging from ca. 2 nA/mM to around 0.3 nA/mM. The resolution behaved similarly and decreased from 1 mM to 5 mM. Response times ranged from 60 s to 320 s.

The decreasing signal and increasing linear range supported the previous findings that higher polymer concentrations gave a denser membrane with a lower permeability. The sensitivity behaved more or less similarly to the permeability for the different polymer concentrations, confirming the anticipated sensor behavior. The fact that polymer concentrations above 6 % did not extend the linear range further could be attributed to a non-sufficient oxygen supply to the enzyme layer under the membrane [13, 42].

Influence of solvent composition

The influence of the solvent composition is depicted in Fig. 3.16. As with the PU concentration a parallel could be drawn between the influence of solvent composition on morphology and diffusion coefficient and on the measurement perfor-

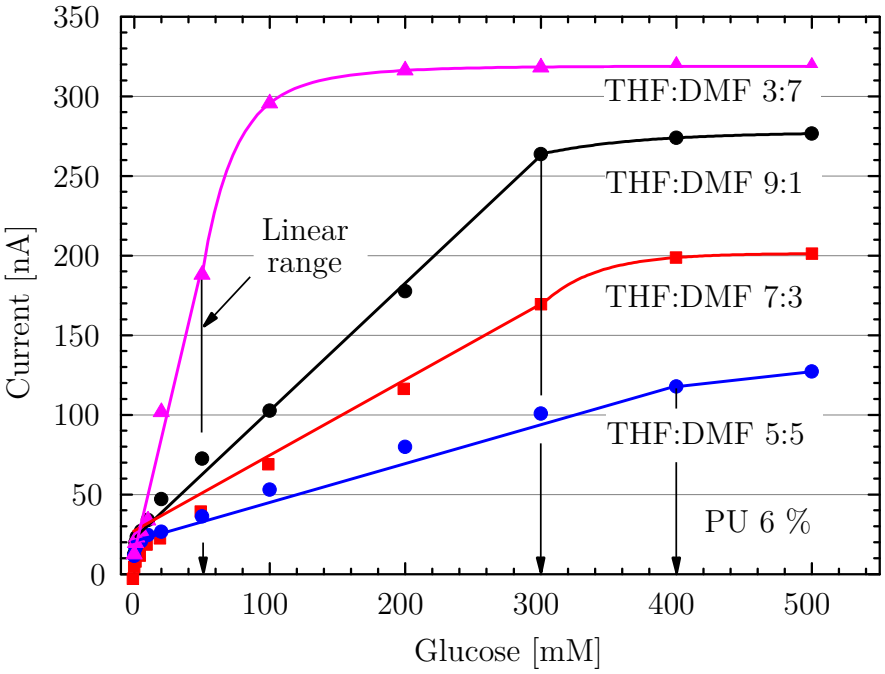

Figure 3.16: Calibration curve of glucose sensor with PU membranes with varying THF-DMF ratios, PU concentration 6 %; linear range up to 400 mM

mance. The linear limit ranged between 300 mM for a solvent ratio of THF:DMF 9:1 and 400 mM for a ratio of THF:DMF 5:5. Sensitivity and resolution were between 0.8 nA/mM and 1 mM and 0.4 nA/mM and 5 mM, respectively. As anticipated, the ratio THF:DMF 3:7 gave the slightest extension to 50 mM, which could be ascribed to the large voids found in the membrane. These presumably did not limit the flux of glucose through the membrane. The sensitivity in general showed the same dependence on the solvent composition as the membrane permeability determined earlier. The limit of the linear measurement scaled approximately linearly with the membrane permeability and thus confirmed the theoretical relationship established in Eq. 2.31 in section 2.1.4.2. However, as pointed out in the discussion of the sensors with PDMS membranes, Eq. 2.31 should be treated as a rough estimation instead of a precise description of the sensor performance.

The thickness of the PU membranes varied between 1.5 µm for membranes with 4 % PU to around 2.5 µm for membranes with 10 % PU, exemplarily determined for a solvent ratio of THF:DMF 5:5. Hence, the membrane thickness played a much smaller role in comparison with sensors with PDMS membranes, where

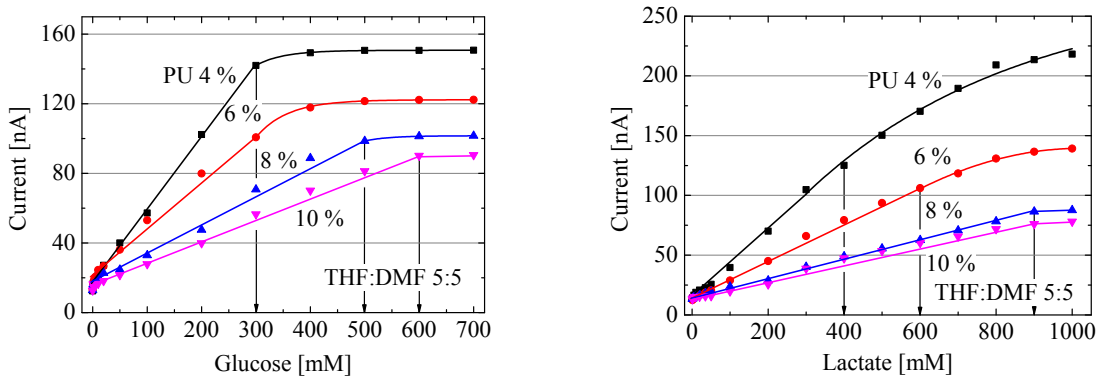

Figure 3.17: Calibration curves of glucose and lactate sensors with optimized PU membranes, PU concentration 4 % to 10 %, ratio THF:DMF 5:5; linear range up to 600 mM for glucose and 900 mM for lactate, covering a significant part of the concentrations found in bioprocesses

thickness was purposefully varied between 4.5 µm and 35 µm. Nevertheless, part of the observed sensor behavior could be ascribed to the effect of PU membranes becoming thicker with increasing polymer concentration.

Since the focus of membrane development was the achievement of a wide linear measurement range the membrane series with THF-DMF ratio of 5:5 was identified as the optimum ratio for diffusion-limiting PU membranes and also used in the fabrication of lactate sensors. In Fig. 3.17 the calibration curves of glucose and lactate sensors with optimized PU membranes are shown. With these membranes the linear range for glucose and lactate could be extended to 600 mM and 900 mM with sensitivities of 0.12 nA/mM and 0.07 nA/mM, respectively, making the sensors more suited for wide-range measurements than determination of small changes in substance concentrations. Both sensors had a resolution of 1 mM at 4 % PU and 5 mM at 10 % PU. The differences between glucose and lactate were likely caused by the different Michaelis constants of glucose oxidase and lactate oxidase, leading to a different behavior of the enzyme layers and hence of the whole sensor. Since lactate oxidase has a smaller Michaelis constant than glucose oxidase (0.7 mM vs. 33 mM [58]), however, a lower limit of the linear range for lactate was expected. This contradicting behavior has to be studied in further experiments.

In conclusion, the enzyme sensors with optimized PU membranes covered a significant range of the glucose and lactate concentrations found in bioprocesses,

THF-DMF ratio	PU conc. [%]	Lin. Range [mM]	Sensitivity [nA/mM]
Glucose			
9:1	4	200	1.96
	6	300	0.82
	8	300	0.48
	10	300	0.25
9:1	6	300	0.82
7:3	6	300	0.64
5:5	6	400	0.37
3:7	6	50	2.76
5:5	4	300	0.4
	6	300	0.37
	8	500	0.17
	10	600	0.12
Lactate			
5:5	4	400	0.26
	6	600	0.17
	8	900	0.11
	10	900	0.07

Table 3.3: Linear range and sensitivity of enzyme sensors with PU membranes

making the sensors well suited for applications in bioprocesses. The performance of the enzyme sensors with the different PU membranes is summarized in Tab. 3.3.

Sterilization

All equipment introduced into bioreactors needs to be sterilized. Physical sensors without biological elements are typically steam sterilized, however, for enzyme sensors the high temperature above 120 °C of this sterilization procedure is prohibitive because of the irreversible denaturation of enzymes at high temperatures, destroying the functionality of the biomolecules. For glucose oxidase

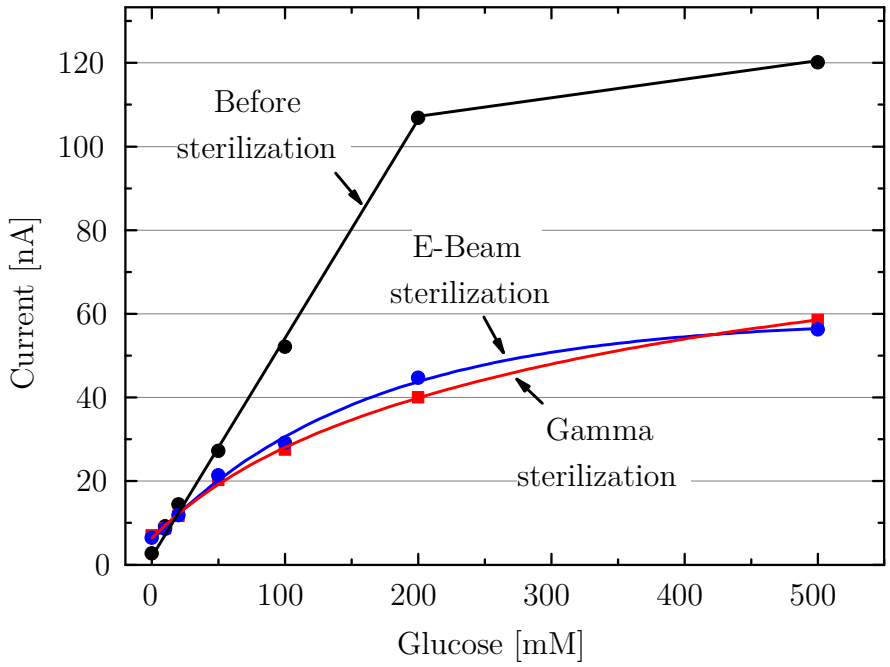

Figure 3.18: Calibration curves of glucose sensors with optimized PU membranes (PU 4 %, THF:DMF 5:5) before and after gamma and electron beam sterilization at a dose of 25 kGy each; sensors remained functional and both sterilization methods had almost the same effect on the sensor sensitivity

denaturation occurs at temperatures above 56 °C [113], for lactate oxidase above 70 °C [114]. As a solution other sterilization procedures have been proposed, among them treatment with chemicals such as glutaraldehyde [115], and gamma or electron beam irradiation [116, 117]. In comparison to chemical treatment, irradiation offers a more convenient and faster way to sterilize sensors. To assess the general suitability of the used functionalization method for sterilization glucose sensors with optimized PU membranes (4 % PU, THF:DMF 5:5) were sterilized using gamma and electron beam irradiation at a dose of 25 kG each (mediscan GmbH, Austria). This dose has been shown to ensure a high sterility assurance level of 1×10^{-6} for many medical devices [118]. As can be seen from the calibration curves in Fig. 3.18 the sensors lost up to 60 % of their sensitivity during the sterilization but remained functional. The impact of both sterilization methods on the sensitivity was almost similar, suggesting that both are equally suited for enzyme sensors. The long-term performance of sterilized sensors has to be investigated in further experiments.

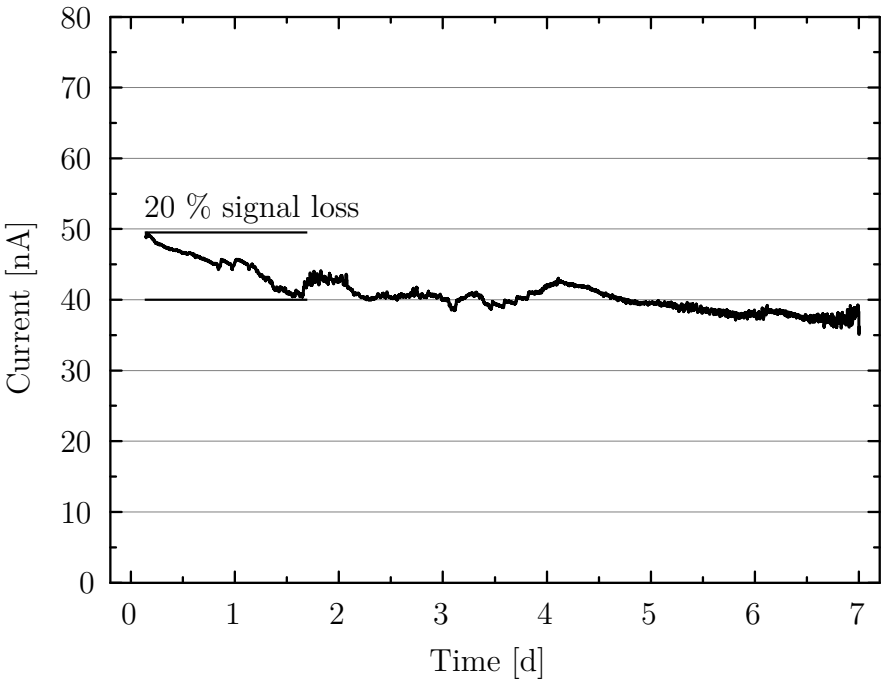

Figure 3.19: Long-term performance of optimized glucose sensor in 200 mM glucose, THF:DMF 5:5, PU 6 %; sensor showed initial signal loss of 20 % but remained functional over the whole measurement duration

Evaluation of Long-Term Performance

After the measurement range and sensitivity of the sensors had been investigated, the long-term performance of an optimized glucose sensor with THF:DMF ratio of 5:5 and an exemplary polymer concentration of 6 % was evaluated in a 200 mM glucose solution. As can be seen from Fig. 3.19 the sensor showed an initial signal loss of around 20 % during the first 36 h, but otherwise had a stable signal. After day 7 the PU membrane detached from the enzyme layer, leading to dissolution of the enzyme layer and loss of sensor signal within a few hours. Improving the adhesion of the PU membrane on the chip surface is expected to have a high chance to increase the sensor lifetime and extend the application range to longer culture runs.

To further assess the long-term performance of the enzyme sensors and verify the found results a prolonged measurement run was simulated by keeping glucose sensors with optimized membranes (PU 4 %, THF:DMF 5:5) in PBS and performing calibration measurements every 7 days. Over this period of permanent contact with aqueous solution changes of the sensor behavior are possible due

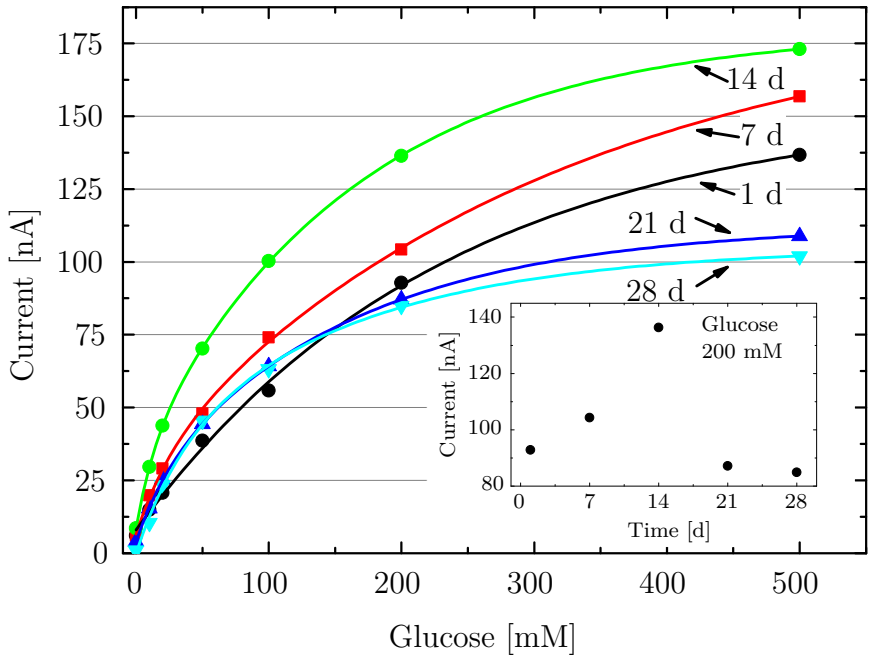

Figure 3.20: Long-term performance of glucose sensors with optimized PU membranes (PU 4 %, THF:DMF 5:5) over 28 days; storage in PBS between calibration measurements; inset shows sensor signal at 200 mM glucose over time

to effects such as changing membrane permeability [16]. As can be seen from Fig. 3.20 the sensitivity of the sensors increased from 0.5 nA/mM at day 1 to 0.9 nA/mM at day 14. At the same time the linear measurement range decreased from 200 mM to 20 mM. During the following 14 days the sensitivity decreased to about the value at the first day. The behavior during the first 14 days could be ascribed to an increasing permeability of the diffusion-limiting membrane, stemming from water uptake of the polymer or changes in the polymer structure [16]. In the second phase of the experiment, possibly, a decreasing enzyme activity acted contrarily to the increasing membrane permeability. For reliable long-term measurements the sensors can be re-calibrated by adding a bolus of known concentration to the cell culture medium and determining the sensitivity from the induced signal increase.

The longer measurement duration achieved in this experiment in comparison to the results shown in Fig. 3.19 pointed to the fact that the membrane adhesion on the chip surface varied from batch to batch. This could be attributed to the small batch sizes and functionalization of the sensors by hand and is expected to be resolved when sensors are produced using automated equipment such as

dispensing robots.

Cell Culture Monitoring

To evaluate the suitability of the fabricated sensors for the monitoring of bioprocesses the glucose level in a yeast culture was monitored using a glucose sensor with an optimized PU membrane (PU 6 %, THF:DMF 5:5). The culture was prepared in PBS with an initial cell density of 1 g/l and a glucose concentration of 50 mM. The culture was continuously stirred and aerated at a rate of 150 l/h, and the pH was kept at pH 6 by addition of potassium hydroxide. Every 24 h glucose solution was added to increase the concentration by 50 mM, and every fourth day the culture was replaced to avoid the fermentation from getting stuck. Samples were drawn immediately before and after the addition of glucose, diluted and analyzed using a spectrophotometric assay, based on a reaction with *o*-dianisidine (Sigma Aldrich, USA). The signal of the glucose sensor is shown in Fig. 3.21. During the first one and a half days the sensor was conditioned and calibrated. Consumption of glucose and replenishment can be clearly seen from the sensor signal, being in good correlation with the reference measurements. The first and third culture, running until day 4 and from day 8 onwards, respectively, turned out to be sluggish and not consume all the glucose, which can be seen from the sensor signal not reaching 0 mM. In general, the sensor signal showed good performance over the whole fermentation duration of 13 days, demonstrating the suitability of the fabricated glucose sensors for bioprocess monitoring.

Conclusion

In conclusion, both PDMS and polyurethane were found to be suitable membrane materials for wide-range enzyme sensors for application in bioprocess monitoring. The wider measurement ranges, shorter response times and easier fabrication put polyurethane in front of PDMS and made sensors possible that cover a significant part of the concentration ranges of glucose and lactate in bioprocesses. These sensors allow to monitor fermentation processes with medium to high substrate concentrations and lactate production with high yield for biodegradable polymers. As for the sensors with PDMS membranes, the sensitivities below 1 nA/mM qualify the sensors for determination of wide concentration ranges of analytes instead of fine differentiations, which was found feasible for the moni-

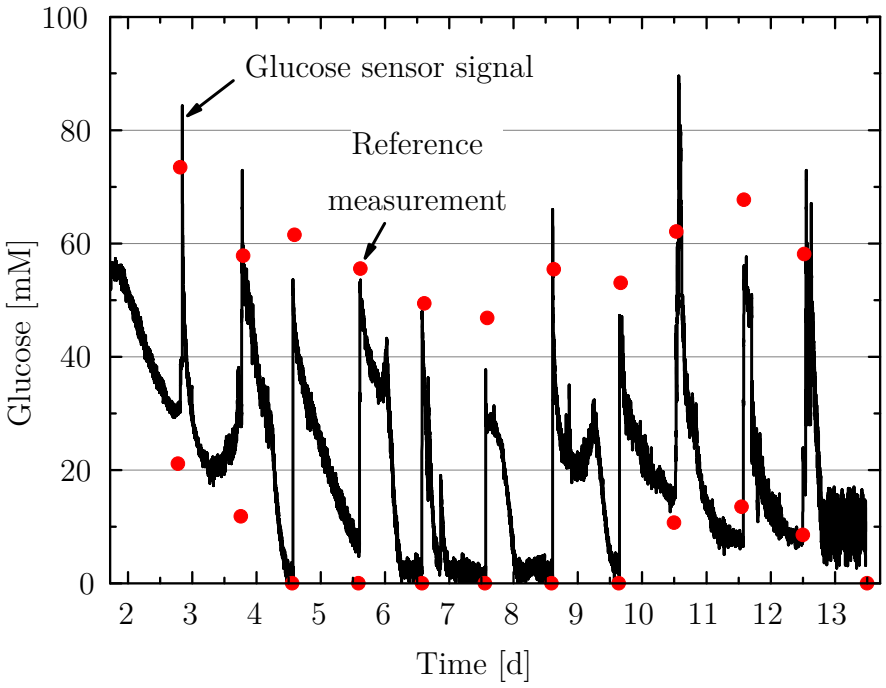

Figure 3.21: Glucose monitoring in a yeast culture over 13 days using a glucose sensor with an optimized PU membrane (PU 6 %, THF:DMF 5:5); glucose was added every 24 h to increase the concentration by 50 mM; curve: sensor signal, red dots: spectrophotometric reference measurements (Sigma Aldrich, USA)

toring of fermentation processes. By lowering the PU concentration in the membrane higher sensitivities could be achieved and the sensor performance adjusted to other applications such as the monitoring of mammalian cell cultures.

3.2 Cell Density Sensor

To determine the general behavior of the fabricated interdigitated electrodes (IDE) the impedance spectra of the IDE variants were determined in 10 mM PBS buffer in a frequency range from 1 kHz to 30 MHz. The results are shown in Fig. 3.22 and listed in Tab. 3.4, where $\hat{f}$ and $\hat{R}$ denote measured values. In Fig. 3.23 the design of the variants is shown for comparison.

The lower cutoff frequencies ranged between 30 kHz and 250 kHz and for most variants were in general agreement with the values calculated in the design phase. The upper cutoff frequencies were between 7 MHz and 10 MHz for all variants, meaning that these frequencies were by 50 % to 65 % lower for variants 1 to 6

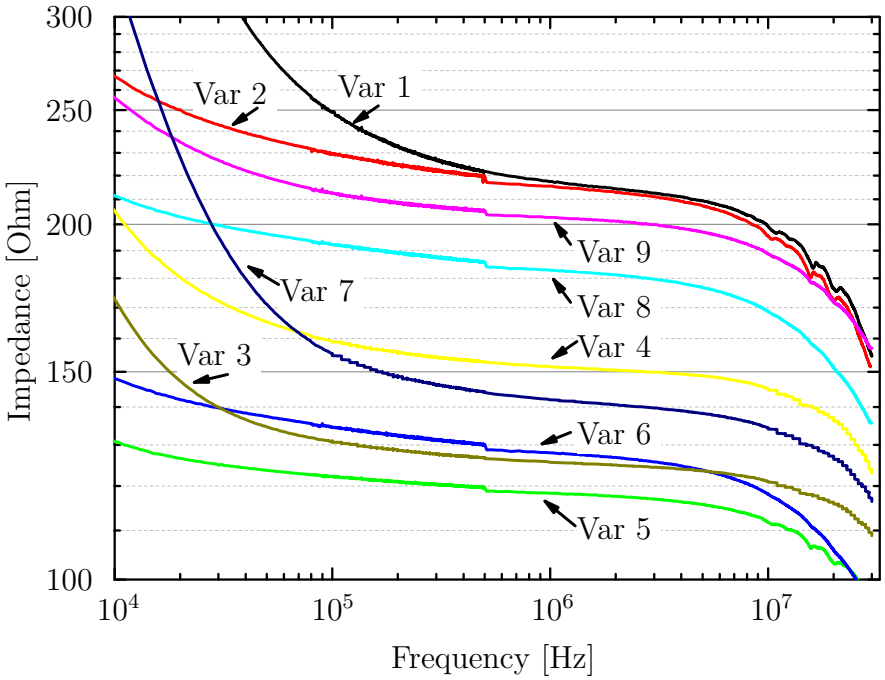

Figure 3.22: Impedance spectra of interdigitated electrodes in 10 mM PBS; sensor variants had ohmic plateaus ranging from 20 kHz to 10 MHz

and by 10 % to 20 % lower for variants 7 to 9 in comparison to what had been calculated in the design phase. From this behavior it was concluded that the estimation of the upper cutoff frequency in Eq. 2.56 introduced a significant error, especially for values above 10 MHz. Since Eq. 2.56 included both the cell constant K_{Cell} and the wiring capacitance C_{Wire} the error could have been introduced by any of the two parameters. Given the facts that the resistances of the ohmic plateaus were consistently higher by a factor of 3 to 6 than the theoretically calculated values and the considered parasitic capacitance of $C_{\mathrm{Wire}} = 200\,\mathrm{pF}$ was in accordance with other work [93], the calculation of K_{Cell} was assumed to be the main source of error.

Assuming the theoretically calculated cell constants of 0.36 1/cm for variants 1 to 6 and 0.76 1/cm for variants 7 to 9 the ohmic plateaus were expected to be at 36 Ω for variants 1 to 6 and 76 Ω for variants 7 to 9. Instead, the curves showed distributed plateaus with resistances ranging from around 120 Ω to 210 Ω, taken in the middle of each plateau. Consequently, the cell constants derived from these resistances at a solution conductivity of 10 mS/cm were between 1.2 1/cm and 2.1 1/cm.

Var	f_{High} [MHz]	$\hat{f}_{\text{High}}$ [MHz]	f_{Low} [kHz]	$\hat{f}_{\text{Low}}$ [kHz]	R [Ω]	$\hat{R}$ [Ω]
1	20	7	112	250	36	210
2	20	7	56.3	50	36	210
3	20	10	56.3	70	36	125
4	20	9	56.3	80	36	150
5	20	8	41.6	30	36	120
6	20	7	20.8	30	36	125
7	10	9	56.3	200	76	140
8	10	8	41.6	30	76	180
9	10	8	20.8	70	76	200

Table 3.4: Results of impedance measurements with IDE variants and comparison with theoretically calculated values; $\hat{f}$ and $\hat{R}$ denote measured cutoff frequencies and resistances of the ohmic plateau, f and R are calculated values

Such deviations of the cell constant have been described in the literature [119] and could be ascribed to fringing electric field lines running through the chip substrate [94]. Also, the existence of inductances, which were not considered in the design phase, has been proposed as an explanation [119]. A clear relationship between the measured resistance and electrode area or spacing could not be established. However, the resistance distinctly corresponded to the length of the electrodes, giving smaller values for longer electrode fingers. Therefore, the finger length was identified as the most determining parameter for the resistance of the IDE and the calculation of the cell constant.

Since the upper measurement frequency for cell density measurements in yeast suspensions was 10 MHz, the found deviations of the upper cutoff frequency could possibly distort these measurement. To evaluate possible impacts on the sensor performance calibration measurements in yeast suspensions were performed.

Evaluation of Measurement Performance

In order to evaluate the measurement performance of the cell density sensor calibration measurements in stirred yeast suspensions were performed. For this, variants 2, 3, 5 and 9 were employed, differing significantly in finger width, spacing and length. In the equivalent circuit diagram in Fig. 3.24 the cells were modeled as

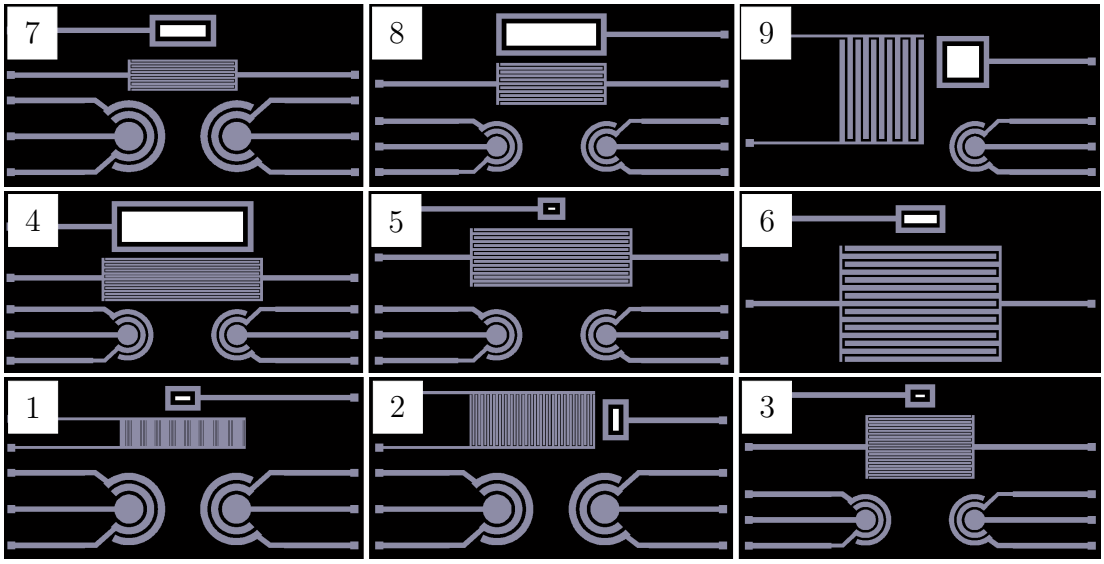

Figure 3.23: Design variants of interdigitated electrodes with enzyme electrodes and pH sensor; platinum layer is shown in gray color, pH sensitive area in white color; figures show detailed views of chip variants

a capacitor with capacitance C_{Cell} and a resistor with resistance R_{Cell}, representing the resistance of the cell cytoplasm. These elements were thought to act in parallel to the branches modeling the electrode behavior.

The measurement signal of variant 3 is shown exemplarily in Fig. 3.25. In general, all evaluated variants were able to measure cell densities between 0 g/l and 20 g/l with linear ranges going up to 10 g/l. Thus, the shifted upper cutoff frequencies observed in the impedance spectra did not prohibit the measurement of cell densities. Sensitivities ranged between 0.15 % per g/l for variant 2 and 0.35 % per g/l for variant 9 in the linear range, being in accordance with the reported performance of similar sensors for cell density [97]. The resolution of the sensors was determined as 0.01 g/l, allowing the measurement of cell density with high resolution.

The combined results in Fig. 3.26 and Fig. 3.27 show that the design parameters had significant influence on the sensitivity. Increasing finger width and spacing resulted in a higher sensitivity and a declining linear measurement range. A possible explanation for this behavior could be that the electric field lines of electrodes with wider spacing reach farther into the cell solution than those with narrower spacing, thereby encountering more cells. The more cells are in the way

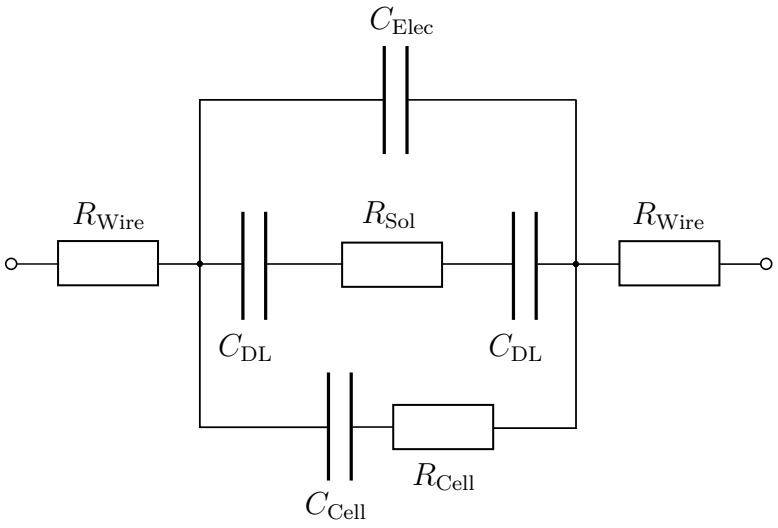

Figure 3.24: Equivalent circuit diagram of interdigitated electrodes in cell suspension; C_{Cell}: capacitance of cells, R_{Cell}: resistance of cell cytoplasm, C_{DL}: capacitance of electrical double layer, C_{Elec}: capacitance between electrodes, R_{Sol}: solution resistance, R_{Wire}: wiring resistance

of the electric field lines, the more the conductivity is lowered, leading to a higher signal change per increase in cell mass.

Another explanation for the observed performance could be that the cell density close to the chip surface is thought to be lower than in the bulk solution [97]. Consequently, electrodes with narrower spacing, measuring in the vicinity of the surface, would detect a lower cell density than those measuring in larger volumes and thus generate a smaller signal.

The relationship between finger length and measurement sensitivity showed in general similar behavior to the finger width. With increasing length the signal per gram of yeast cells rose, the reason of which could be that the electric field lines of longer fingers pass through a larger volume of cell suspension and hence exhibit a larger influence of the cells. This result was in compliance with the observed relationship between the finger width and spacing and the sensitivity.

The relation between the IDE design parameters and the sensitivity of the cell density sensor variants, calculated at a cell density of 10 g/l, is summarized in Fig. 3.27. Since there were two variants with the same finger length, spacing and width, respectively, for these values a mean sensitivity is shown in the diagrams.

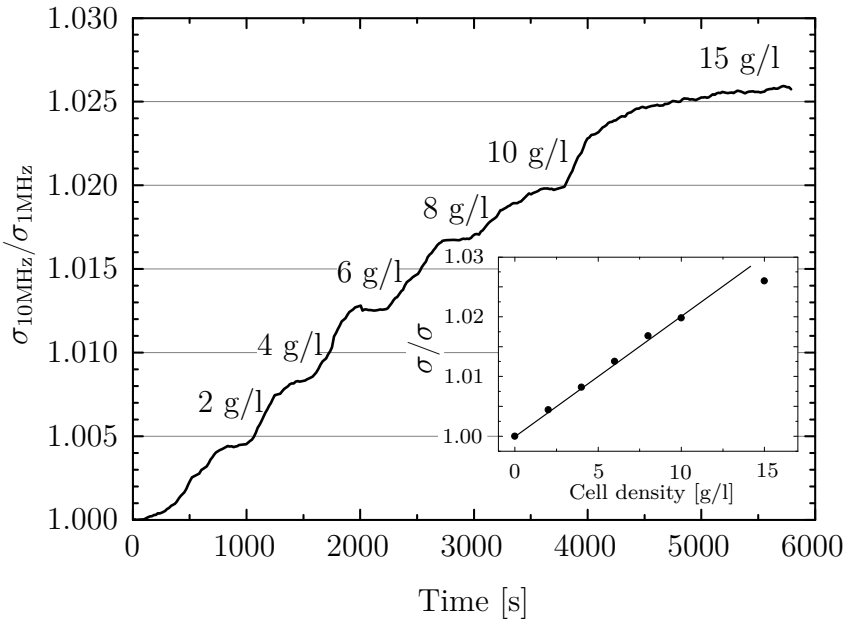

Figure 3.25: Measurement signal of IDE variant 3 in yeast suspensions of increasing concentration; inset shows calibration curve

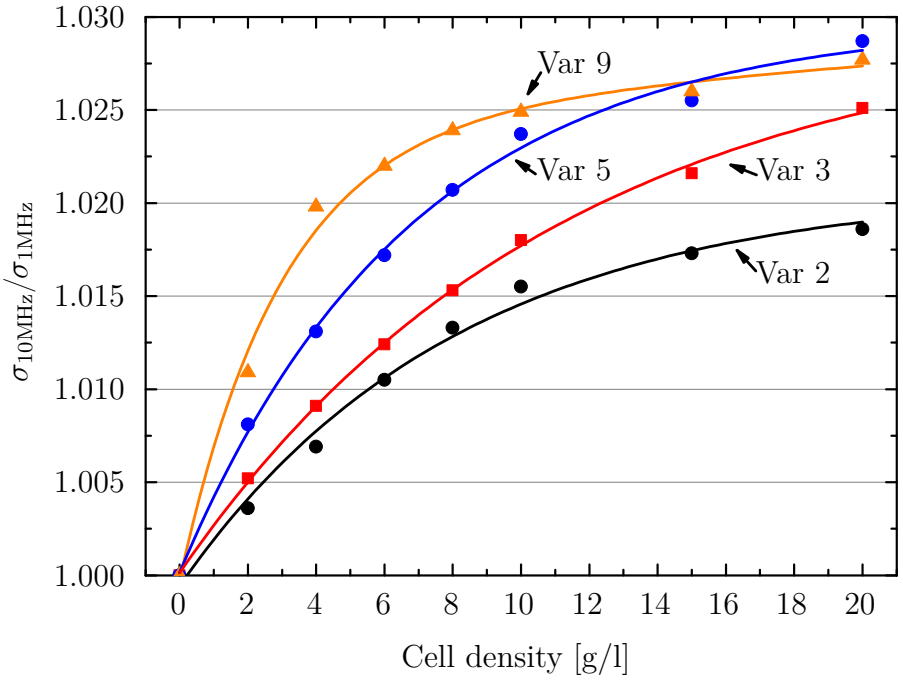

Figure 3.26: Combined results of cell density measurements for variants 2, 3, 5 and 9

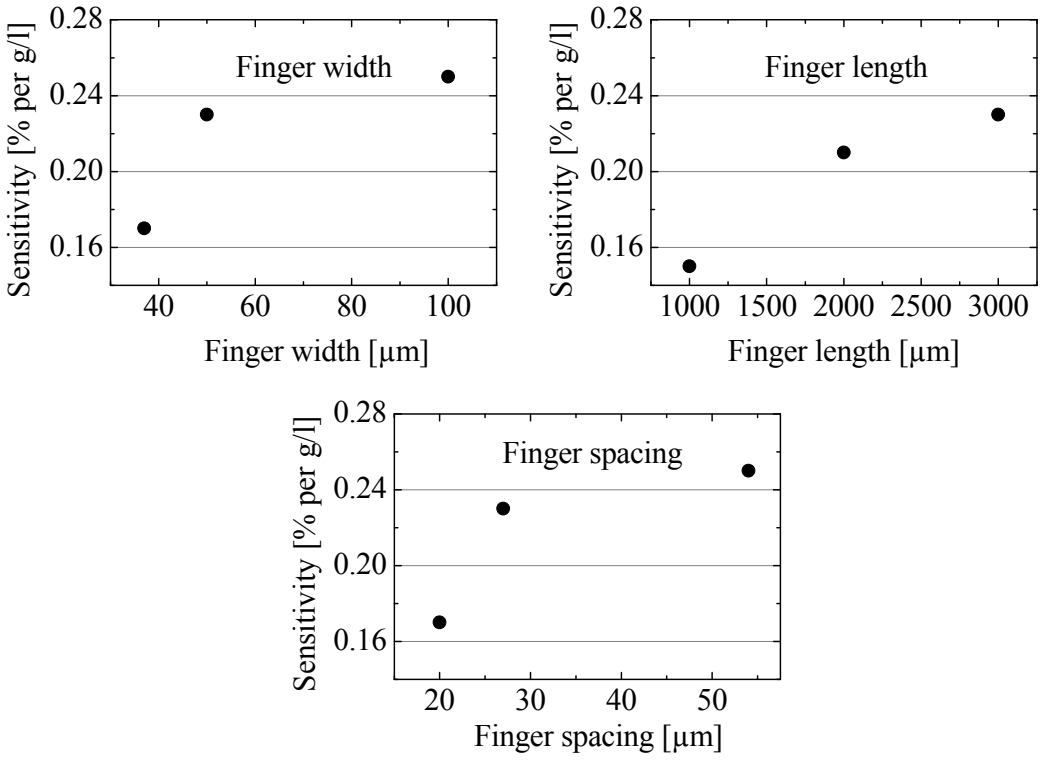

Figure 3.27: Relationship between IDE design parameters and sensitivity of the cell density sensor variants, calculated at a cell density of 10 g/l

Conclusion

Taken as a whole, the achieved sensitivities and resolution together with the low noise even at high stirring speeds allowed precise and reliable determination of the cell density despite the found deviations in the impedance spectra. The signals of all variants showed low noise even at high stirring speeds and response times between 800 s and 1000 s for concentration increments of 2 g/l and approximately 2000 s for increments of 5 g/l, as can be seen from Fig. 3.25. These response times are adequate for cell culture monitoring since the doubling time even of fast organisms is in the order of 20 min [3], and concentration changes are typically lower than what was applied in the calibration experiments.

Considering the fact that measurements were performed with instant yeast and the relation between the weight of instant yeast and the weight of dried yeast samples taken from a culture has been given as approximately 2:1 [120], the sensors were assumed to measure cell densities up to around 40 g/l. This

measurement range is suitable for mammalian cell cultures as well as many fermentation processes. To cover a wider range of fermentation processes with cell densities of 80 g/l and above [120] an expansion of the measurement range is necessary. Such ranges have been achieved in measurements relying solely on the phase angle of the impedance signal [90], offering a promising approach for future work.

3.3 pH Sensor

To study the general behavior of the pH sensor C-V measurements were performed with the fabricated variants in PBS buffer with pH 7.4. Before measurements, the chips were stored in PBS overnight to allow possibly slow first binding and release reactions of the surface hydroxy groups to take place. As depicted in Fig. 3.28 the C-V curves showed capacitances between 4.5 nF and 11.5 nF and, except for variant 3, had a threshold voltage of approximately 250 mV. Variant 3 had a threshold voltage around 150 mV. The curve of variant 9 is not shown in the diagram since it showed a capacitance in the range of 900 pF, which was much smaller than the other variants. This low capacitance could have been caused by a faulty attachment of the chip on the die attach pad of the printed circuit board, leading to a badly conducting connection. The measured capacitances together with the theoretically calculated values are listed in Tab. 3.5, where $\hat{C}_{\mathrm{pH,Diff}}$ and $\hat{C}_{\mathrm{Total}}$ indicate measured values.

The capacitance step C_{Diff}, originating from the formation of the depletion layer, matched the calculated values well for most variants, confirming the calculations in the design phase. The overall capacitances were consistently higher by 4 nF to 7 nF than the calculated values. This deviation stemmed mainly from the fact that the chip, after having been mounted on a printed circuit board, was entirely immersed in the measurement solution. This setup differed from the original plan that included a fluidic chamber confining the solution to the sensor area of the chip. Consequently, the capacitance of the circumferential chip edge, which now contacted the measurement solution, had not been considered in the design phase. Also, the SiO_2 grown in the remaining chip area was found to be 20 % thinner than what had been assumed. Depending on the amount of potting compound applied on the chip edges this parallel capacitance was between 3 nF

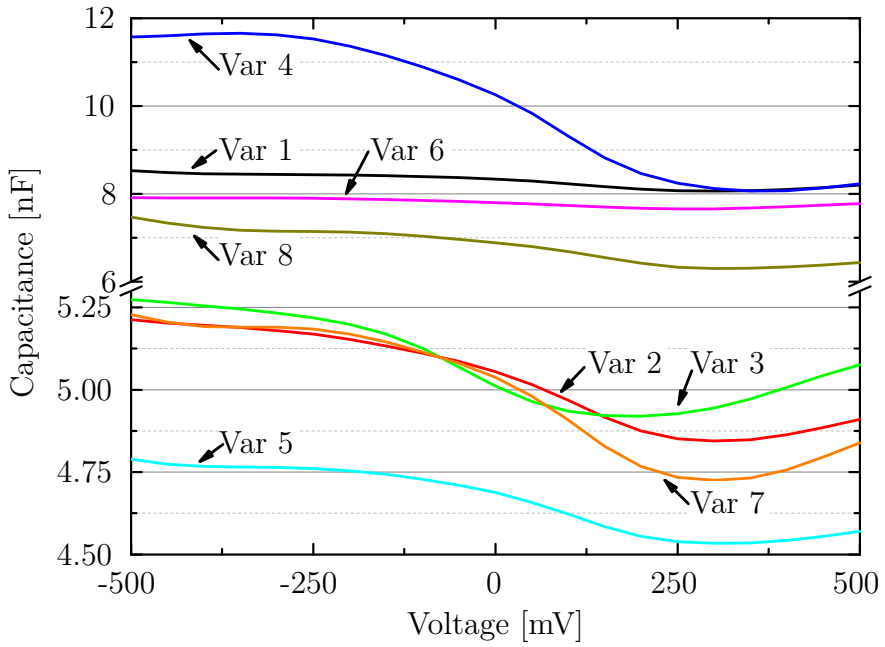

Figure 3.28: C-V curves of pH sensor variants 1 to 8

and 4.5 nF. Adding to this were parallel capacitances stemming from the PCB partly immersed into solution, mainly the lead connecting the die attach pad with the pin contact on the upper side of the PCB.

The threshold voltages were about 500 mV lower than what had been expected for pH 7.4. The deviation between calculated and measured voltage was mainly attributed to the neglected flatband voltage of the EIS structure in the theoretical calculations. However, during the measurements, an initial strong drift towards higher voltages was observed, decaying with increasing number of measurement runs and measurement duration but remaining present. Due to the constant drift a definite value for the threshold voltage could not be determined.

The higher capacitances found in the C-V measurement lowered the ratio Γ of C_{pH} and C_{Total}, possibly affecting the detection of the threshold voltage shift in the depletion zone of the C-V curve. Calibration measurements in solutions with differing pH were performed to assess a possible impact on the measurement performance.

Evaluation of Measurement Performance

Calibration measurements were performed in buffer solutions with pH values ranging from pH 3 to pH 12 by measuring C-V curves in a DC voltage range

Var	Γ	S $[\frac{\text{mV}}{\text{pH}}]$	$C_{\text{pH,Step}}$	$\hat{C}_{\text{pH,Step}}$	C_{Total}	$\hat{C}_{\text{Total}}$
1	0.05	56.3	51.5 pF	300 pF	1.03 nF	8.5 nF
2	0.1	56.7	108.4 pF	350 pF	1.09 nF	5.25 nF
3	0.02	52.3	20 pF	350 pF	1 nF	5.25 nF
4	0.8	53.1	3.43 nF	3.4 nF	4.28 nF	11.5 nF
5	0.01	56.7	9.9 pF	230 pF	989 pF	4.8 nF
6	0.2	54	242.6 pF	300 pF	1.21 nF	7.9 nF
7	0.33	56.1	474 pF	470 pF	1.44 nF	5.25 nF
8	0.67	60.8	1.85 nF	900 pF	2.77 nF	7.5 nF
9	0.5	-	945.3 pF	15 pF	1.89 nF	920 pF

Table 3.5: Measurement performance of pH sensor variants and comparison with theoretically calculated values; Γ is the ratio of pH-sensitive and remaining chip area, S is sensitivity, $C_{\text{pH,Step}}$ is the capacitance step and C_{Total} is the overall capacitance of the chip variant; C indicates calculated values

from $-0.8\,\text{V}$ to $0.8\,\text{V}$. This range ensured that for all pH values the whole C-V curve was recorded. The superimposed AC voltage was set to $20\,\text{mV}$. An exemplary set of C-V curves, recorded using chip variant 4, is shown in Fig. 3.29. The threshold voltages of the curves were between 300 mV for pH 3 and 690 mV for pH 12. The higher voltages in comparison to the ones shown in Fig. 3.28 were likely to be caused by the drift observed in all pH measurements. Since several measurements had been conducted between the initial recording of the C-V curves and the calibration of the sensors, the drifts during these measurements could have easily added up to the difference seen between the two diagrams.

The threshold voltage change in response to a pH change amounted to 43 mV/pH, being significantly lower than what had been calculated. This deviation was ascribed to the nonlinear relationship between voltage and capacitance in this voltage range. However, for pH measurements the voltage in the middle of the depletion region was taken rather than the threshold voltage. Since the sensitivity in this region was consistently higher the low sensitivity at threshold was not seen as a problem.

To determine the sensitivity of the sensors a fixed capacitance was determined for every variant, which for all pH values was in the linear regime of the C-V

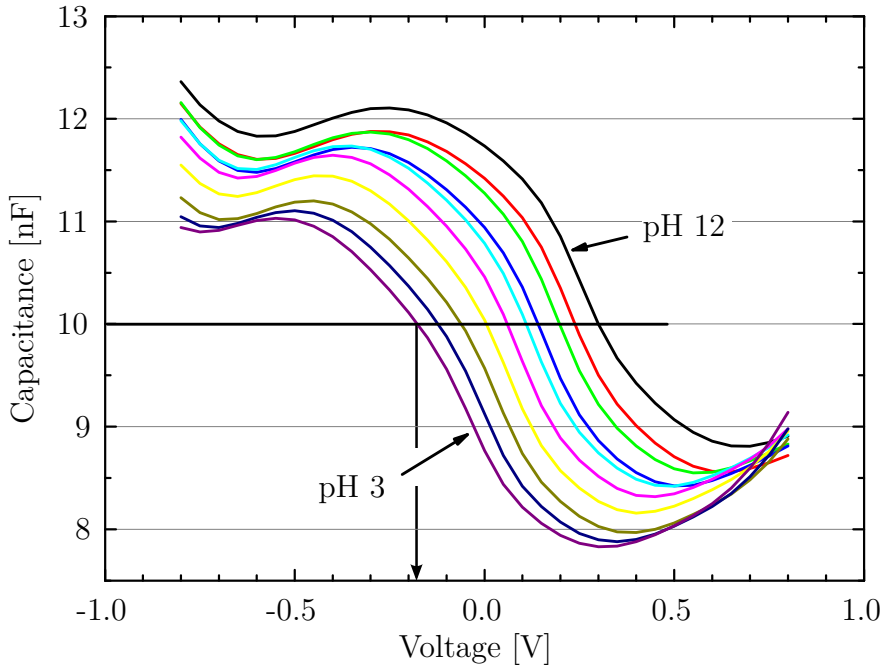

Figure 3.29: C-V measurement with pH sensor variant 4 in buffer solutions of pH 3 to pH 12; a fixed capacitance of 10 nF was chosen and the voltage taken at this capacitance was related to the pH

curves. For variant 4 this capacitance is highlighted in Fig. 3.29, amounting to 10 nF. The voltages at this capacitance at the different pH values were taken and plotted against the pH. The resulting calibration curves of variant 4 are shown in Fig. 3.30. All variants except variant 9 showed a linear behavior between pH 3 and pH 12 with sensitivities S between 52.3 mV/pH and 60.8 mV/pH, as given in Tab. 3.5. The average sensitivity was 55.8 mV/pH, being only slightly lower than the theoretical Nernst limit of 59.1 mV/pH. Together with the high resolution this performance should enable precise pH measurements in biotechnological processes. The results allowed the conclusion that the area of the pH sensors could be further reduced below the minimum area of 0.004 mm^2 in relation to the remaining chip area. This would mean that a new reference capacitance had to be determined at which the voltage shift would be detected.

The resolution throughout all variants was pH 0.05. This resolution was expected to be sufficient to detect even small variations in the order of pH 0.1 found in mammalian cell cultures. Variant 9 showed a response to differing pH values, but it did not reliably correspond to the applied solutions. This was ascribed to

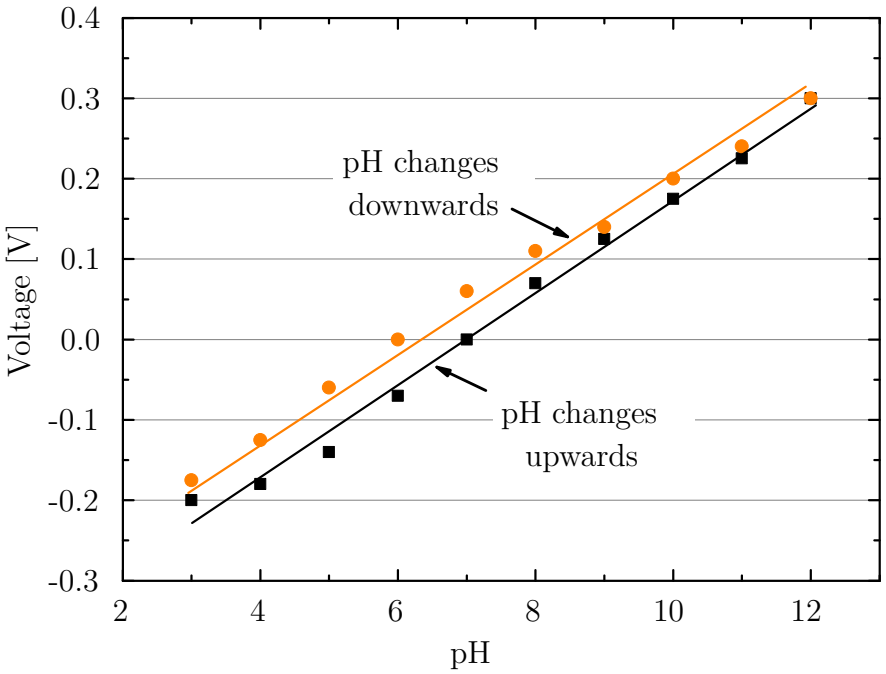

Figure 3.30: Calibration curves of pH sensor variant 4 with pH changing upwards and downwards; hysteresis of around 40 mV

the supposed faulty attachment of the chip on the PCB. The deviations between the sensitivities were in the order of the variation coefficient of the measurements and could not be related to any design parameters. They were hence ascribed to randomly varying measurement conditions.

The direction of the pH change was found to have influence on the measured voltage. As can be seen from Fig. 3.30 the calibration curves of sensor variant 4, shown here exemplarily, differed by 40 mV on average, depending on whether the pH was changed upwards or downwards. This behavior has been reported for pH ISFETs and is ascribed to a delayed pH response and the action of OH^- ions present in the solution [121]. After longer operation of the pH sensors over two days, however, the hysteresis decayed to a difference around 5 mV. While such a hysteresis is regarded as acceptable for cultures where the pH is allowed to vary in the order of several tenths of pH units, it might be prohibitive for cultures which need a very fine pH adjustment. Unfortunately, a definite solution to the hysteresis of semiconductor-based pH sensors is still to be found [122] and beyond the scope of this work.

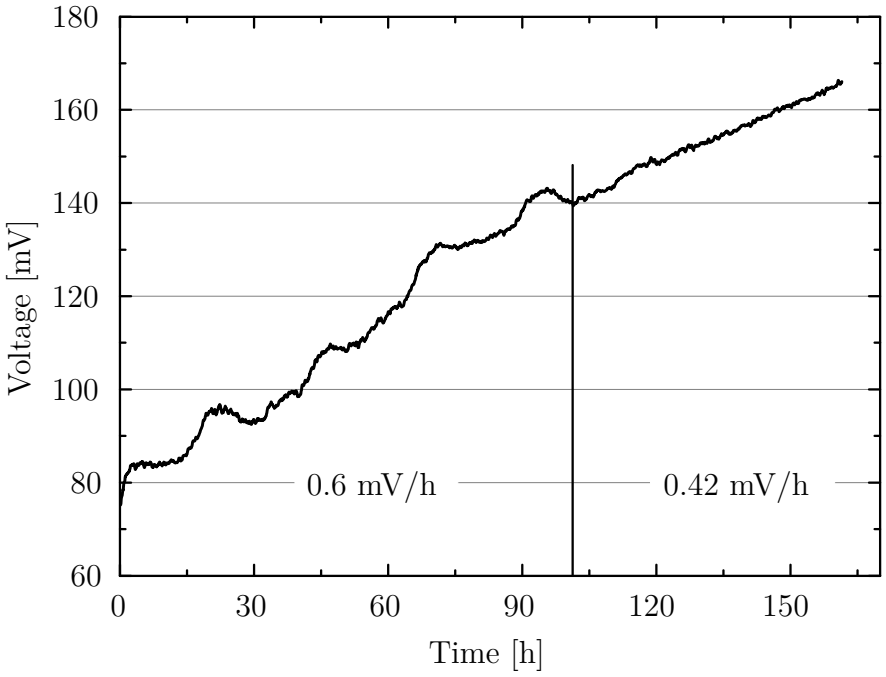

Figure 3.31: Long-term performance of pH sensor variant 2 in PBS; a quasi-linear drift was found, which could be split into two phases

Evaluation of Drift Behavior

Since a drift had been observed in all experiments long-term measurement runs were performed to determine the magnitude and behavior of this phenomenon. Before the measurements, chips were kept dry to evaluate the influence of dry storage. After immersion into PBS, a preliminary measurement with approximately 300 curves was recorded to assess the initial strong drift. This drift was found to stop after around 180 C-V cycles and 1800 s, during which a voltage shift of 90 mV to 100 mV was observed.

After the first stage of the experiment, the measurement frequency was increased to one cycle per 10 min and long-term runs performed in PBS over 7 days. The measurement signal of variant 2 is exemplarily shown in Fig. 3.31. The signal could be split into two phases. In the first phase, lasting about 100 h, a drift of 0.6 mV/h was recorded. In the second phase the drift declined to 0.42 mV/pH and the signal showed a stabler behavior. The other variants showed a similar behavior with slightly different values for the two phases. Such a drift behavior is well known for pH ISFETs [123], and a magnitude of around 0.5 mV/h has been reported by others [20]. Several reasons have been proposed for the drift, includ-

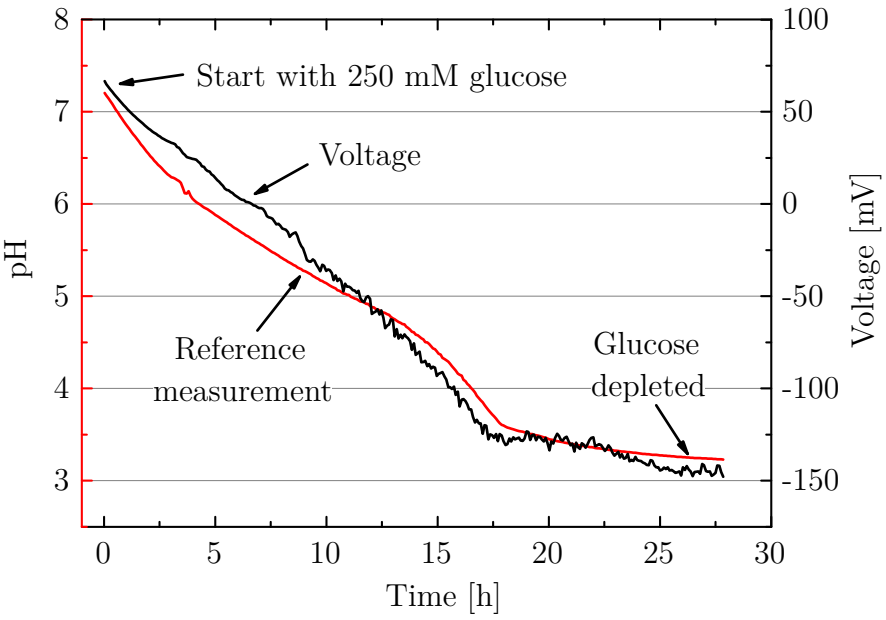

Figure 3.32: pH monitoring in a yeast culture; good agreement of sensor signal with reference measurement, performed using a pH glass electrode (Sentix 980, WTW GmbH, Germany)

ing ion migration into the insulator material, leading to buried proton adsorption sites [124], and alterations of the insulator surface over longer time scales [123]. These effects proved to be persistent and could not be reversed by the sweeping DC voltage applied during the measurements. Nevertheless, several measures can be taken to compensate for the drift, including compensation algorithms. The linear drift of the fabricated pH sensors would allow to apply such an algorithm.

Cell Culture Monitoring

To evaluate the suitability of the pH sensor for cell culture monitoring the pH of a yeast culture was monitored using variant 4 and the sensor data compared to the signal of a commercial pH glass electrode (Sentix 980, WTW GmbH, Germany). The culture was set up in PBS with an initial cell density of 2 g/l and a glucose concentration of 250 mM and allowed to rehydrate for 2 h before measurements were started. As can be seen from Fig. 3.32 the signal of the pH sensor matched the reference signal well over the entire culture duration of 28 h and retained the sensitivity found in the calibration measurements.

Conclusion

The wide measurement range of the fabricated pH sensors covered the whole range of culture media from acid to very alkaline solutions. This, the high sensitivity and the good performance in the cell culture monitoring demonstrated the suitability of the fabricated pH sensors for the monitoring of bioprocesses. Drift and hysteresis behavior, however, need to be improved to obtain a reliable sensor. A further reduction of the sensor area below 0.004 mm^2 would allow a further miniaturization of the multi-sensor system. The extent of this miniaturization, however, has to be determined in further experiments.

3.4 Parallel Measurements

After the sensor elements had been characterized individually, they were applied in parallel measurements. The parallel operation of the sensors integrated on the same chip could lead to interferences between the single sensors. Products of the enzymatic reaction, i.e. H_2O_2, or a byproduct of the amperometric detection, i.e. H^+ ions, could be transported - by diffusion or convection - to the interdigitated electrodes and distort the measured conductivity. There could also be electrical interferences due to parasitic capacitances of wiring and sensor elements and the high frequency signals generated by the impedance measurement.

In order to demonstrate the feasibility of the parallel operation and assess possible interferences a parallel measurement of glucose and conductivity was performed in a stirred 50 mM glucose solution. For this, sensor variant 3 was chosen. The measurement was started with a conductivity measurement. After 6 h, the amperometric glucose detection was added. From Fig. 3.33 it can be seen that the signal of the conductivity ratio showed some noise in the first part of the experiment but otherwise remained stable with a slight decline from 1 to 0.99 over the whole experiment. The amperometric signal stabilized after approx. 3 h and then remained stable with some noise with an amplitude of approx. 3 nA.

No mutual influences between the sensors could be found except the fact that the noise of the conductivity signal decreased at the time the potentiostat was turned on. This behavior was also observed in measurements in PBS without glucose and could therefore be attributed to electrical interferences. These, however, did not impair the sensor performance.

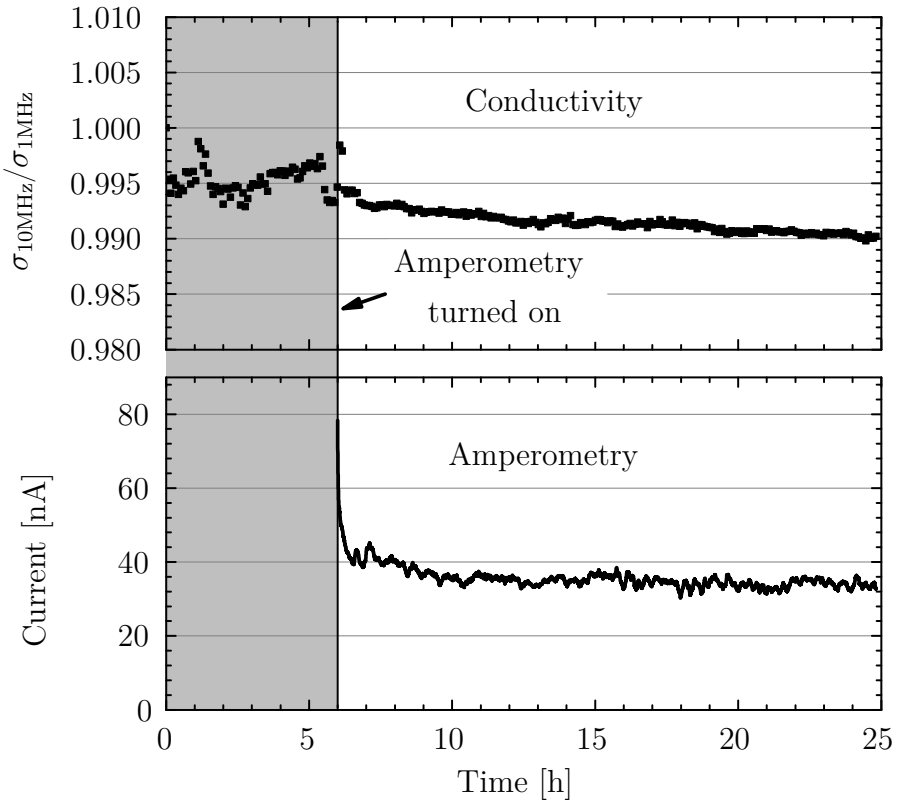

Figure 3.33: Parallel monitoring of conductivity and glucose in glucose solution; no significant mutual interferences were detected

After the parallel mode of operation had been shown feasible, a concurrent monitoring of a yeast culture was performed using variant 3. The culture was prepared in PBS with an initial cell density of 2 g/l and a glucose concentration of 200 mM. Before measurements were started, the yeast was allowed to rehydrate for 2 h. During the culture temperature and pH were held constant at 31 °C and pH 5, respectively, and the culture was continuously aerated and stirred. Samples were taken every 30 minutes for reference measurements.

Glucose concentration was determined in 50-fold dilution using a spectrophotometric assay, based on a reaction with *o*-dianisidine (Sigma Aldrich, USA), and cell density was measured in 40-fold dilution by measurement of absorbance (both measurements conducted using a Jasco FP-8500 spectrometer, Germany).

The signal of both sensors showed good correlation with the reference measurements, as depicted in Fig. 3.34.

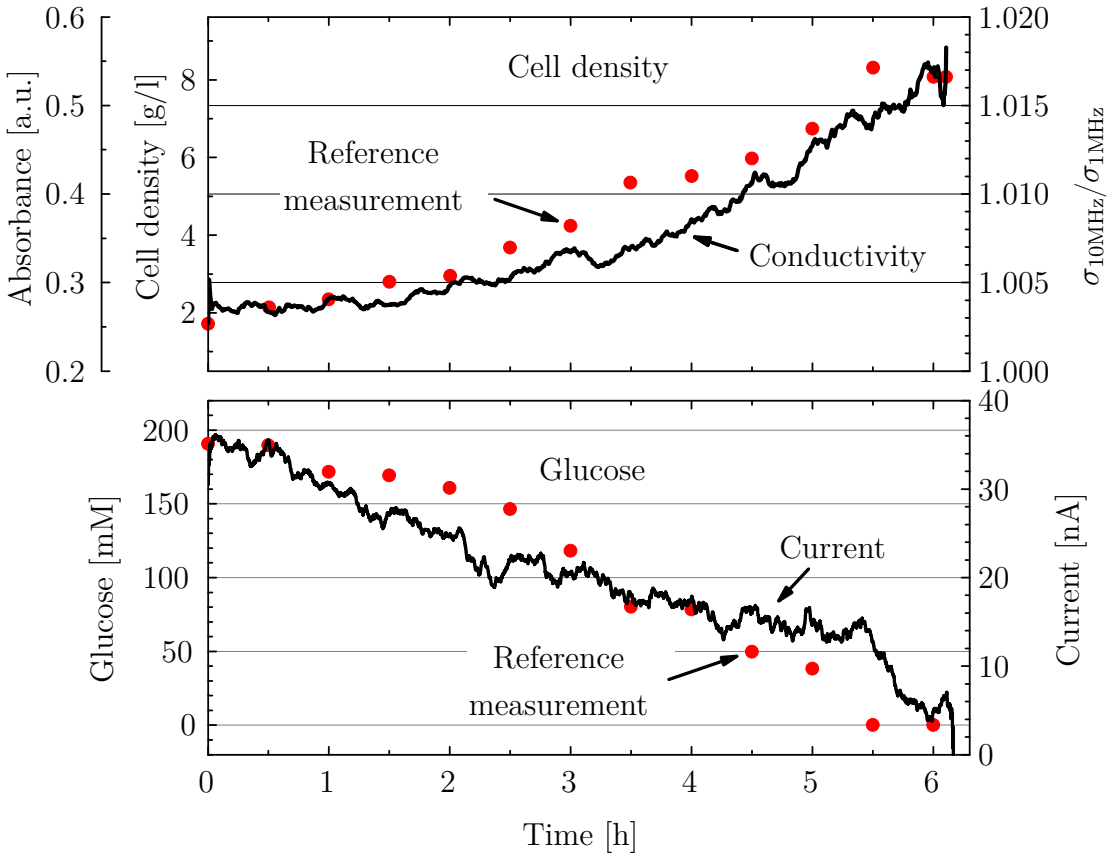

Figure 3.34: Parallel monitoring of cell density and glucose in a yeast culture; curves: sensor signals, red dots: spectrophotometric reference measurements

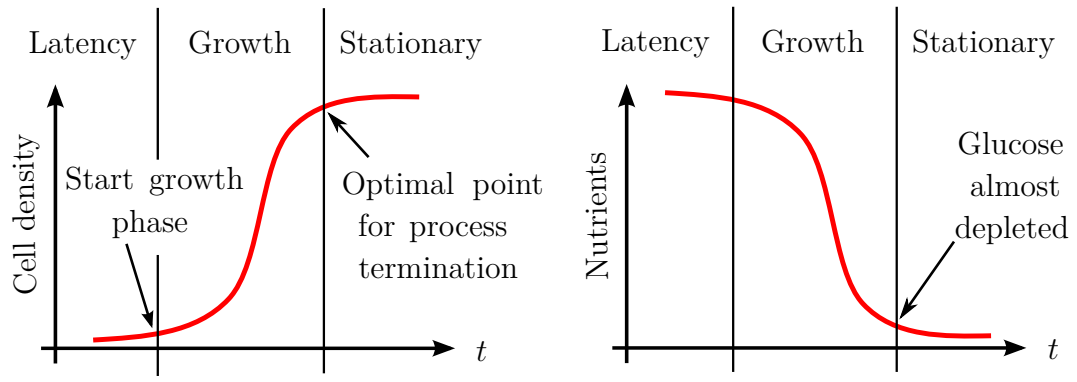

Figure 3.35: Typical behavior of cell density and nutrient concentration in a batch culture with additional information; schematic representation

Conclusion

Especially the signal of the cell density sensor showed the typical growth curve of a yeast culture with lag phase, exponential growth and stationary phase. Together with the glucose sensor data the signals were close to the behavior of batch cultures, anticipated in the introductory section and schematically shown in Fig. 3.35. Consequently, the results of the cell culture monitoring demonstrated the feasibility and potential of the proposed device for parallel in-situ monitoring of biotechnological processes. From the gained data a multitude of information about the process can be obtained, and tight control becomes possible.

Chapter 4

Conclusion and Outlook

In this thesis an integrated multi-sensor system for the parallel in-situ monitoring of glucose, lactate, cell density and pH in biotechnological processes was developed. The work demonstrated two novelties. First, the developed enzymatic glucose and lactate sensors for wide concentration ranges extended the rare reports about sensors with such a performance and met the requirements found in biotechnology, being it fermentation processes or lactate production in high concentrations. In this context the detailed characterization of morphology and permeability of diffusion-limiting polyurethane membranes for enzyme sensors was conducted for the first time to the author's best knowledge. Second, the enzyme sensors were integrated with other sensor elements on one chip and employed in the monitoring of yeast cultures. This integration had not been demonstrated before to the author's best knowledge. All sensor elements were characterized and showed good performance for applications in biotechnological processes.

The benefits of the demonstrated multi-sensor chip for biotechnological processes are manifold. Thanks to the multitude of monitored parameters, which can easily be extended by further sensors, optimal control of bioprocesses becomes possible. Possibly, even new processes that cannot be realized today due to insufficient control will become feasible. The low production costs of the device and the single sterilization procedure significantly reduce the investment costs for bioprocesses and thereby help to establish production facilities for small volume products and those in emerging markets. The latter two factors are regarded as important trends in biotechnology, and single-use technologies have been pro-

posed to meet the changing requirements of the industry [11]. The small chip size reduces the occupied space, allows integration into standard PG 13.5 sensor housings but also enables usage in single-use bioreactors, such as foil bags.

The close proximity of the sensor elements allows to use the data of one sensor to correct or complement other sensor signals. For the demonstrated device the measured pH could be used to compensate for the dependence of the enzyme sensors on this parameter. The integration of a temperature sensor would provide further data for compensation. The data of the glucose and lactate sensors could complement the cell density sensor to provide information about the cell viability and the growth phase of the cells. Thus, synergies of the parallel application of the sensors arise, which rely on the analysis of several parameters.

This work demonstrated the general feasibility of the integration of enzyme sensors with additional sensor principles for in-situ applications. Further work is necessary to reach commercial maturity. Every item introduced into a bioreactor needs to be sterilized. In this work first results of sterilization by gamma and e-beam irradiation have been demonstrated. Further work on the long-term stability of sterilized sensors is necessary. Since the proposed platform is mainly intended for single use, fabricated devices could be sterilized at the production site and shipped in sterile bags. The end-user would then only have to remove the device in a sterile environment and install it in the already sterilized bioreactor. In the case of single-use reactors the chip could be already installed in the reactor before shipment and the setup sterilized as a whole. This would provide the customer with a ready-to-use product without the need for purchase, sterilization and installation of separate sensors.

Another issue regarding the enzyme sensors is the dependence of oxidases on a redox mediator. In this work the sensors relied on oxygen present in the culture medium. There are, however, processes that proceed without oxygen, e.g. anaerobic fermentations. To enable glucose and lactate monitoring in these processes and eliminate the dependence on oxygen in the culture medium in general an artificial redox mediator, such as Prussian Blue, could be incorporated into the enzyme layer [125, 126]. This would also lower the required oxidation potential and therefore reduce the influence of interfering substances, such as ascorbic acid, on the sensor signal.

A third point that needs to be mentioned is biofouling. Almost any surface

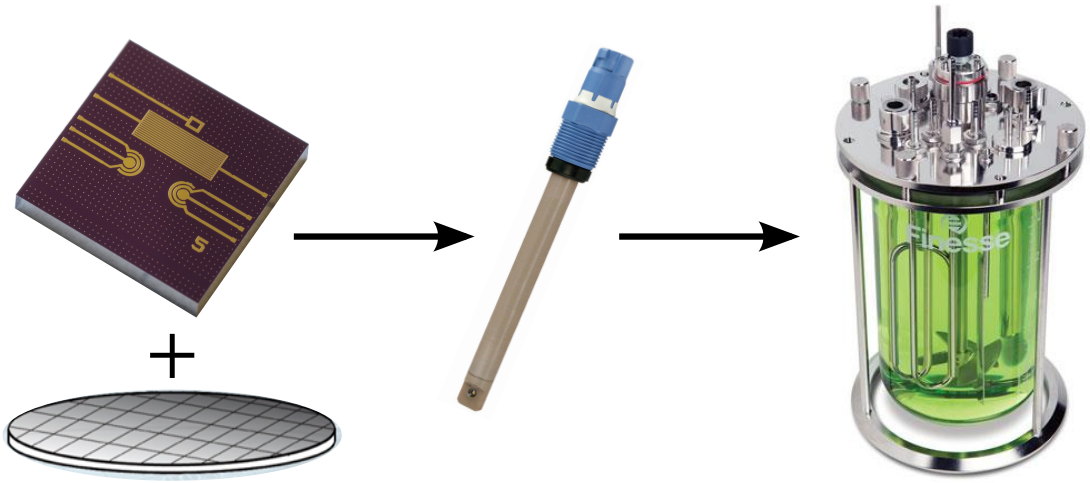

Figure 4.1: Combination of multi-sensor chip with CMOS readout electronics and integration of the measurement system into a PG 13.5 housing for application in bioreactors; bioreactor image © Finesse Solutions [127], PG 13.5 sensor housing image © Endress+Hauser [128]

surrounded by a solution containing proteins or cells is prone to adhesion of these components. The prevention of biofilm formation has been studied for decades and is still subject to ongoing research [129,130]. An effective anti-fouling strategy has to prevent the formation of a biofilm but not impair the sensor performance. Ideally, the sensors would be rendered repellent for cells and proteins during the fabrication, i.e. the surface chip layer had to be deposited in a way that it would prevent fouling. Alternatively, an anti-fouling agent, such as poly(ethylene) glycol, could be applied to the chip surface after fabrication. Either way, the performance of such measures would have to be assessed in cultures of different cell types, i.e. mammalian, bacterial and fungal cells, and different medium compositions.

The proposed platform can be extended by further sensors without substantial modifications. By replacing the used enzymes with other oxidases, such as glutamine oxidase or glutamate oxidase, the range of analytes can easily be broadened. The incorporation of further electrodes would produce a Clark electrode for oxygen measurements or a temperature sensor. Mass-sensitive sensors, which could be functionalized with antibodies or aptamers, could sense cytokines or other secreted products of the cell metabolism and thereby provide valuable information for complex fabrication processes of therapeutic proteins.

To obtain a complete measurement system the developed sensor elements could be fabricated on top of a CMOS substrate with readout circuits and interfaces to external control equipment. Possible specifications for a readout circuit for the developed sensor elements are listed in Tab. 4.1. These were based on the theoretical calculations of the sensor elements, the settings of the used measurement equipment as well as the obtained measurement results and were exemplarily adjusted to the performance of chip variant 2. The feasibility of realizing these performance characteristics in an integrated circuit would have to be examined in detail.

Since 8-inch production facilities were used throughout the work the fabrication of the sensor elements and the integrated readout electronics could be carried out on a scale suitable for mass fabrication. By integrating the system into a PG 13.5 sensor housing a self-contained product could be realized, being compatible with standard bioreactor ports and integrable into a wide variety of processes. These development steps, schematically shown in Fig. 4.1, would be a prerequisite for the multi-sensor chip demonstrated in this work to be successful on the market.

As the complexity of bioprocesses and the number of important process parameters is ever increasing tight process monitoring and control becomes more and more important for high product quality, safety and yield. Multi-sensor platforms with their ability to potentially monitor all of these parameters in a miniaturized setup are expected to have great potential in all kinds of processes and significant impact on biotechnology and the way processes will be monitored in the future.

Sensor	Specification	Value
pH	Measurement principle	Detection of voltage shift at fixed capacitance
	Capacitance range	1 nF - 10 nF
	Capacitance resolution	100 pF
	DC Voltage range	-1 ÷ +2 V
	AC Frequency	1 kHz
	AC Voltage	20 mV
Cell density	Measurement principle	Comparison of conductance at two frequencies
	Frequency range	1 - 20 MHz
	Impedance range	100 - 300 Ω
	Phase angle range	0° - 10°
	Impedance resolution	⩽ 0.5 %
	Phase angle resolution	⩽ 0.1°
Enzyme	Measurement principle	Amperometric
	Voltage between WE and RE	700 mV
	Voltage between WE and CE	700 - 1000 mV
	Current measurement range	0 - 500 nA
	Current resolution	1 nA
	Parallel measurement	Multiplexed WE, shared RE and CE

Table 4.1: Possible specifications of a readout circuit for the developed sensor elements

Peer-Reviewed Journal Articles

S. Mross, T. Zimmermann, S. Zenzes, M. Kraft and H. Vogt, "Study of Enzyme Sensors with Wide, Adjustable Concentration Ranges for In-Situ Monitoring of Biotechnological Processes", *Sens. Actuat. B-Chem.*, **241**, 2017, 48–54.

S. Mross, T. Zimmermann, N. Winkin, M. Kraft and H. Vogt, "Integrated Multi-Sensor System for Parallel In-Situ Monitoring of Cell Nutrients, Metabolites, Cell Density and pH in Biotechnological Processes", *Sens. Actuat. B-Chem.*, **236**, 2016, 937–946.

S. Mross, P. Fürst, S. Pierrat, T. Zimmermann, H. Vogt and M. Kraft, "Enzyme Sensor With Polydimethylsiloxane Membrane and CMOS Potentiostat for Wide-Range Glucose Measurements", *IEEE Sens. J.*, **15**, 2015, 7096–7104.

S. Mross, S. Pierrat, T. Zimmermann and M. Kraft, "Microfluidic Enzymatic Biosensing Systems: A Review", *Biosens. Bioelectron.*, **70**, 2015, 376–391.

M. S. Darup, M. Kastsian, **S. Mross** and M. Mönnigmann, "Efficient Computation of Spectral Bounds for Hessian Matrices on Hyperrectangles for Global Optimization", *J. Global Optim.*, **58**, 2014, 631–652.

Conference Proceedings

S. Mross, T. Zimmermann, N. Winkin, M. Kraft and H. Vogt, "Integrated Multi-Sensor System for Parallel In-Situ Monitoring of Cell Nutrients, Metabolites and Cell Mass in Biotechnological Processes", *Eurosensors 2015, Proc. Eng.*, **120**, 2015, 372–375.

S. Mross, P. Fürst, S. Pierrat, T. Zimmermann and M. Kraft, "CMOS Potentiostat and Sensor with Multilayer Membrane for Wide Range Measurements of Glucose Concentrations", *IEEE Sensors 2014 Proceedings*, 2014, 1096–1099.

Master Thesis in the Context of This Work

S. Zenzes, "Entwicklung einer Enzymsensorik zur Überwachung großer Konzentrationsbereiche von Glukose und Laktat in Bioprozessen", Hochschule Niederrhein, Krefeld, Germany, 2015.

Bibliography

[1] D. S. Dimitrov, "Therapeutic Proteins", *Methods Mol. Biol.*, **899**, 2012, 1–26.

[2] B. Leader, Q. J. Baca and D. E. Golan, "Protein Therapeutics: A Summary and Pharmacological Classification", *Nat. Rev. Drug Discov.*, **7**, 2008, 21–39.

[3] M. Pohlscheidt, S. Charaniya, C. Bork, M. Jenzsch, T. L. Noetzel and A. Luebbert, "Bioprocess and Fermentation Monitoring", in M. C. Flickinger, "Upstream Industrial Biotechnology", Wiley, Hoboken, USA, 2013, 1471–1491.

[4] P. Hossler, S. F. Khattak and Z. J. Li, "Optimal and Consistent Protein Glycosylation in Mammalian Cell Culture", *Glycobiology*, **19**, 2009, 936–949.

[5] E. D. Vieira, M. d. G. Stupiello Andrietta and S. R. Andrietta, "Yeast Biomass Production: A New Approach in Glucose-Limited Feeding Strategy", *Brazil. J. Microbiol.*, **44**, 2013, 551–558.

[6] FDA Guidance for PAT, *www.fda.gov/AboutFDA/CentersOffices/OfficeofMedicalProductsandTobacco/CDER/ucm088828.htm.*

[7] A. A. Arroyo, "Advances in Sensor and Sampling Technologies in Fermentation and Mammalian Cell Culture", in R. H. Baltz, J. E. Davies and A. L. Demain, "Manual of Industrial Microbiology and Biotechnology", ASM Press, Washington, USA, 2010, 700–718.

[8] S. S. Farid, "Process Economics of Industrial Monoclonal Antibody Manufacture", *J. Chromatogr. B-Analyt. Technol. Biomed. Life Sci.*, **848**, 2007, 8–18.

[9] Lambda Instruments, *www.lambda-instruments.com.*

[10] R. Eibl, C. Löffelholz and D. Eibl, "Single-Use Bioreactors - An Overview", in R. Eibl and D. Eibl, "Single-Use Technology in Biopharmaceutical Manufacture", Wiley, Hoboken, USA, 2010, 33–51.

[11] A. A. Shukla and U. Gottschalk, "Single-Use Disposable Technologies for Biopharmaceutical Manufacturing", *Trends Biotechnol.*, **31**, 2013, 147–154.

[12] Trace Analytics GmbH, *www.trace.de.*

[13] Y. H. Xu, A. S. Jeevarajan, J. M. Fay, T. D. Taylor and M. M. Anderson, "On-Line Measurement of Glucose in a Rotating Wall Perfused Vessel Bioreactor Using an Amperometric Glucose Sensor", *J. Electrochem. Soc.*, **149**, 2002, H103–H106.

[14] Y. H. Xu, J. J. Sun, G. Mathew, A. S. Jeevarajan and M. M. Anderson, "Continuous Glucose Monitoring and Control in a Rotating Wall Perfused Bioreactor", *Biotechnol. Bioeng.*, **87**, 2004, 473–477.

[15] S. Spichiger and U. E. Spichiger-Keller, "Process Monitoring with Disposable Chemical Sensors Fit in the Framework of Process Analysis Technology (PAT) for Innovative Pharmaceutical Development and Quality Assurance", *Chimia*, **64**, 2010, 803–807.

[16] S. Mross, P. Fürst, S. Pierrat, T. Zimmermann, H. Vogt and M. Kraft, "Enzyme Sensor With Polydimethylsiloxane Membrane and CMOS Potentiostat for Wide-Range Glucose Measurements", *IEEE Sens. J.*, **15**, 2015, 7096–7104.

[17] F. Gódia and J. Cairó, "Cell Metabolism", in S. S. Ozturk and W.-S. Hu, "Cell Culture Technology for Pharmaceutical and Cell-Based Therapies", Taylor & Francis, Boca Raton, USA, 2005, 81–112.

[18] L. Olsson, U. Schulze and J. Nielsen, "On-Line Bioprocess Monitoring - an Academic Discipline or an Industrial Tool?", *Trac-Trend Anal. Chem.*, **17**, 1998, 88–95.

[19] Y.-S. Tsao, A. Cardoso, R. Condon, M. Voloch, P. Lio, J. Lagos, B. Kearns and Z. Liu, "Monitoring Chinese Hamster Ovary Cell Culture by the Analysis of Glucose and Lactate Metabolism", *J. Biotechnol.*, **118**, 2005, 316–327.

[20] E. E. Krommenhoek, M. van Leeuwen, H. Gardeniers, W. M. van Gulik, A. van den Berg, X. Li, M. Ottens, L. A. M. van der Wielen and J. J. Heijnen, "Lab-Scale Fermentation Tests of Microchip with Integrated Electrochemical Sensors for pH, Temperature, Dissolved Oxygen and Viable Biomass Concentration", *Biotechnol. Bioeng.*, **99**, 2008, 884–892.

[21] C. Ress, A. Adami, L. Lorenzelli, C. Collini, A. Tindiani, A. Maglione and G. Soncini, "Development and Characterization of a Multiparametric Microsensor for Yeast Cell Growth Monitoring", *Proceedings of the Eurosensors XXIII Conference*, 2009, 1059–1062.

[22] A. Weltin, K. Slotwinski, J. Kieninger, I. Moser, G. Jobst, M. Wego, R. Ehret and G. A. Urban, "Cell Culture Monitoring for Drug Screening and Cancer Research: A Transparent, Microfluidic, Multi-Sensor Microsystem", *Lab. Chip*, **14**, 2014, 138–146.

[23] S. Mross, S. Pierrat, T. Zimmermann and M. Kraft, "Microfluidic Enzymatic Biosensing Systems: A Review", *Biosens. Bioelectron.*, **70**, 2015, 376–391.

[24] S. Mross, P. Fürst, S. Pierrat, T. Zimmermann and M. Kraft, "CMOS Potentiostat and Sensor with Multilayer Membrane for Wide Range Measurements of Glucose Concentrations", *IEEE Sensors 2014 Proceedings*, 2014, 1096–1099.

[25] S. Mross, T. Zimmermann, S. Zenzes, M. Kraft and H. Vogt, "Study of Enzyme Sensors with Wide, Adjustable Concentration Ranges for In-Situ Monitoring of Biotechnological Processes", *Sens. Actuat. B-Chem.*, **241**, 2017, 48–54.

[26] S. Mross, T. Zimmermann, N. Winkin, M. Kraft and H. Vogt, "Integrated Multi-Sensor System for Parallel In-Situ Monitoring of Cell Nutrients, Metabolites and Cell Mass in Biotechnological Processes", *Proc. Eng.*, **120**, 2015, 372–375.

[27] S. Mross, T. Zimmermann, N. Winkin, M. Kraft and H. Vogt, "Integrated Multi-Sensor System for Parallel In-Situ Monitoring of Cell Nutrients, Metabolites, Cell Density and pH in Biotechnological Processes", *Sens. Actuat. B-Chem.*, **236**, 2016, 937–946.

[28] D. Grieshaber, R. MacKenzie, J. Voros and E. Reimhult, "Electrochemical Biosensors - Sensor Principles and Architectures", *Sensors*, **8**, 2008, 1400–1458.

[29] N. J. Ronkainen, H. B. Halsall and W. R. Heineman, "Electrochemical Biosensors", *Chem. Soc. Rev.*, **39**, 2010, 1747–1763.

[30] J. Janata, *Principles of Chemical Sensors*, Springer, Dordrecht, The Netherlands, 2009.

[31] T. Cass and F. S. Ligler, *Immobilized Biomolecules in Analysis, A Practical Approach*, Oxford University Press, New York, USA, 1999.

[32] M. C. Moreno-Bondi and E. Benito-Pena, "Fundamentals of Enzyme-Based Sensors", in F. Baldini, A. N. Chester, J. Homola and S. Martellucci, "Optical Chemical Sensors", Springer, Dordrecht, The Netherlands, 2006, 323–352.

[33] R. A. Copeland, *Enzymes: A Practical Introduction to Structure, Mechanism, and Data Analysis*, Wiley, New York, USA, 2000.

[34] L. Li, L. Mi, Q. Feng, R. Liu, H. Tang, L. Xie, X. L. Yu and Z. N. Chen, "Increasing the Culture Efficiency of Hybridoma Cells by the Use of Integrated Metabolic Control of Glucose and Glutamine at Low Levels", *Biotechnol. Appl. Biochem.*, **42**, 2005, 73–80.

[35] A. F. Europa, A. Gambhir, P. C. Fu and W. S. Hu, "Multiple Steady States with Distinct Cellular Metabolism in Continuous Culture of Mammalian Cells", *Biotechnol. Bioeng.*, **67**, 2000, 25–34.

[36] M. Bely, J.-M. Sablayrolles and P. Barre, "Automatic Detection of Assimilable Nitrogen Deficiencies during Alcoholic Fermentation in Oenological Conditions", *J. Ferment. Bioengineer.*, **70**, 1990, 246–252.

[37] L. F. Bisson and C. E. Butzke, "Diagnosis and Rectification of Stuck and Sluggish Fermentations", *Am. J. Enol. Viticult.*, **51**, 2000, 168–177.

[38] M. Kudo, P. Vagnoli and L. F. Bisson, "Imbalance of pH and Potassium Concentration as a Cause of Stuck Fermentations", *Am. J. Enol. Viticult.*, **49**, 1998, 295–301.

[39] F. N. Arroyo-López, S. Orlić, A. Querol and E. Barrio, "Effects of Temperature, pH and Sugar Concentration on the Growth Parameters of Saccharomyces Cerevisiae, S. Kudriavzevii and Their Interspecific Hybrid", *Int. J. Food Microbiol.*, **131**, 2009, 120–127.

[40] B. Choudhury and T. Swaminathan, "Lactic Acid Fermentation in Cell-Recycle Membrane Bioreactor", *Appl. Biochem. Biotechnol.*, **128**, 2006, 171–183.

[41] S. Kwon, I.-K. Yoo, W. G. Lee, H. N. Chang and Y. K. Chang, "High-Rate Continuous Production of Lactic Acid by Lactobacillus Rhamnosus in a Two-Stage Membrane Cell-Recycle Bioreactor", *Biotechnol. Bioeng.*, **73**, 2001, 25–34.

[42] D. J. Harrison, R. F. B. Turner and H. P. Baltes, "Characterization of Perfluorosulfonic Acid Polymer Coated Enzyme Electrodes and a Miniaturized Integrated Potentiostat for Glucose Analysis in Whole-Blood", *Anal. Chem.*, **60**, 1988, 2002–2007.

[43] M. Koudelka, S. Gernet and N. F. de Rooij, "Planar Amperometric Enzyme-Based Glucose Microelectrode", *Sens. Actuat.*, **18**, 1989, 157–165.

[44] R. Vaidya and E. Wilkins, "Effect of Interference on Amperometric Glucose Biosensors with Cellulose-Acetate Membranes", *Electroanalysis*, **6**, 1994, 677–682.

[45] A. Maines, D. Ashworth and P. Vadgama, "Diffusion Restricting Outer Membranes for Greatly Extended Linearity Measurements with Glucose Oxidase Enzyme Electrodes", *Anal. Chim. Acta*, **333**, 1996, 223–231.

[46] T. Matsumoto, M. Furusawa, H. Fujiwara, Y. Matsumoto and N. Ito, "A Micro-Planar Amperometric Glucose Sensor Unsusceptible to Interference Species", *Sens. Actuat. B-Chem.*, **49**, 1998, 68–72.

[47] W. H. Mullen, F. H. Keedy, S. J. Churchouse and P. M. Vadgama, "Glucose Enzyme Electrode with Extended Linearity - Application to Undiluted Blood Measurements", *Anal. Chim. Acta*, **183**, 1986, 59–66.

[48] F.-G. Banica, *Chemical Sensors and Biosensors*, Wiley, Chichester, United Kingdom, 2012.

[49] C. H. Ahn, J. W. Choi, G. Beaucage, J. H. Nevin, J. B. Lee, A. Puntambekar and J. Y. Lee, "Disposable Smart Lab on a Chip for Point-of-Care Clinical Diagnostics", *Proc. IEEE*, **92**, 2004, 154–173.

[50] O. Frey, S. Talaei, P. D. van der Wal, M. Koudelka-Hep and N. F. de Rooij, "Continuous-Flow Multi-Analyte Biosensor Cartridge with Controllable Linear Response Range", *Lab. Chip*, **10**, 2010, 2226–2234.

[51] I. A. Ges and F. Baudenbacher, "Enzyme-Coated Microelectrodes to Monitor Lactate Production in a Nanoliter Microfluidic Cell Culture Device", *Biosens. Bioelectron.*, **26**, 2010, 828–833.

[52] I. A. Ges and F. Baudenbacher, "Enzyme Electrodes to Monitor Glucose Consumption of Single Cardiac Myocytes in Sub-Nanoliter Volumes", *Biosens. Bioelectron.*, **25**, 2010, 1019–1024.

[53] B. A. Palfey, D. P. Ballou and V. Massey, "Oxygen Activation by Flavins and Pterins", in J. S. Valentine, C. S. Foote, A. Greenberg and J. F. Liebman, "Active Oxygen in Biochemistry", Springer, Dordrecht, The Netherlands, 1995, 37–83.

[54] Glucose Oxidase from Aspergillus niger, Data Sheet, Kikkoman.

[55] I. Y. Huang, S.-H. Wang, C.-C. Chu and C.-T. Chiu, "Improved Solid-State Planar Ti/Pd/Ag/AgCl/KCl-Gel Microreference Electrode by Silicon Cap Sealing Package", *J. Micro. Nanolithogr. MEMS MOEMS*, **8**, 2009, 033050–1–033050–9.

[56] C. H. Hamann and W. Vielstich, *Elektrochemie*, Wiley-VCH, Weinheim, Germany, 2005.

[57] M. Alvarez-Icaza and U. Bilitewski, "Mass-Production of Biosensors", *Anal. Chem.*, **65**, 1993, A525–A533.

[58] J. S. White and D. C. White, *Source Book of Enzymes*, CRC Press, Florida, USA, 1997.

[59] C. Li, P.-M. Wu, J. Han and C. H. Ahn, "A Flexible Polymer Tube Lab-Chip Integrated with Microsensors for Smart Microcatheter", *Biomed. Microdevices*, **10**, 2008, 671–679.

[60] C. Y. Li, L. A. Shutter, P. M. Wu, C. H. Ahn and R. K. Narayan, "Potential of a Simple Lab-on-a-Tube for Point-of-Care Measurements of Multiple Analytes", *Lab. Chip*, **10**, 2010, 1476–1479.

[61] J. Trzebinski, S. Sharma, A. R. B. Moniz, K. Michelakis, Y. Y. Zhang and A. E. G. Cass, "Microfluidic Device to Investigate Factors Affecting Performance in Biosensors Designed for Transdermal Applications", *Lab. Chip*, **12**, 2012, 348–352.

[62] E. L. Cussler, *Diffusion: Mass Transfer in Fluid Systems*, Cambridge University Press, New York, USA, 2013.

[63] T. Melin and R. Rautenbach, *Membranverfahren - Grundlagen der Modul- und Anlagenauslegung*, Springer, Berlin, Germany, 2007.

[64] K. Ohlrogge and K. Ebert, *Membranen - Grundlagen, Verfahren und industrielle Anwendungen*, Wiley-VCH, Weinheim, Germany, 2005.

[65] M. Mulder, *Basic Principles of Membrane Technology*, Springer, Dordrecht, The Netherlands, 1996.

[66] P. Bartlett and C. S. Toh, "Kinetic Modeling for Biosensors", in J. M. Cooper and A. E. G. Cass, "Biosensors - A Practical Approach", Oxford University Press, New York, USA, 2004, 59–96.

[67] Y. Chen and T. C. Tan, "Mathematical Model on the Sensing Behavior of a Biooxidation Biosensor", *AIChE J.*, **41**, 1995, 1025–1036.

[68] D. S. Bindra, Y. N. Zhang, G. S. Wilson, R. Sternberg, D. R. Thevenot, D. Moatti and G. Reach, "Design and Invitro Studies of a Needle-Type Glucose Sensor for Subcutaneous Monitoring", *Anal. Chem.*, **63**, 1991, 1692–1696.

[69] W. K. Ward, L. B. Jansen, E. Anderson, G. Reach, J. C. Klein and G. S. Wilson, "A New Amperometric Glucose Microsensor: In Vitro and Short-Term in Vivo Evaluation", *Biosens. Bioelectron.*, **17**, 2002, 181–189.

[70] A. P. Soldatkin, A. V. Elskaya, A. A. Shulga, A. S. Jdanova, S. V. Dzyadevich, N. Jaffrezic-Renault, C. Martelet and P. Clechet, "Glucose-Sensitive Conductometric Biosensor with Additional Nafion Membrane - Reduction of Influence of Buffer Capacity on the Sensor Response and Extension of its Dynamic-Range", *Anal. Chim. Acta*, **288**, 1994, 197–203.

[71] BST Biosensor Technology GmbH, Personal communication, 2013.

[72] T. Romaskevic, S. Budriene, K. Pielichowski and J. Pielichowski, "Application of Polyurethane-Based Materials for Immobilization of Enzymes and Cells: A Review", *Chemija*, **17**, 2006, 74–89.

[73] W. Kaiser, *Kunststoffchemie für Ingenieure - Von der Synthese bis zur Anwendung*, Hanser, München, Germany, 2007.

[74] N. Wang, K. Burugapalli, W. Song, J. Halls, F. Moussy, Y. Zheng, Y. Ma, Z. Wu and K. Li, "Tailored Fibro-Porous Structure of Electrospun Polyurethane Membranes, Their Size-Dependent Properties and Trans-Membrane Glucose Diffusion", *J. Membr. Sci.*, **427**, 2013, 207–217.

[75] ICSC database, N,N-Dimethylformamide, Tetrahydrofuran.

[76] J. E. Mark, H. R. Allcock and R. West, *Inorganic Polymers*, Oxford University Press, New York, USA, 2005.

[77] J. H. Koschwanez, R. H. Carlson and D. R. Meldrum, "Thin PDMS Films Using Long Spin Times or Tert-Butyl Alcohol as a Solvent", *PLoS One*, **4**, 2009, e4572.

[78] W. Zhang, G. Ferguson and S. Tatic-Lucic, "Elastomer-Supported Cold Welding for Room Temperature Wafer-Level Bonding", *Proceedings of the IEEE MEMS Conference 2004*, 2004, 741–744.

[79] W. Chen, R. H. W. Lam and J. Fu, "Photolithographic Surface Micromachining of Polydimethylsiloxane (PDMS)", *Lab. Chip*, **12**, 2012, 391–395.

[80] B. Krajewska and A. Olech, "Pore Structure of Gel Chitosan Membranes. I. Solute Diffusion Measurements", *Polym. Gels. Netw.*, **4**, 1996, 33–43.

[81] C.-H. Lin, Y.-H. Yeh, W.-C. Lin and M.-C. Yang, "Novel Silicone Hydrogel Based on PDMS and PEGMA for Contact Lens Application", *Colloids Surf. B-Biointerfaces*, **123**, 2014, 986–994.

[82] V. Stepankova, S. Bidmanova, T. Koudelakova, Z. Prokop, R. Chaloupkova and J. Damborsky, "Strategies for Stabilization of Enzymes in Organic Solvents", *Acs Catalysis*, **3**, 2013, 2823–2836.

[83] A. Wolf, "Environmental Degradation Factors, Their Characterisation and Effects on Sealed Building Joints", in A. Wolf, "Durability of Building Sealants - State-of-the-Art Report of RILEM TC 139-DBS", RILEM Publications SARL, Bagneux, France, 1999, 41–71.

[84] R. Keshavaraj, R. W. Tockt and C. V. G. Vallabhan, "Effects of Moisture on Structural Silicone Rubber Sealants Used in Window Glazing Applications", *Constr. Build. Mater.*, **8**, 1994, 227–232.

[85] K. Konstantinov, S. Chuppa, E. Sajan, Y. Tsai, S. J. Yoon and F. Golini, "Real-Time Biomass-Concentration Monitoring in Animal-Cell Cultures", *Trends Biotechnol.*, **12**, 1994, 324–333.

[86] B. Sonnleitner, G. Locher and A. Fiechter, "Biomass Determination", *J. Biotechnol.*, **25**, 1992, 5–22.

[87] J. P. Carvell and J. E. Dowd, "On-Line Measurements and Control of Viable Cell Density in Cell Culture Manufacturing Processes Using Radio-Frequency Impedance", *Cytotechnology*, **50**, 2006, 35–48.

[88] C. M. Harris, R. W. Todd, S. J. Bungard, R. W. Lovitt, J. G. Morris and D. B. Kell, "Dielectric Permittivity of Microbial Suspensions at Radio Frequencies - a Novel Method for the Real-Time Estimation of Microbial Biomass", *Enzyme Microb. Technol.*, **9**, 1987, 181–186.

[89] K. Asami and T. Yonezawa, "Dielectric Analysis of Yeast-Cell Growth", *Biochim. Biophys. Acta-Gen. Subj.*, **1245**, 1995, 99–105.

[90] S. Hauttmann and J. Müller, "In-Situ Biomass Characterisation by Impedance Spectroscopy Using a Full-Bridge Circuit", *Bioprocess Biosyst. Eng.*, **24**, 2001, 137–141.

[91] M. Ibrahim, "Geometric Parameters Optimization of Planar Interdigitated Electrodes for Bioimpedance Spectroscopy", *J. Electr. Bioimpedance*, **4**, 2013, 10.

[92] R. E. G. van Hal, J. C. T. Eijkel and P. Bergveld, "A Novel Description of ISFET Sensitivity with the Buffer Capacity and Double-Layer Capacitance as Key Parameters", *Sens. Actuat. B-Chem.*, **24**, 1995, 201–205.

[93] M. Bäcker, "Chip-Based (Bio-)Chemical Sensors for Bioprocess Monitoring", Ph.D. thesis, FH Aachen, 2013.

[94] W. Olthuis, W. Streekstra and P. Bergveld, "Theoretical and Experimental Determination of Cell Constant of Planar-Interdigitated Electrolyte Conductivity Sensors", *Sens. Actuat. B-Chem.*, **24**, 1995, 252–256.

[95] B. Timmer, W. Sparreboom, W. Olthuis, P. Bergveld and A. van den Berg, "Optimization of an Electrolyte Conductivity Detector for Measuring Low Ion Concentrations", *Lab. Chip*, **2**, 2002, 121–124.

[96] G. Langereis, "An Integrated Sensor System for Monitoring Washing Processes", Ph.D. thesis, Universiteit Twente, 1999.

[97] E. E. Krommenhoek, J. G. E. Gardeniers, J. G. Bomer, X. Li, M. Ottens, G. W. K. van Dedem, M. V. Leeuwen, W. M. van Gulik, L. A. M. van der Wielen, J. J. Heijnen and A. van den Berg, "Integrated Electrochemical Sensor Array for On-Line Monitoring of Yeast Fermentations", *Anal. Chem.*, **79**, 2007, 5567–5573.

[98] A. Jupe, Fraunhofer IMS, Personal communication, 2014.

[99] P. V. Gerwen, W. Laureyn, W. Laureys, G. Huyberechts, M. O. D. Beeck, K. Baert, J. Suls, W. Sansen, P. Jacobs, L. Hermans and R. Mertens, "Nanoscaled Interdigitated Electrode Arrays for Biochemical Sensors", *Sens. Actuat. B-Chem.*, **49**, 1998, 73–80.

[100] P. Bergveld, "Development of an Ion-Sensitive Solid-State Device for Neurophysiological Measurements", *IEEE Trans. Bio-Med. Eng.*, **BM17**, 1970, 70–71.

[101] D. E. Yates, S. Levine and T. W. Healy, "Site-Binding Model of Electrical Double-Layer at Oxide-Water Interface", *J. Chem. Soc.-Faraday Trans.*, **70**, 1974, 1807–1818.

[102] T. Windbacher, "Engineering Gate Stacks for Field-Effect Transistors", Ph.D. thesis, Technische Universität Wien, 2010.

[103] S. Takeda, M. Fukawa, Y. Hayashi and K. Matsumoto, "Surface OH Group Governing Adsorption Properties of Metal Oxide Films", *Thin Solid Films*, **339**, 1999, 220–224.

[104] M. Bäcker, S. Pouyeshman, T. Schnitzler, A. Poghossian, P. Wagner, M. Biselli and M. J. Schöning, "A Silicon-Based Multi-Sensor Chip for Monitoring of Fermentation Processes", *Phys. Status Solidi A*, **208**, 2011, 1364–1369.

[105] L. Bousse, S. Mostarshed, B. Vandershoot, N. F. de Rooij, P. Gimmel and W. Gopel, "Zeta Potential Measurements of Ta2O5 and SiO2 Thin-Films", *J. Colloid Interface Sci.*, **147**, 1991, 22–32.

[106] L. Bousse, N. F. de Rooij and P. Bergveld, "Operation of Chemically Sensitive Field-Effect Sensors as a Function of the Insulator-Electrolyte Interface", *IEEE Trans. Electron Devices*, **30**, 1983, 1263–1270.

[107] A. J. Bard and L. R. Faulkner, *Electrochemical Methods: Fundamentals and Applications*, Wiley, Hoboken, USA, 2007.

[108] M. D. Groner and S. M. George, "High-k Dielectrics Grown by Atomic Layer Deposition: Capacitor and Gate Applications", in S. P. M. E. K. Sinha, "Interlayer Dielectrics for Semiconductor Technologies", Academic Press, San Diego, USA, 2003, 327–348.

[109] P. R. Gray, *Analysis and Design of Analog Integrated Circuits*, Wiley, Hoboken, USA, 2010.

[110] B. van Zeghbroeck, *Principles of Semiconductor Devices*, Colorado University, Colorado, USA, 2004.

[111] S. M. Sze, *Physics of Semiconductor Devices*, Wiley, New York, 1981.

[112] R. W. Baker, *Membrane Technology and Applications*, Wiley-Blackwell, Chichester, United Kingdom, 2012.

[113] G. Zoldak, A. Zubrik, A. Musatov, M. Stupak and E. Sedlak, "Irreversible Thermal Denaturation of Glucose Oxidase from Aspergillus Niger Is the Transition to the Denatured State with Residual Structure", *J. Biol. Chem.*, **279**, 2004, 47601–47609.

[114] H. Minagawa, Y. Yoshida, N. Kenmochi, M. Furuichi, J. Shimada and H. Kaneko, "Improving the Thermal Stability of Lactate Oxidase by Directed Evolution", *Cell. Mol. Life Sci.*, **64**, 2007, 77–81.

[115] T. von Woedtke, W. D. Jülich, V. Hartmann, M. Stieber and P. U. Abel, "Sterilization of Enzyme Glucose Sensors: Problems and Concepts", *Biosens. Bioelectron.*, **17**, 2002, 373–382.

[116] M. Koudelka-Hep, D. J. Strike and N. F. de Rooij, "Miniature Electrochemical Glucose Biosensors", *Anal. Chim. Acta*, **281**, 1993, 461–466.

[117] K. Rebrin, G. M. Steil, W. P. van Antwerp and J. J. Mastrototaro, "Subcutaneous Glucose Predicts Plasma Glucose Independent of Insulin: Implications for Continuous Monitoring", *Am. J. Physiol. Endocrinol. Metab.*, **277**, 1999, E561–E571.

[118] J. B. Kowalski, C. Herring, L. Baryschpolec, J. Reger, J. Patel, M. Feeney and A. Tallentire, "Field Evaluations of the VDmax Approach for Substantiation of a 25 kGy Sterilization Dose and Its Application to Other Preselected Doses", *Radiat. Phys. Chem.*, **64**, 2002, 411–416.

[119] M. Bäcker, S. Beging, M. Biselli, A. Poghossian, J. Wang, W. Zang, P. Wagner and M. J. Schöning, "Concept for a Solid-State Multi-Parameter Sensor System for Cell-Culture Monitoring", *Electrochim. Acta*, **54**, 2009, 6107–6112.

[120] V. Moses, R. E. Cape and D. Springham, *Biotechnology: The Science and the Business*, Harwood Academic, Amsterdam, The Netherlands, 1999.

[121] L. Bousse, H. van den Vlekkert and N. de Rooij, "Hysteresis in Al2O3-Gate ISFETs", *Sens. Actuat. B-Chem.*, **2**, 1990, 103 – 110.

[122] Y. Sasaki and H. Kawarada, "Low Drift and Small Hysteresis Characteristics of Diamond Electrolyte-Solution-Gate FET", *J. Phys. D-Appl. Phys.*, **43**, 2010, 374020–1–374020–8.

[123] K.-M. Chang, C.-T. Chang, K.-Y. Chao and C.-H. Lin, "A Novel pH-Dependent Drift Improvement Method for Zirconium Dioxide Gated pH-Ion Sensitive Field Effect Transistors", *Sensors*, **10**, 2010, 4643–4654.

[124] L. Bousse and P. Bergveld, "The Role of Buried OH-Sites in the Response Mechanism of Inorganic-Gate pH-Sensitive ISFETs", *Sens. Actuat.*, **6**, 1984, 65–78.

[125] W. Dungchai, O. Chailapakul and C. S. Henry, "Electrochemical Detection for Paper-Based Microfluidics", *Anal. Chem.*, **81**, 2009, 5821–5826.

[126] M. M. Picher, S. Kupcu, C. J. Huang, J. Dostalek, D. Pum, U. B. Sleytr and P. Ertl, "Nanobiotechnology Advanced Antifouling Surfaces for the

Continuous Electrochemical Monitoring of Glucose in Whole Blood Using a Lab-on-a-Chip", *Lab. Chip*, **13**, 2013, 1780–1789.

[127] Finesse Solutions, *www.finesse.com*.

[128] Endress+Hauser Messtechnik GmbH+Co. KG, *www.de.endress.com*.

[129] G. D. Bixler and B. Bhushan, "Biofouling: Lessons from Nature", *Philos. Trans. A Math. Phys. Eng. Sci.*, **370**, 2012, 2381–2417.

[130] V. Kochkodan and N. Hilal, "A Comprehensive Review on Surface Modified Polymer Membranes for Biofouling Mitigation", *State-of-the-Art Reviews in Desalination*, **356**, 2015, 187–207.